Lawrence Berkeley National Laboratory
Recent Work

Title

EXPLORATORY CELL RESEARCH AND FUNDAMENTAL PROCESSES STUDY IN SOLID STATE ELECTROCHEMICAL CELLS

Permalink

https://escholarship.org/uc/item/0w55053r

Authors

Smyrl, W.H.
Owens, B.B.
White, H.S.

Publication Date

1988-10-01

eScholarship.org Powered by the California Digital Library
University of California

LBL-26134 c.2
UC-210

Lawrence Berkeley Laboratory
UNIVERSITY OF CALIFORNIA

APPLIED SCIENCE DIVISION

Exploratory Cell Research and Fundamental Processes Study in Solid State Electrochemical Cells

Final Report

RECEIVED
LAWRENCE
BERKELEY LABORATORY

FEB 15 1989

LIBRARY AND
DOCUMENTS SECTION

W.H. Smyrl, B.B. Owens, and H.S. White

October 1988

TWO-WEEK LOAN COPY

This is a Library Circulating Copy which may be borrowed for two weeks.

APPLIED SCIENCE DIVISION

LBL-26134 c.2

Prepared for the U.S. Department of Energy under Contract Number DE-AC03-76SF00098.

DISCLAIMER

This document was prepared as an account of work sponsored by the United States Government. While this document is believed to contain correct information, neither the United States Government nor any agency thereof, nor the Regents of the University of California, nor any of their employees, makes any warranty, express or implied, or assumes any legal responsibility for the accuracy, completeness, or usefulness of any information, apparatus, product, or process disclosed, or represents that its use would not infringe privately owned rights. Reference herein to any specific commercial product, process, or service by its trade name, trademark, manufacturer, or otherwise, does not necessarily constitute or imply its endorsement, recommendation, or favoring by the United States Government or any agency thereof, or the Regents of the University of California. The views and opinions of authors expressed herein do not necessarily state or reflect those of the United States Government or any agency thereof or the Regents of the University of California.

LBL-26134

EXPLORATORY CELL RESEARCH AND FUNDAMENTAL PROCESSES STUDY IN SOLID STATE ELECTROCHEMICAL CELLS

Final Report

October 1988

by

William H. Smyrl
Boone B. Owens
Henry S. White

University of Minnesota
Department of Chemical Engineering & Materials Science
112 Mines & Metallurgy Building
221 Church Street, S.E.
Minneapolis, Minnesota 55455

for

Applied Science Division
Lawrence Berkeley Laboratory
1 Cyclotron Road
Berkeley, California 94720

This work was supported by the Assistant Secretary for Conservation and Renewable Energy, Office of Energy Storage and Distribution, Energy Storage Division of the U.S. Department of Energy under Contract No. DE-AC03-76SF00098, Subcontract No. 4536610 with the Lawrence Berkeley Laboratory.

Summary of Progress

Effort was focussed on 3 major areas: (1) Exploratory Cell Research, (2) Fundamental Studies of Reaction and Transport in Polymeric Electrolytes, (3) Voltammetry Studies using Microstructured Electrodes.

(1) Cells of Mg and Na were constructed using polymer films of $Mg(ClO_4)_2$-$(PEO)_x$ (x=4,8,10), $MgCl_2$-$(PEO)_x$)x=6,8,10 and NaI-$(PEO)_8$, with V_6O_{13} as the positive electrode material. Open circuit voltages were measured and cycling tests were performed. The Mg cells were resistive, but the Na cells could be cycled. A second type of Mg cell was sealed in the dry box and tested in the lab. Preliminary results suggest that the performance of these cells may be limited by a passivation film at the planar magnesium electrode.

Solid state polymer electrolyte cells of the type M/M-salt in PEO/V_6O_{13} have been fabricated where M=Mg, Ca, Zn, and Cu. Cycling tests have been performed. The initial open circuit voltages of several experimental cells have been tabulated and the cycling test data are reported. The results indicate that copper and zinc systems to be reversible. Extensive studies on the zinc system shows no evidence of passivation and appears to be especially promising. However, the cell performance may be limited by the conductivity of the polymer electrolyte. This phase of the program is still in progress. Cells where M=Mg or Ca have been found to be completely resistive and are not being pursued further.

To support the cell fabrication tests, electrolytes of $Mg(CF_3SO_3)_2$, $MgCl_2$, $Cu(ClO_4)_2$, $CuCl_2$, $Zn(CF_3SO_3)_2$ and $Zn(ClO_4)_2$ were prepared by the solvent technique. A hot-press method for preparing electrolytes has also been developed which required no auxiliary solvents to dissolve the salts and PEO. This is particularly advantageous when using salts of multivalent metal ions which are very difficult to dissolve in casting solvents.

(2) The electrical impedance of insertion electrodes is being studied in order to examine the comparisons between redox polymer films, electronically conducting polymer films, and inorganic oxide films such as V_6O_{13} and WO_3. The investigation of highly

smooth poly(vinylferrocene) films which are spin-cast on gold-covered Si wafers has demonstrated that the properties of such films are suitable for ultra-thin-film cell fabrication techniques. The roughness of the films was determined to be below 20 nm peak-to-valley, as measured by Phase Detection Microscopy. Films of thickness 20-800 nm have been fabricated successfully and studied by impedance measurements. The diffusivity in the films is of the order of 10^{-7} cm^2/sec, which is more than 2 orders of magnitude higher than ordinary solvent-cast films. If such films are used as the negative electrode with PEO electrolytes, where diffusion coefficients are of order 10^{-9} cm^2/sec, diffusion limitations in the electrolyte may be more important than in the redox polymer films.

Electrochemical impedance measurements were made on electronically conducting polymers to study electrode reactions as well as transport phenomena in the electrolyte. The observed behavior of poly(3-methylthiophene), poly(thiophene), and poly(pyrrole) was found to be similar to the behavior of the redox polymer poly(vinylferrocene) studied earlier in this laboratory. The materials show "porous electrode" properties that are influenced by the concentration of injected charge in the films.

Charge vs voltage curves were measured by coulometric techniques on poly(1-trimethylsilyl-2-bromoacetylene), a derivative of poly(acetylene), in two conditions. In the first, coulometry measurements were conducted in a solvent in which the polymer was fully soluble in both the oxidized and reduced forms. In this case, the charge-voltage relationship was Nernstian with approximately 60 mV/decade slope. The same material was studied as a cast film in another solvent where both the oxidized and reduced forms were insoluble. In the latter case, the change of voltage with concentration was much larger (of the order of 150 mV/decade) and changed with concentration level. These studies are the first of their kind for high molecular weight polymers and should lead to important developments in the use of such materials for energy storage.

Cation intercalation studies of Li^+ into single crystal V_6O_{13} confirmed previously reported data in the literature. The studies were done by coulometric titration and have

provided the basis for studies of the insertion of Na^+ and multivalent ions like Mg^{+2}, Ca^{+2}, Zn^{+2}, and Cu^{+2}, into V_6O_{13}. Successful intercalation would mean that positive electrodes of V_6O_{13} which have been used in Li polymer electrolyte cells may also be used with the other cations.

Development of the theory for transference number measurements in polymer electrolytes, based on dilute solution theory, was completed. It was shown that measurement of electrolyte thickness, initial concentration of the salt, initial conductivity, steady-state current, and steady-state voltage across the cell will allow the determination of the diffusion coefficients and transference numbers of both ions in a binary electrolyte. This will provide a foundation for rigorous experimental measurements of transference numbers in solid-state batteries.

(3) Microelectrode structures for measuring transport rates have been constructed and tested in polymer electrolytes containing Li^+, Fe^{+2}, Fe^{+3}, and Cu^{+2} ions. Cyclic voltammetry under semi-infinite solution conditions has been used to measure the apparent diffusion coefficients of the metal ions. The electrochemical reversibility of these metal ions was also determined. The use of microelectrode voltammetry provides a quick and reliable means of measuring transport rates and chemical reversibility of metal ions in PEO solution.

Table of Contents

1. Exploratory Cell Research

This program was initiated to develop thin film solid state cells using anode materials other than lithium. Although lithium has many attractive features, certain other materials offer advantages in such areas as cost, possibly cycle behavior, and manufacturability. Huggins (1985) has recommended the use of Li alloys as the negative electrode in advanced cell systems. Certain alloys may offer high rates of lithium diffusion with improved cyclability. Because of the nature of the thin film polymer electrolyte cell concept involving cells of extremely low electrode loading, unique and novel methods of fabrication must be investigated. However, prior to engineering activities, there is a need for careful research on these types of materials and their properties in cells.

A research cell that can be fabricated in a dry room or ambient laboratory environment is requisite for the cell studies. Utilizing equipment available at the University of Minnesota and industrial laboratories (e.g., Medtronics), cells have been fabricated for evaluation of electrode materials and electrolytes. Some of the cells reported below were modifications of present lithium polymer electrolyte cells have been fabricated for evaluation of electrode materials and electrolytes. The lithium-type cell is nominally a 6.5 cm^2 area cell with thickness of 100-200 microns. The cells were hermetically sealed to permit experimental tests outside of the controlled atmosphere. Other cells of a novel design were used for survey tests with several metals.

In the results to be reported below, experimental cells utilizing thin film poly(ethylene oxide) electrolytes with either Na or bivalent metals (Mg, Ca, Zn, and Cu) were fabricated for study. The metals were chosen because of their availability as thin foils (bivalent metals), and low cost. Cells using Mg, Ca, Zn, and Cu as the anodes were fabricated with V_6O_{13} as the positive electrode. The positive electrode material has been studied in our laboratory (in another program) and was shown to have excellent properties in Li cells. The results reported below have shown that the Zn and Cu cells may be cycled, but neither Mg nor Ca were successfully cycled. Because of the question of whether the

problems in the latter cells were caused by the metal electrode or by the V_6O_{13} positive electrode (i.e., can the bivalent metal ions be intercalated into the oxide material), other cells were constructed and separate intercalation studies were performed. The alternate cells also indicated that Mg could not be cycled, and those results are reported in the present section of the report. The intercalation studies with single crystal V_6O_{13} are reported in Section 2.

Electrolyte preparation methods used here and elsewhere for lithium salts were not acceptable for the bivalent metal salts because of their low solubility in make-up solvents such as acetonitrile. Two alternate techniques were devised and were successful to some degree. Two make-up solvents were used, one to dissolve the metal salt and the other to dissolve the PEO. The solutions were mixed, thin films were cast with the doctor blade technique, and the two make-up solvents were evaporated. This technique mixed the metal salt with PEO intimately, but one of the solvents (dimethyl sulfoxide) was difficult to remove by evaporation. A second technique was devised in which the metal salt and PEO solids were mixed and compressed into a thin film by a Hot Press Method (HPM). Comparison of the properties of the electrolytes made by both techniques have been started, but not completed.

1A. APPLICATIONS OF MULTIVALENT IONIC CONDUCTORS TO POLYMERIC ELECTROLYTE BATTERIES

- J.Y. Cherng, M.Z.A. Munshi, B.B. Owens, W.H. Smyrl

INTRODUCTION

Polymer electrolytes have been widely investigated over the last ten years because of their potential use in high energy density solid state batteries. Polyethylene oxide (PEO) has been the most extensively studied polymer. It was found that PEO doped with a lithium salt such as $LiCF_3SO_3$ could give conductivity values of about $10^{-4}(\Omega cm)^{-1}$ at 100°C [1]. Cells utilizing the monovalent salt-polymer electrolyte, lithium anodes and cathodes based on insertion compounds such as V_6O_{13} have demonstrated good cycling and good reversibility at 100°C.

These encouraging results have led to the investigations of other alkali ion systems such as those based on sodium ion conduction. For example, West et al., [2], reported a Na/MoS_3 cell using $(PEO)_{10}$•NaI as the electrolyte at 90°C. Worrell et al. reported on a cell Na/TiS_2, that was operated with $PEO_{4.5}$-NaSCN electrolyte at 80°C [3].

Although exploratory research has also been made on divalent salt systems such as Mg^{2+}, Ca^{2+}, Pb^{2+}, Zn^{2+} and Cu^{2+} [4-8], little attention has been given to these electrolytes in the studies of solid state batteries. The only report to date has been made by Patrick et al. [8] on a primary Mg/TiS_2 cell using $(PEO)_{15}$•$Mg(SCN)_2$ as the electrolyte at room temperature.

The present paper describes the possibility of using V_6O_{13} as the cathode in sodium and magnesium cells and compares the results (where possible) to the performance of lithium cells. The major limitations associated with these cells are also discussed.

EXPERIMENTAL

Lithium, sodium and magnesium were chosen as the anode material and V_6O_{13} as the cathode. The technique for preparing the lithium based polymer electrolyte $(PEO)_8$•$LiCF_3SO_3$ has been described elsewhere [9]. The sodium ion conductors,

$(PEO)_{10}$•NaI, $(PEO)_{10}$•NaBr and $(PEO)_{10}$•$NaCF_3SO_3$ and the magnesium ion conductors, $(PEO)_8$•$MgCl_2$ and $(PEO)_8$•$Mg(ClO_4)_2$ were prepared as follows.

Polyethylene oxide (Polyscience, MW=$5x10^6$), was dissolved in the appropriate amount of acetonitrile. The salts, NaI, NaBr, $NaCF_3SO_3$, $MgCl_2$ and $Mg(ClO_4)_2$ were dissolved separately in the appropriate amount of anhydrous ethanol. Each salt solution was mixed with a PEO solution with constant stirring. Once homogenized, the mixture was cast on a PTFE sheet using a doctor blade technique. Using this method, thin films of 15 to 35 μm polymer electrolytes were obtained.

The cathode was prepared by a complex mixing process involving V_6O_{13}(80 w/o), PEO (15 w/o) and Shawinigan carbon black (5 w/o).

A thin, flat sodium electrode was made by placing a piece of sodium on a thin stainless steel surface, covering this with polymer film and compressing the electrode between two glass-slides. Once thin enough, the polymer film was removed from the sodium remaining on the stainless steel current collector. Finally a scalpel blade was used to remove excess sodium and to ensure a smooth, oxide-free surface. The thickness of the sodium film prepared by this means was about 30 μm.

The lithium electrode was obtained as a thin foil (thickness 55 μm) and used with no further treatment. The magnesium electrode was also obtained as thin foil (thickness 125 μm) and after cleaning the surface, the final thickness was about 25 μm.

Cells were assembled as shown in Figure 1. The diameter of the electrolyte was 1 cm. Adhesive tape (thickness = 5 μm) was used as the spacer to separate the two electrodes. All the electrolytes were vacuum-dried after casting and stored in an argon atmosphere glove-box for two weeks prior to use. The cell assembly was also carried out in the glove box. Once sealed with epoxy, the cells were tested outside the glove box. Sodium cells were tested at 90°C and lithium and magnesium cells at 100°C.

RESULTS AND DISCUSSIONS

The initial open circuit voltages (OCV) of the experimental cells are listed in Table 1. The cells, NaI$(PEO)_{10}$•NaBr|V_6O_{13} and NaI$(PEO)_{10}$•$NaCF_3SO_3$|V_6O_{13} show an OCV of about 3.1 V at 90°C. In contrast, the NaI$(PEO)_{10}$•NaI|V_6O_{13} cell has an OCV of only 2.76V at 90°C. This value is close to the NaI_2 cell which has an OCV of 2.8 V or 2.9 V, obtained from the free energy of formation of NaI(l) or NaI(s) [10]. This suggests the possibility of a reaction between the NaI and the V_6O_{13}. Two possible reaction schemes are:

$$xNaI + V_6O_{13} + xC \rightarrow Na_xV_6O_{13} + xI\text{-}C \quad (1)$$

$$xNaI + V_6O_{13} \rightarrow x/2\ I_2 + Na_xV_6O_{13} \quad (2)$$

Reaction (1) occurs with the adsorption of iodine on the carbon surface and (2) occurs with the liberation of free iodine. In any case both reactions would contribute to a lowering of the OCV.

Both magnesium cells demonstrated an OCV of 2.0 V at 100°C whereas the lithium cell value was greater than 3.2V. The lithium cell was the most extensively studied system in our investigation. Figure 2 shows the performance of LiI$(PEO)_8$•$LiCF_3SO_3$|V_6O_{13} at three discharge rates. The charging was carried out at constant potential using a limiting resistor in series with the circuit to control the current. At the C/5 rate over a hundred cycles was obtained with greater than 35% of the theoretical capacity ($8Li/V_6O_{13}$). Figure 3 shows the load voltage of the cell against utilization of V_6O_{13}. It is seen that greater than 80% of the theoretical capacity is possible at the C/10 and C/20 rates.

Figure 2 also shows a NaI$(PEO)_{10}$•NaI|V_6O_{13} cell operating at the C/4 rate. The cell appears to cycle with constant capacity but is limited to only one Na per V_6O_{13} between the voltage limits of 2.8 V and 1.5 V. A typical charge-discharge curve for the NaI$(PEO)_{10}$•NaI|V_6O_{13} cell is shown in Figure 4. The initial stages of discharge appears to

be flatter than the latter stages which shows a rapid decline in capacity. The first part is attributed to the reaction of I_2 as shown in sequences (1) and (2) above and the second part to a combination of sodium intercalation with V_6O_{13} and I_2 reaction. During charge the cell potential exceeds 2.8 V when a 51 $\mu A/cm^2$ charge current is applied. This sudden increase suggests that the intercalation of Na into V_6O_{13} may not be as reversible as Li.

Cyclic voltammetry results on the sodium cells are shown in Figure 5a and 5b. For $NaI(PEO)_{10}{\bullet}NaI|V_6O_{13}$, the curve (Figure 5a) shows a distinct inflection at 2.8 V. This is normally representative of a reaction involving

$$Na + 1/2\ I_2 \rightarrow NaI \qquad (3)$$

rather than an intercalation reaction ($xNa + V_6O_{13} \rightarrow Na_xV_6O_{13}$). A typical intercalation curve was found in the $NaI(PEO)_{10}{\bullet}NaCF_3SO_3|V_6O_{13}$ cell (Figure 5b). This does not show a distinct inflection corresponding to a single reaction but rather a series of reactions.

Due to the low ionic conductivity of the $(PEO)_{10}{\bullet}NaBr$ electrolyte, the corresponding cyclic voltammetry curve for the $NaI(PEO)_{10}{\bullet}NaBr|V_6O_{13}$ cell exhibited much lower currents (by a factor of 0.001). The curve was representative of a high resistance cell associated with a large iR drop. In contrast the currents were about four times higher in the $NaI(PEO)_{10}{\bullet}NaI|V_6O_{13}$ cell than in the $NaI(PEO)_{10}{\bullet}NaCF_3SO_3|V_6O_{13}$ cell. Furthermore the latter cell demonstrated an order of magnitude increase in the cell internal resistance upon storage for one day at 90°C. This increase in resistance with time was not observed in the other sodium cells. Previous work [11] on the lithium system has demonstrated that $LiCF_3SO_3$ is not thermodynamically stable with lithium metal. The metal is, however, protected by a passive film formed by a reaction involving the lithium and $LiCF_3SO_3$. It is envisaged that $NaCF_3SO_3$ is also not thermodynamically stable with sodium metal. However, in this case, the protective film appears to be less protective and less ionically conducting than the film on lithium metal. This gives rise to a large build-up

of the passive layer which subsequently results in an increase in the interfacial resistance and hence an increase in the observed cell impedance with time.

The cyclic voltammetry curves for the magnesium electrode against a magnesium reference electrode in cells of the type $Mg|(PEO)_8{\cdot}MgCl_2|V_6O_{13}$ and $Mg|(PEO)_8{\cdot}Mg(ClO_4)_2|V_6O_{13}$ are shown in Figure 6a and 6b. In either case the anodic currents are considerably higher than the corresponding cathodic currents. Furthermore the anodic current in the forward potential sweep is less than the anodic current in the backward sweep. In the forward sweep, the potential of the magnesium electrode increases with a corresponding increase in the slope of the curve. This phenomena does not occur in the backward potential sweep. This clearly suggests the formation of a passive layer on the magnesium electrode surface and, hence, the need to activate the magnesium electrode at a certain potential. However, as the passive film grows with time, the required activation potential increases.

This passivation phenomena can also be confirmed from the voltage delay observed in the constant current discharge curves of the magnesium cells (Figure 7a and 7b). The constant current charge curve shows a poor rechargeability of the magnesium electrodes in both cells.

The cyclic voltammetry curve (Fig. 8) for the V_6O_{13} electrode against a magnesium reference electrode in cells of the type $Mg|(PEO)_8{\cdot}Mg(ClO_4)_2|V_6O_{13}$ does suggest some reversibility of magnesium intercalation in V_6O_{13}. The current output in this case is larger than that observed for the magnesium working electrodes.

CONCLUSION

The lithium polymer electrolyte battery system is thus far the best candidate that exhibits good cycling and good reversibility with cathodes such as V_6O_{13}.

Preliminary investigation suggests that the cell $NaI|(PEO)_{10}{\cdot}NaI|V_6O_{13}$ behaves as a $NaI|I_2$ cell with and OCV of 3.1V at 90°C. In addition, passivation in the

$NaI(PEO)_{10}$•$NaCF_3SO_3|V_6O_{13}$ cell and low ionic conductivity of the $(PEO)_{10}$•NaBr electrolyte severely limits the performance of this system.

The magnesium system is limited by the magnesium electrode rather than the cathode. Further work is continuing to confirm some of the above observations and to investigate other electrode couples for solid-state polymer-electrolyte batteries.

REFERENCES

[1] B.E. Fenton, J.M. Parker and P.V. Wright, Polymer, 14, 589 (1973).

[2] K. West, B. Zachau-Christiansen, T. Jacobsen, and S. Atlung, J. Electrochem. Soc., 132, 3061 (1985).

[3] P.G.M. Mehrotra and W.L. Worrell, Presented at the 164th Electro. Soc. Meeting, Extended Abstract, Vol 83-2, No. 86 (1983).

[4] A. Moryoussef, M. Bonnat, M. Fouletier, and P. Hicter, 6th Risφ International Symposium on Metallurgy and Materials Science, ed. F.W. Paulsen, N. Hessel Andersen, K. Clausen, S. Skaarup and O. Toft Sorensen, 335 (1985).

[5] L.L. Yang, A.R. McGhie, and G.C. Farrington, J. Electrochem. Soc., 133, 1380 (1986).

[6] T.M.A. Abrantes, L.J. Alcacer, and C.A.C. Sequeira, Solid State Ionics, 18 & 19, 315 (1986).

[7] R. Huq, G. Chiodelli, P. Ferloni, A. Magistris, and G.C. Farrington, J. Electrochem. Soc., 134, 364 (1987).

[8] A. Patrick, M. Glasse, R. Latham and R. Linford, Solid State Ionics, 18 & 19, 1063 (1986).

[9] M.Z.A. Munshi and B.B. Owens, Appl Phys. Comm., 6 (4), 279 (1987).

[10] JANAF Thermochemical Tables, Aug. 1965.

[11] D. Fauteux, Solid State Ionics, 17, 133 (1985).

TABLE 1. INITIAL OCV OF POLYMER ELECTROLYTE CELLS

	OCV (v)	T(C°)
$Li/PEO_8LiCF_3SO_3/V_6O_{13}$	3.2	100
$Na/PEO_{10}{\bullet}NaI/V_6O_{13}$	2.76	90
$Na/PEO_{10}{\bullet}NaBr/V_6O_{13}$	3.09	90
$Na/PEO_{10}{\bullet}NaCF_3SO_3/V_6O_{13}$	3.12	90
$Mg/PEO_8{\bullet}Mg(ClO_4)_2/V_6O_{13}$	2.0	100
$Mg/PEO_8{\bullet}MgCl_2/V_6O_{13}$	2.0	100

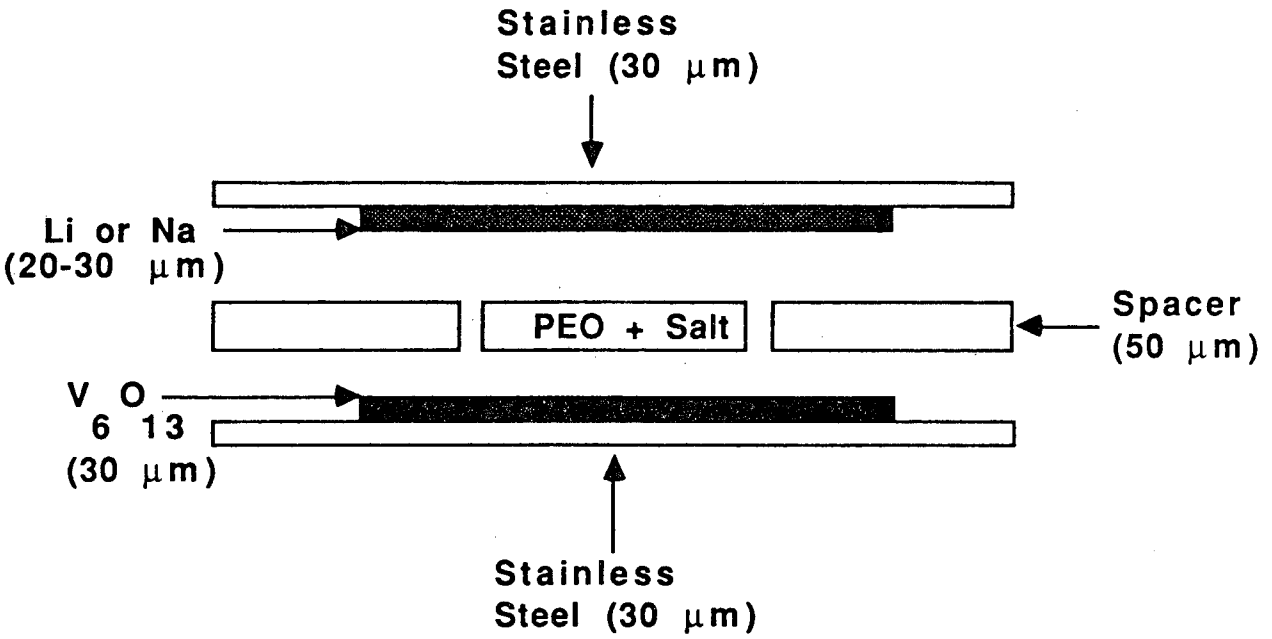

Figure 1. Schematic of a polymer electrolyte cell.

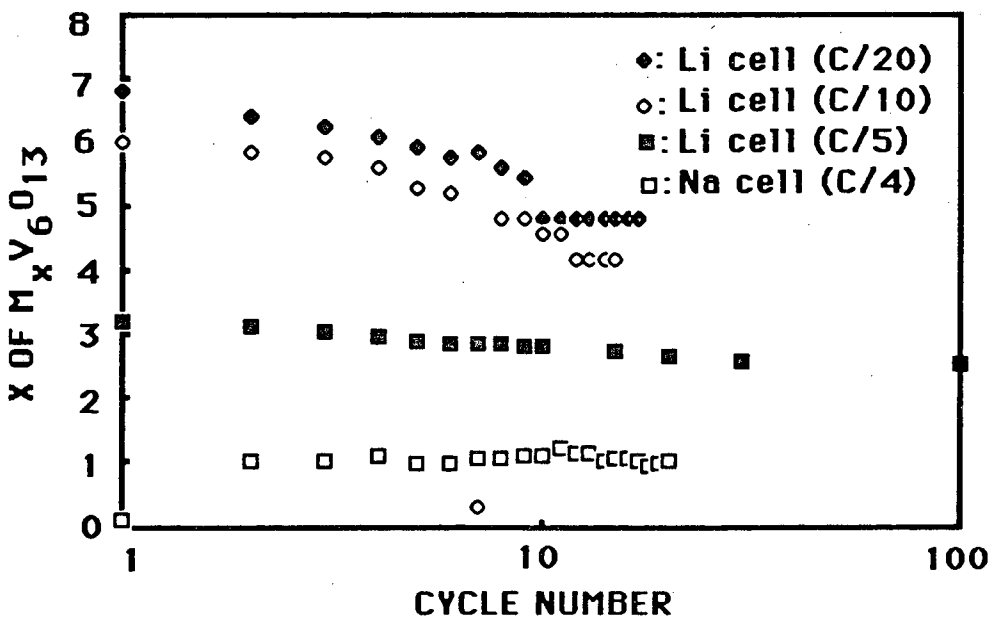

Figure 2. Performance of polymer electrolyte cells.

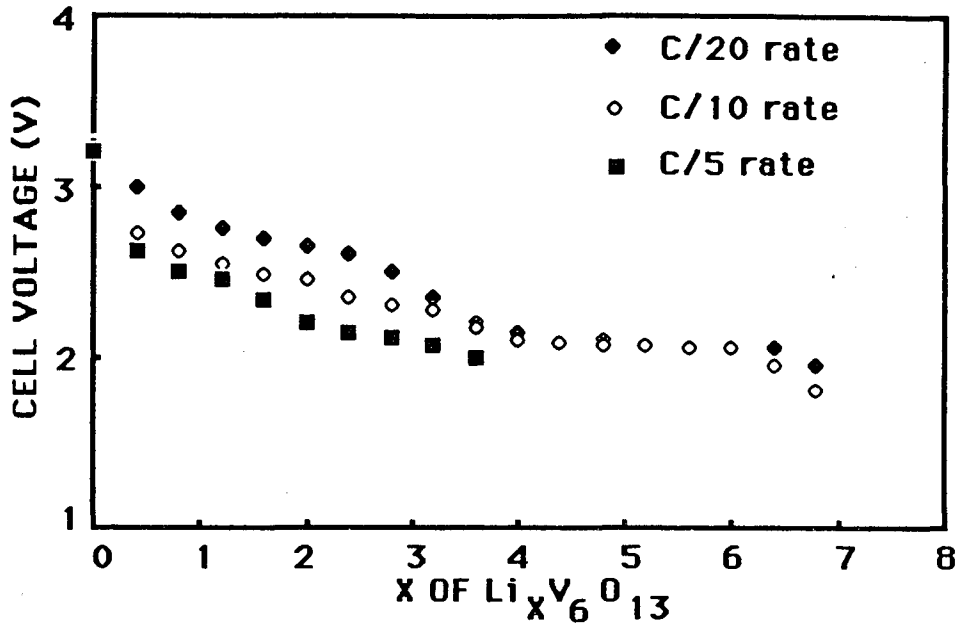

Figure 3. Discharge curve of a Li/V_6O_{13} cell.

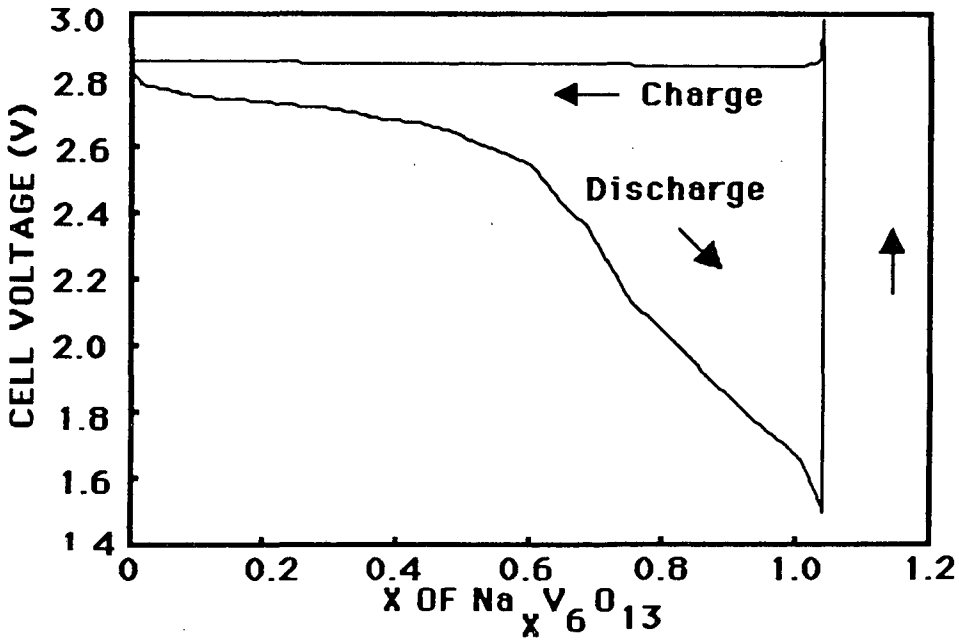

Figure 4. Discharge-charge curve of a Na/PEO_{10}-NaI/ V_6O_{13} cell at a constant current ($51\mu A/cm^2$).

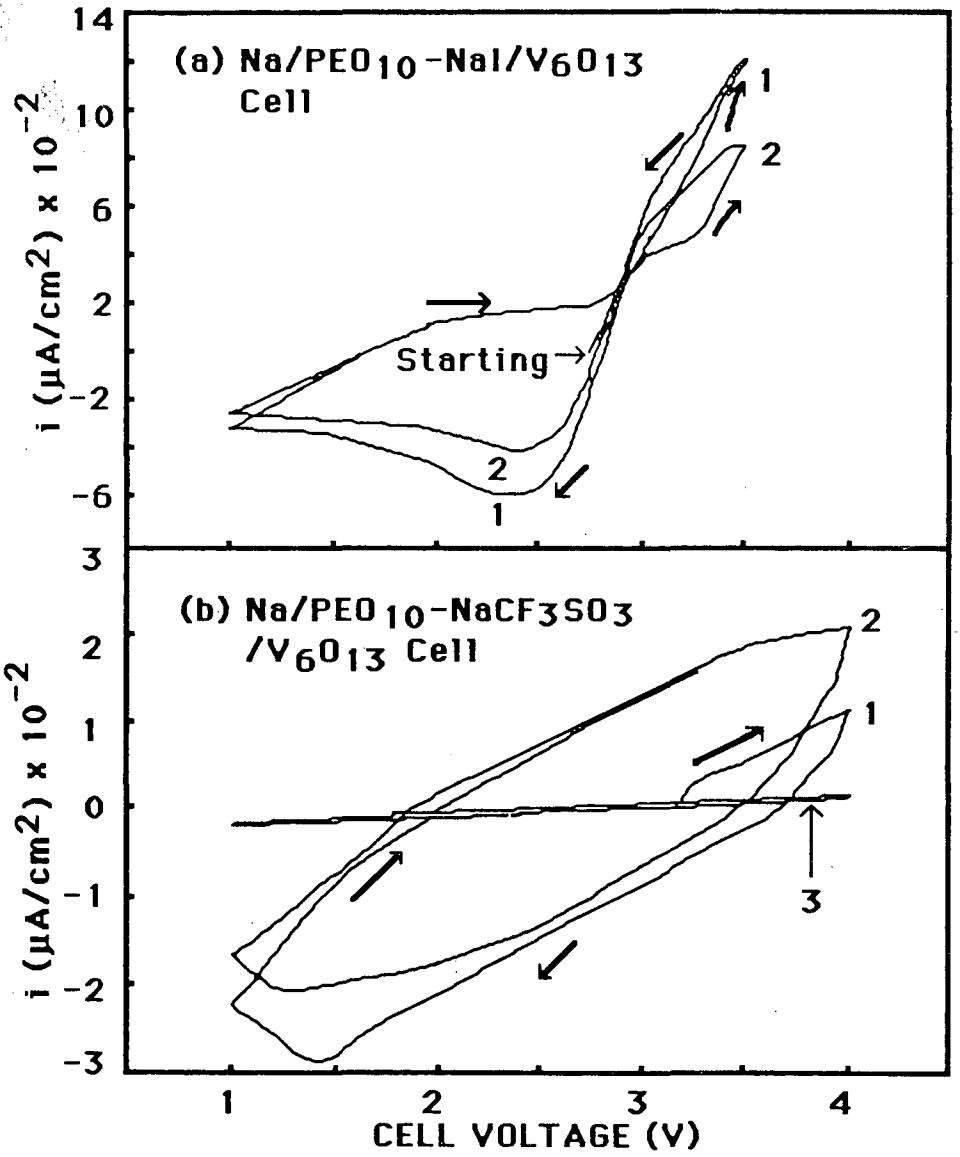

Figure 5. Cyclic voltammograms of sodium cells at 10 mV/s (Cycle 3, after 26 hours storage at 90 °C).

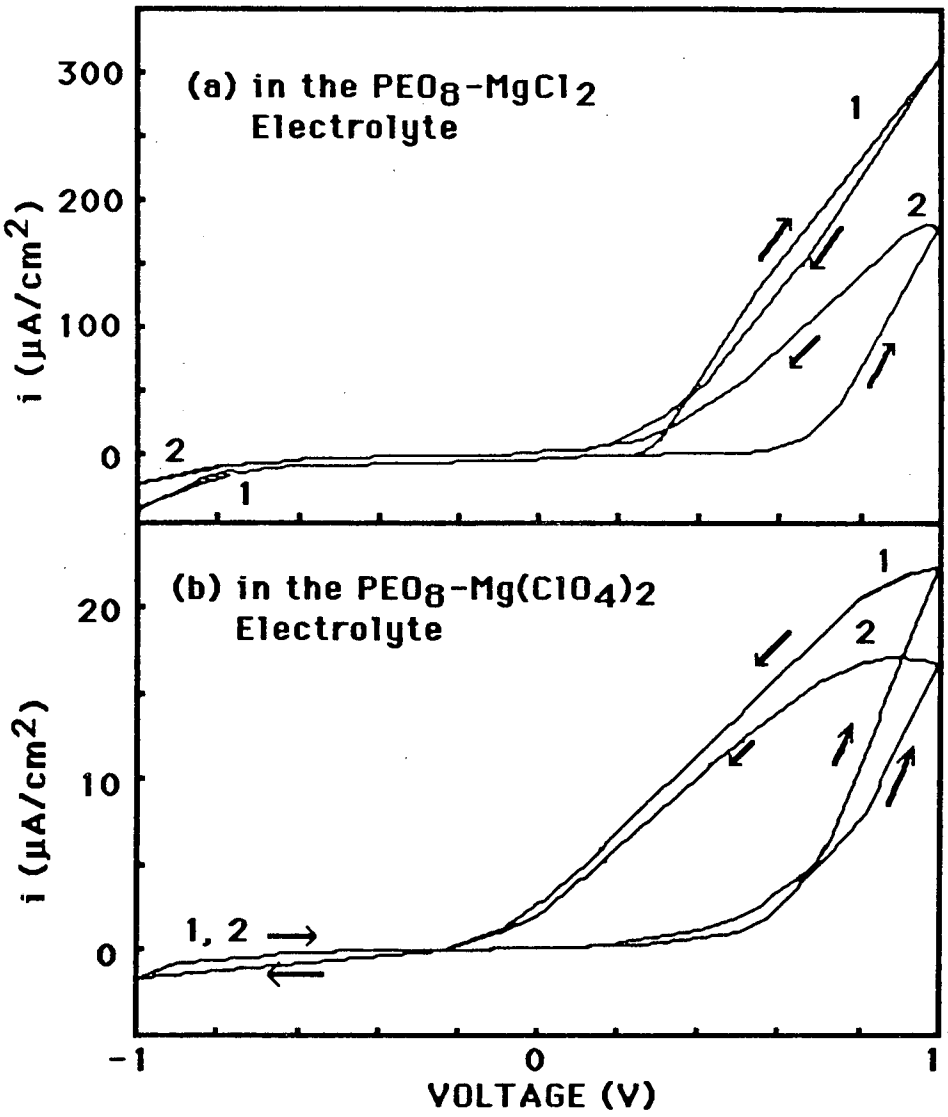

Figure 6. Cyclic voltammograms at 10 mV/s of magnesium electrodes with respect to magnesium ref. electrodes.

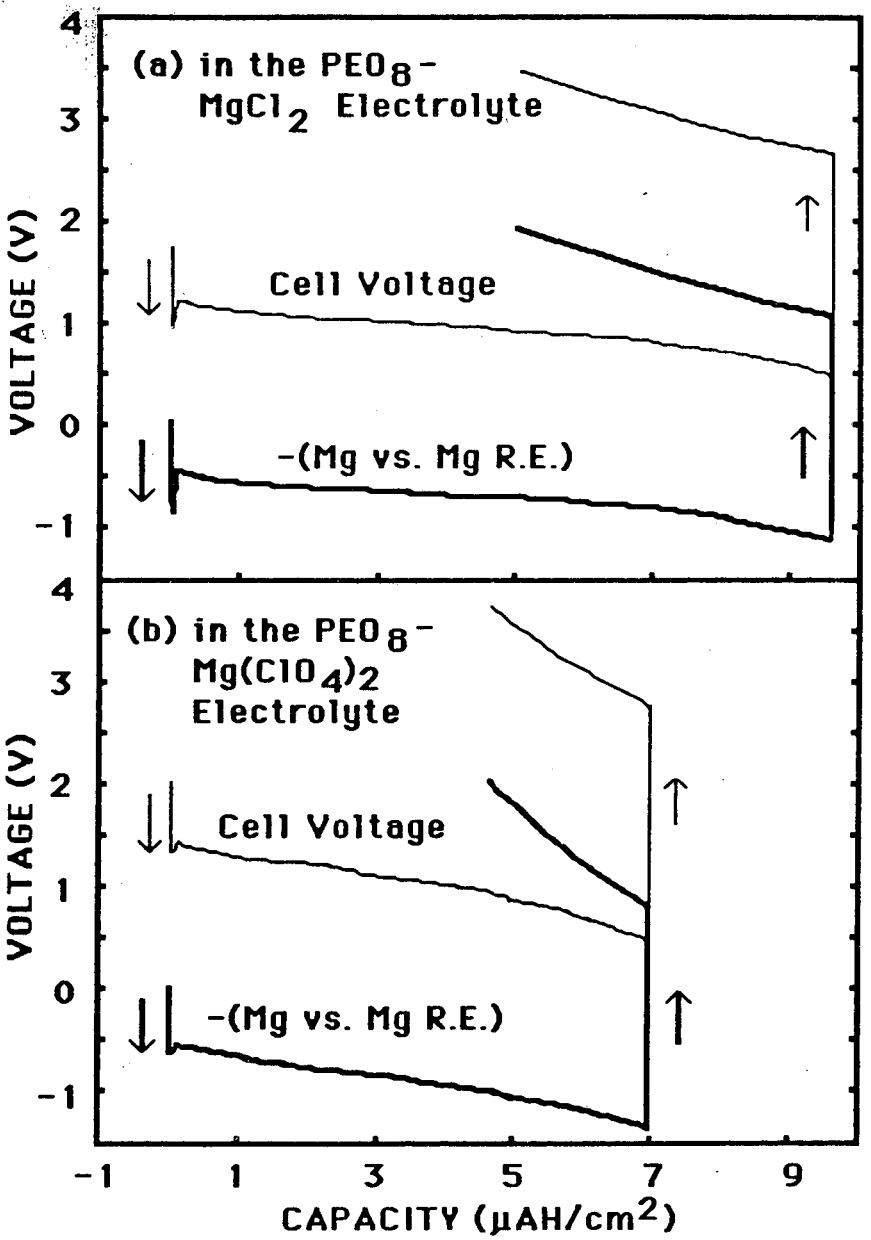

Figure 7. Discharge-charge curves of magnesium cells at a constant current (16.7 μA/cm^2).

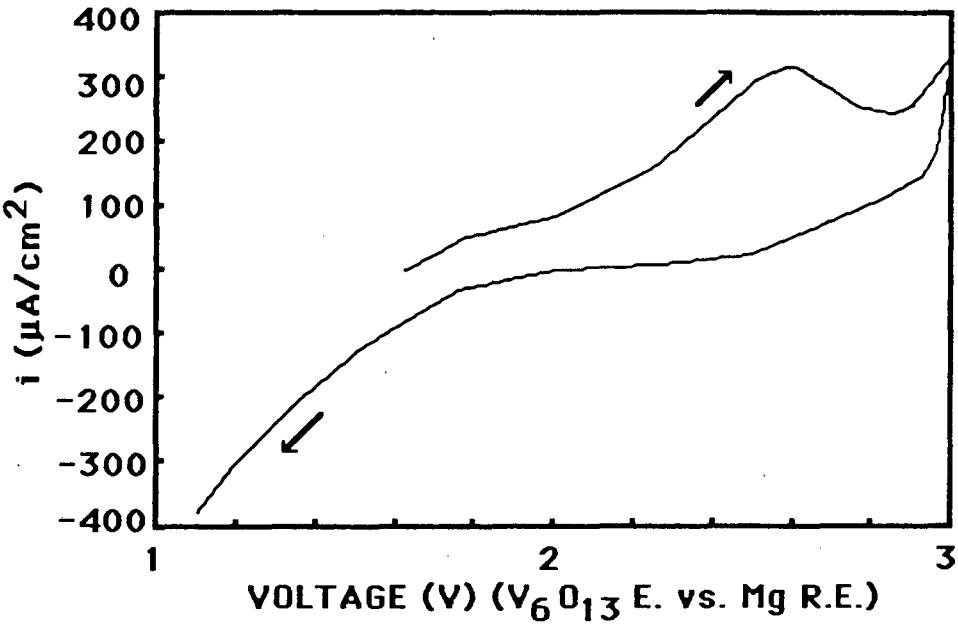

Figure 8. Cyclic voltammogram at 10 mV/s of the V_6O_{13} electrode in the PEO_8-$Mg(ClO_4)_2$ electrolyte.

1B. APPLICATION OF MULTIVALENT POLYMER ELECTROLYTES TO SOLID STATE BATTERIES

- Alison Gilmour, B.B. Owens

INTRODUCTION

In recent years new macromolecular materials based on polyethers have been proposed as solid electrolytes suitable for applications in batteries of high specific energy (1,2). One of the major problems in this field is the absence of solid electrolytes that exhibit adequately high ionic conductivities for appropriate ionic species. Some solid electrolyte batteries have been designed for operation at elevated temperatures where the electrical conductivity permits reasonable power levels; however, there is more interest in solid-state batteries that would be operable at ambient temperatures and in this area the material problem remains challenging (3).

Most work to date has been based on alkali metal salt systems, with particular attention being focussed on lithium because of the attractiveness of metallic lithium as a lightweight, high specific energy negative electrode material. Very little work has been reported on other metal systems such as zinc, lead or copper; the alkaline earth metals have been particularly neglected. Of the metals not widely studied, magnesium is one of particular interest because of its diagonal relationship in the periodic table with lithium, and because it has a divalent charge there will be a consequent increase in anion to cation ratio of 2:1. The solid electrolyte magnesium perchlorate: polyethylene oxide, PEO_8 $Mg(ClO_4)_2$, has been shown by Patrick et al. (4) to give conductivities between 10^{-5} - 10^{-6} S cm^{-1} at 80°C, and this is comparable with that for lithium polymeric electrolytes (i.e., PEO_8 $LiClO_4$) at similar temperatures. However, preliminary work carried out as part of the present program by J.Y. Cherng et. al. (5) (see also previous section) suggests that although the magnesium is readily oxidized, the deposition reaction is severely hindered. Despite this, magnesium polymeric electrolytes, in particular, offer an interesting alternative to lithium systems for room temperature, solid-state battery systems and were investigated as part of a systematic analysis of polymeric-electrolyte cell systems.

EXPERIMENTAL

Magnesium, calcium, copper and zinc were chosen as the anode material and V_6O_{13} was initially selected as the cathode, since it showed very promising results with lithium cell systems (6-9) and was found by Patrick et. al. (10) to give higher OCV values for Mg, Ca and Zn systems than other cathode systems such as TiS_2. The cathode was prepared by adaptation of a previously developed, complex mixing process involving V_6O_{13} (80 w/o), PEO (15 w/o) and Shawinigan carbon black (5 w/o)(11). The anode material was obtained as a thin foil which was mechanically cleaned just before cell fabrication to remove any oxide film which might be present on the foil. Two techniques were used for preparing the polymer electrolytes.

I) Solvent Method (S.M.)

The electrolytes were prepared in the same way as those in the previous section (p. 4), except that the following salts were used:

$Mg(CF_3SO_3)_2$, $MgCl_2$, $Cu(ClO_4)_2$ $CaCl_2$, $CuCl_2$, $Zn(CF_3SO_3)_2$, and $Zn(ClO_4)_2$ The salts were chosen because solubilities and conductivities were expected to be high in PEO.

II) Hot-Press Method (H.P.M.) (12)

Ground PEO and ground salt were mixed together in 5 g samples using a 100 ml shaker at liquid nitrogen temperature for 2-3 minutes. Steel balls were used in this mixing process to help decrease the particle size of the PEO and salt and hence get better mixing. About 0.03g of this salt/PEO mixture was put into a 5-mm die and pressed at 2 tons at room temperature. The electrolyte pellet was then transferred to a 13-mm die and pressed at 5 tons so that a thin film of salt/PEO mixture is obtained. After releasing the pressure, the electrolyte was heated to 130°C for 3 hours while still in the die. After 3 hours, the electrolyte was cooled to room temperature with a pressure of 2 tons being exerted at 70°C and below. Using this method, 13-mm diameter thin film wafers of 35- to 50-μm thick polymer electrolytes were obtained.

All electrolyte and cathode materials were dried in a vacuum desiccator over P_2O_5 for at least one week before use. Cell assembly (Figure 1) was carried out in a dry room and the cells were tested at 100°C inside the glove box.

Conductivity Measurements

Conductivity measurements were carried out using a Solartron 1260 impedance analyzer. This instrument is in the process of being interfaced to a Hewlett Packard 9816 computer for easier data collection. The electrolyte material being studied was placed between two stainless steel blocking electrodes in the conductivity apparatus which could be evacuated and heated. The temperature inside the apparatus was monitored using a chromel-alumel thermocouple, as shown in Figure 9. Before the measurements were carried out, the electrolyte was heated to 120°C and then cooled to the appropriate temperature for measurement. This was done to improve the electrical contact between the electrolyte and electrodes.

RESULTS AND DISCUSSION

Electrolytes of the following compositions, $Mg(CF_3SO_3)_2 \cdot PEO_{16}$, $MgCl_2 \cdot PEO_{16}$, $Cu(ClO_4)_2 \cdot PEO_{16}$, $CuCl_2 \cdot PEO_{16}$, $CuCl_2 \cdot PEO_{16}$, $Zn(CF_3SO_3)_2 \cdot PEO_{16}$ and $Zn(ClO_4)_2 \cdot PEO_{16}$ were prepared by the solvent technique and some magnesium salts by the hot-press method (12). This method requires no auxiliary solvents to dissolve the salts and PEO which is particularly important when working with salts of certain metals such as Mg which are very difficult to dissolve. Also electrolytes prepared by the hot-press technique have been shown (12) to have superior conductivities to those prepared by the solvent technique.

Conductivity measurements of the above electrolytes are being carried out at present using the Solartron 1260. Preliminary results obtained show that $MgCl_2$:PEO_{16} has a conductivity of 10^{-7} to 10^{-8} $(\Omega\ cm)^{-1}$ at 100°C which is much lower than that obtained by Huq et. al. (13) who obtained values of 10^{-5} $(\Omega\ cm)^{-1}$ at 140°C. However, Huq et. al. used DMSO to dissolve their salts, and this was found during our investigations to be very

difficult to remove. The effect of solvent retention on material resistivity should be ascertained; generally it could reduce resistivity. The conductivity data of the two preparative techniques will be compared, for a number of salt/PEO systems and compositions, and transference number measurements will also be carried out.

Cells of the type M/M-salt in PEO/V_6O_{13} have been fabricated where M = Mg, Ca, Zn and Cu and cycling tests have been performed. The cells where M = Mg or Ca have been found to be completely resistive and neither charging nor discharging was observed. This is probably due to passivation at the metal surface (5) even though great care was taken not to expose the metal anode to the atmosphere and the anode surface was mechanically cleaned just before cell fabrication. The initial open circuit voltages (OCV) of the divalent cation experimental cell systems are listed in Table 2.

Preliminary results indicate that the copper and zinc systems are reversible. Some results obtained from these systems can be seen in Figures 10 and 11, respectively. For both the copper and zinc cell systems the initial starting voltage decreases with cycling. This phenomena may be due to either self-discharge which becomes enhanced as the cell is cycled or the cells are not completely reversible. However, on looking at the discharge curves for the copper system (Figure 10) we can see that the second discharge curve is at a higher voltage than the first discharge curve; and also the second discharge curve appears to level off more than the first one and exhibits a higher capacity value. These three points suggest that the cell has reversibility and more work on the system is required to help overcome the problems mentioned above. The discharge curves for a zinc cell are shown in Figure 11. The first, third and fourth discharge curves show two plateaus, one at the beginning of the discharge process and the other just before the cut-off voltage. The third and fourth discharge curves have low voltages at the beginning of the discharge process which may be due to the low voltage cut-off point during the second discharge, i.e., overdischarge has occurred, which may have resulted in a loss of complete reversibility. In order to understand some of the behavior mentioned above, more work is being carried out

in this area, (see abstract in Appendix I) as well as some fundamental studies, such as DSC analysis of divalent salt: PEO electrolytes and x-ray analysis of these electrolytes.

References

1. M.B. Armand, J.M. Chabagno, M.J. Duclot, Polyethers as solid electrolytes, in Frast Ion Transport in Solids, ed. P. Vashista (North Holland, Amsterdam, 1979) 131-136.

2. M.B. Armand, Solid State Ionics 9-10 (1983) 745.

3. M.Z.A. Munshi and B.B. Owens, Proceedings of the 169th Meeting of the Electrochemistry Society, Boston, MA, May 1986.

4. A. Patrick, M. Glasse, R. Latham and R. Linford, Solid State Ionics 18 & 19 (1986) 1063.

5. J.Y. Cherng, M.Z.A. Munshi, B.B. Owens and W.H. Smyrl, accepted for publication in proceeding volume of Solid State Ionics, Garmisch-Partenkirchen, West Germanyu, 1987.

6. M.Z.A. Munshi, B.B. Owens, Proc. of the Symp. on Primary and Secondary Ambient Temperature Lithium Batteries, Eds. J.P. Gabano, Z. Takehara and P. Bro, Proc. Vol. 88-6, The Electrochem. Soc., p. 737 (1988).

7. R. Gopaliengar, M.Z.A. Munshi and B.B. Owens, ibid, p 726 (1988).

8. B.B. Owens, M.Z.A. Munshi and P.M. Skarstad, Extended Abstract, 38th Meeting of the Int. Soc. of Electrochemistry, Maastricht, The Netherlands, Sept. 13-18, 1987.

9. M.Z.A. Munshi and B.B. Owens, Solid State Ionics 26 (1988) 41.

10. A. Patrick, M. Glasse, R. Latham and R. Linford, Solid State Ionics, 18 & 19 (1986) 1063.

11. M.Z.A. Munshi and B.B. Owens, Submitted to Solid State Ionics.

12. F.M. Gray, J.R. MacCallum & C.A. Vincent, Solid State Ionics, 18 & 19, (1986) 282.

13. R. Huq, G. Chiodelli, P. Ferloni, and A. Magistris, and G. Farrington, J. Electrochem. Soc. 132(2), 1988, 364.

Table 2

Cell	OCV
$Cu\|CuCl_2 \cdot PEO_{16}\|V_6O_{13}$	0.574 V
$Zn\|Zn(ClO_4)_2 \cdot PEO_{16}\|V_6O_{13}$	1.3021 V
$Zn\|ZnCl_2 . PEO_{16}\|V_6O_{13}$	1.073 V
$Cu\|CuCl_2 \cdot PEO_{16}\|V_6O_{13}$	2.162 V
$Cu\|Cu(ClO_4)_2 \cdot PEO_{16}\|V_6O_{13}$	2.387 V
$Mg\|MgCl_2 \cdot PEO_{16}\|V_6O_{13}$	1.81 V

Temp = 100°C

Figure 9

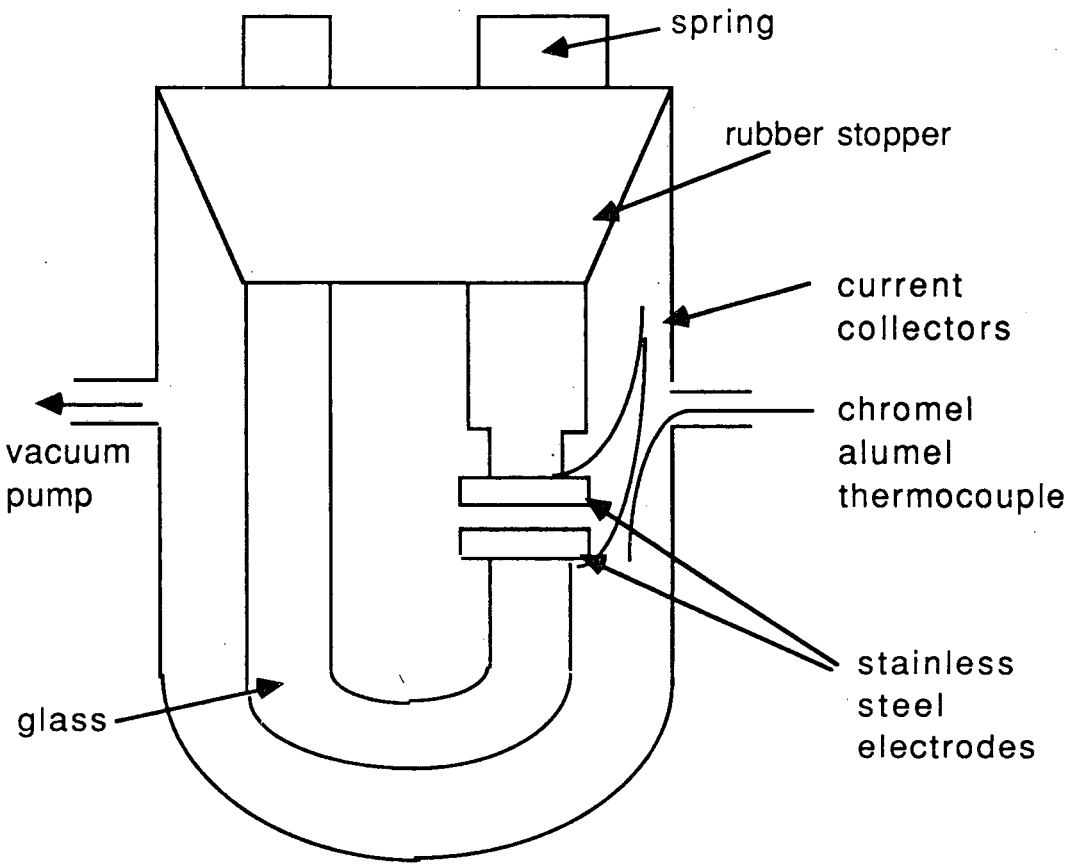
spring
rubber stopper
current collectors
chromel alumel thermocouple
vacuum pump
glass
stainless steel electrodes

Figure 10

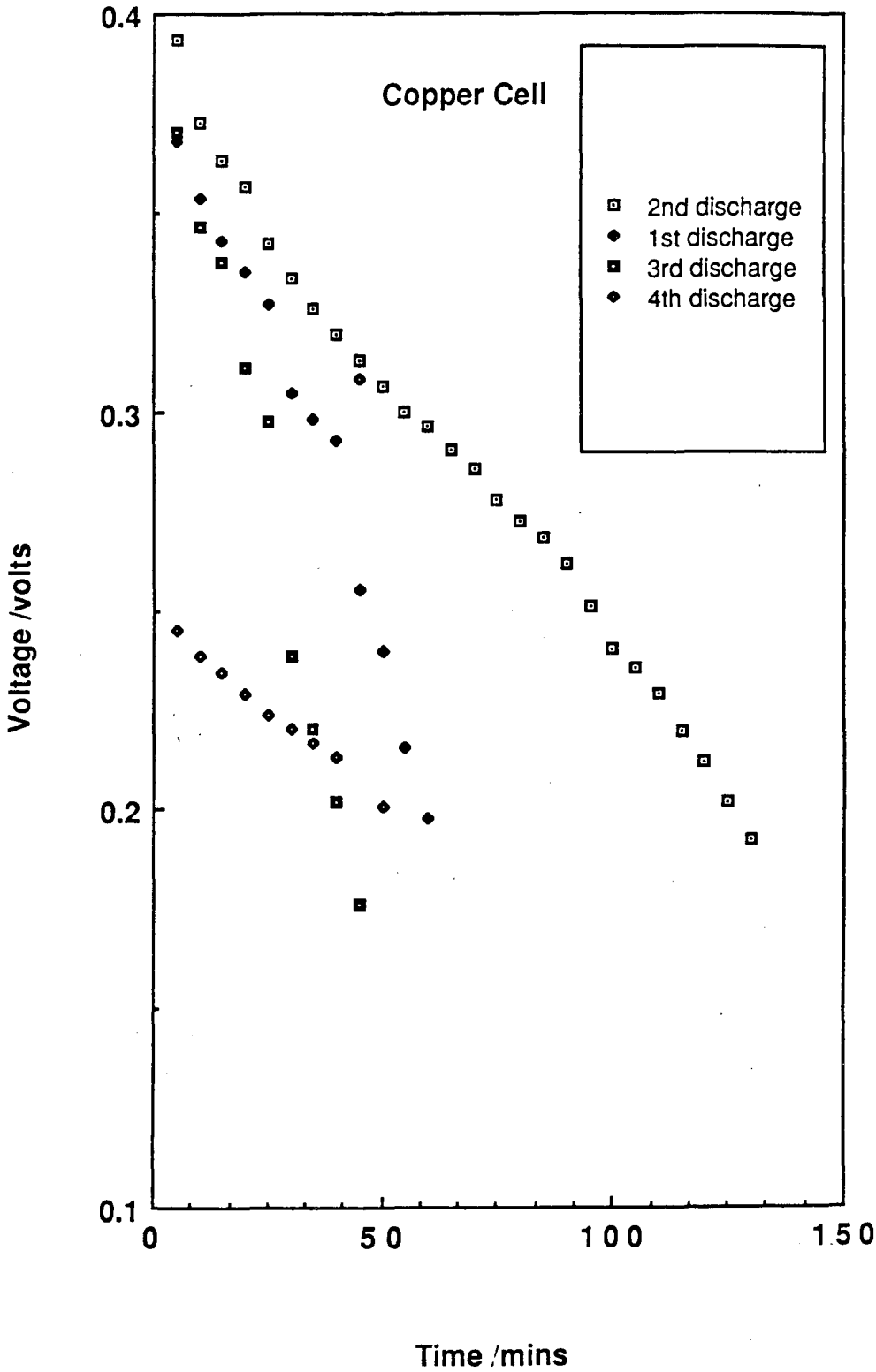

Capacity values

uAhr

1st = 31

2nd = 63

3rd = 22.25

4th = 6.33

Figure 11

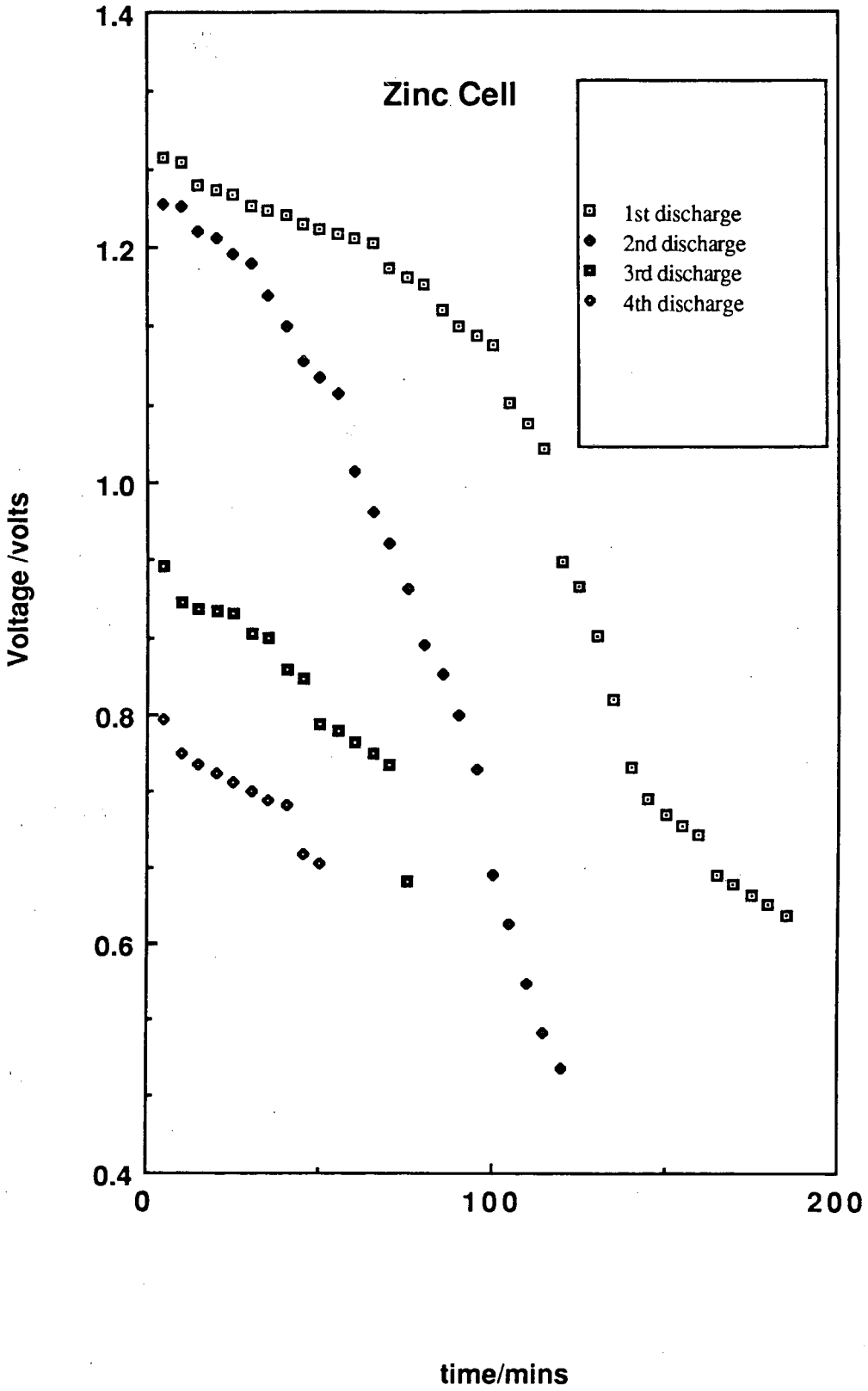

Capacity values

uAhr

1st = 74.75

2nd = 151

3rd = 16.25

4th = 6.5

2. FUNDAMENTAL STUDIES OF REACTION AND TRANSPORT IN POLYMERIC ELECTROLYTES

The objective of these investigations was to apply advanced techniques for assessing the basic mechanisms occurring at the electrode-electrolyte interfaces of novel electrochemical cells. The successful development of any thin-film electrochemical cell with cell thickness of ~100 microns requires a sound understanding of the interfacial phenomena. Although interface reactions are essential in all the importance of these properties is greater batteries, the importance of these properties is greater because of the high interfacial surface area to volume ratio. The studies of interfaces have included the optical studies of interfaces and complex impedance spectroscopy of species and reactions. The possible scope of interfacial processes which may be studied at electrode-electrolyte interfaces range from the elementary charge-transfer steps and the physics of the charged interface, to the nucleation and growth of second-phase reaction products, and may include the influence of diffusion and convection on the surface events. The present investigation is more limited in scope, although it touches several of these areas. The studies have been driven by the need to understand the reacting interfaces at a fundamental level. The aim is to identify the controlling events at the surface and to predict the limits on cell performance which these events dictate.

The results reported below have used intercalation-type positive electrode interfaces. Impedance studies have been carried out with both electronically conducting and redox polymer film electrodes. The kinetics and rate of the intercalation process are of interest in the present program. It was found here that the charge injection process is the charge-transfer reaction at the conducting polymer interface with the electrolyte, and that this process is in parallel with a double layer capacitance. The rate of the charge injection process and charging of the double layer are fundamental parameters that have been determined by impedance techniques on poly(3-methylthiophene), poly(thiophene), poly(pyrrole), and poly(vinylferrocene). These studies have also revealed that the diffusion coefficients range up to the order of 10^{-7} cm^2/sec in the polymer phase for the

materials. Since diffusion coefficients of the order of 10^{-9} cm^2/sec have been reported in PEO solutions, diffusion effects in the electrolyte may be more important in the thin-film cells than would be expected for liquid electrolytes.

Coulometry studies have been carried out on a conducting polymer that is available in both a soluble form and as an insoluble film on a metal substrate. Such materials could be laid down as thin films from solution either in the fully charged or discharged state. The soluble conducting polymer (soluble in both oxidized and reduced forms) shows a classic 60 mV/decade dependence on the concentration of injected anion. This is contrasted with the behavior of the same material when deposited as a film on a metal current collector. These studies complement the impedance work on conducting polymer electrode materials.

Cation intercalation studies have been carried out on single crystal V_6O_{13} to support the exploratory cells studies in Section 1, and to complement the impedance studies of insertion electrode materials. Coulometric titration studies on Li^+ insertion confirmed earlier work in the literature, and provided a baseline for studies with Na^+ and bivalent metal systems for the present program. Successful intercalation has been shown in preliminary studies with Zn^{+2} and Cu^{+2}, but not with Na^+, Mg^{+2}, and Ca^{+2}. If confirmed with more complete studies, the results would imply that V_6O_{13} could be used as the positive electrode material for Zn and Cu cells, but alternate materials (such as the conducting polymers) would have to be utilized for metals in the latter group.

Development of the foundation for transference number measurements in polymer electrolytes was completed. It was shown that measurement of the electrolyte thickness, initial concentration of the salt, initial conductivity, steady state current, and steady state voltage across the cell would allow the determination of the diffusion coefficients and transference numbers of both ions in a binary electrolyte.

2A. ELECTRICAL IMPEDANCE OF INSERTION ELECTRODES

- W.H. Smyrl, Mary Lien

INTRODUCTION

The impedance analysis proposed by Ho et al. (1) is applicable for thin-film electrodes of insertion compounds. In this report, some results using this technique on poly(vinyl ferrocene) (PVF) and V_6O_{13} are presented. The diffusion coefficient calculated by this analysis represents the diffusion of the counterion in the film in the case of a highly conductive film such as WO_3.

The process of electron conduction in PVF occurs by "electron hopping" between the redox centers of the film and may be facilitated by segmental motions of the polymer backbone bringing these centers into close proximity. As the electrode becomes more fully charged, the number of ferrocene (PVF reduced) sites decreases. For V_6O_{13}, the process of reduction converts V^{+5} to V^{+4} and finally to V^{+3} with the accompanying insertion of a metal ion. V_6O_{13} becomes less conductive in highly reduced states.

For redox polymer films, the diffusion coefficient is an effective diffusion coefficient for counter ion diffusion and electron diffusion. As the amount of "free volume" increases within the film, significant effects on the value of the effective diffusion coefficient result. For a liquid electrolyte which penetrates the film, counterion diffusion will be enhanced by increase in "free volume". The process of "electron hopping" may become rate-limiting as the density of PVF filaments decreases.

Subtle variations in polymer composition, structure, and means of casting can have profound effects on permeability. The most important parameter affecting this is the amount of "free volume" within the polymer. Electrochemical behavior of redox polymer films is a strong function of the density of packing of the polymer chains.

Solvents and even non-solvents penetrate glassy polymers and induce high-frequency, short-range segmental backbone motions. In the presence of any low molecular

weight liquid, the polymer is swollen, and the free volume fluctuaties. Ionized polymers are typically swollen to a much larger extent than neutral films.

Many films reveal gross changes in their morphology after electrochemical cycling. This effect is not always "reversible". A "break-in" process occurs during initial cycling of the polymer. During the oxidation sweep the entire unswollen film is characterized by small diffusion coefficients for solvent and electrolyte and only a small outer portion of the film is oxidized before sweep reversal. The rate-limiting process during oxidation is typically the transport of counterions through the polymer phase.

During reversal, much higher diffusion coefficients are observed as only the oxidized, swollen portion of the film is involved. If the oxidation sweep then begins before all of the solvent desorbs, the initial diffusion coefficients will be larger. This cycling process finally results in an activation of the entire film. Thus, the current passed during successive sweeps increases until the entire film is activated.

When polymers were "doped" with highly insoluble monomer units during the spin-casting process (2), these monomers leach out shortly after exposure to the electrolyte solution. This creates a larger "free volume" and has been shown to increase diffusion coefficients by a factor of 10^3, as long as the polymer was able to maintain this open structure. In some cases, the change in polymer density was significant enough to change the rate-limiting step to the ability of electrons to "hop" between active polymer sites.

From this, one might expect large variations in diffusion coefficients on films prepared by different methods. This effect is primarily due to changes in "free volume" of the polymer.

PREVIOUS STUDIES OF IMPEDANCE OF PVF (POLYVINYL FERROCENE) FILMS

Some prior work has been done by Tyler, et al. (3) on the redox reaction mechanisms of PVF in perchlorate solutions. The overall chemical reaction can be written:

$$[(PVF)^{n+} \cdot nClO_4^-] + ne^- \rightleftharpoons PVF + nClO_4^-$$

where n represents the number of electroactive polymer sites. The reduction of the oxidized polymer involves electron injection at the metal/PVF interface, concurrent with ClO_4^- transfer at the solution interface.

The charge transfer resistance, R_{CT}, for charge injection into the film, was determined from the diameter of the charge transfer semicircle at high frequencies. (See Figure 12.) The characteristic frequency at which $Z_{imaginary}$ is at a maximum on the semi-circle gives the double-layer capacitance at the electrolyte/electrode interface, C_{DL} from:

$$\omega = \frac{1}{R_{CT}C_{DL}} \tag{1}$$

In the diffusion controlled regime, the magnitude of the impedance is given by:

$$|Z| = \left(\frac{dE}{dQ}\right) \frac{L}{\sqrt{D_{CT}}\sqrt{\omega}} \tag{2}$$

where $\left(\frac{dE}{dQ}\right)^{-1}$ = low frequency redox capacitance, C_L

D_{CT} = diffusion coefficient for charge transport in the polymer film

L = polymer film thickness

Then $C_L^{-1} = \frac{d(-Z_i)}{d(\omega^{-1})}$

The low frequency polymer resistance, R_L, was obtained by extrapolating the low-frequency data to the x-axis (3). Then,

$$R_L = \frac{1}{C_L} \frac{L^2}{3 D_{CT}} \qquad (3)$$

The phase angle in the diffusion-controlled region was $\pi/2$, as expected and 3 regimes, kinetic control, diffusion control, and charge saturation were found for films ranging from 2500-7000 A. Diffusion coefficients, D_{CT}, for these films were of the order of 10^{-9} cm^2/sec, for the salt TBAP (tetrabutylammonium perchlorate) in acetonitrile.

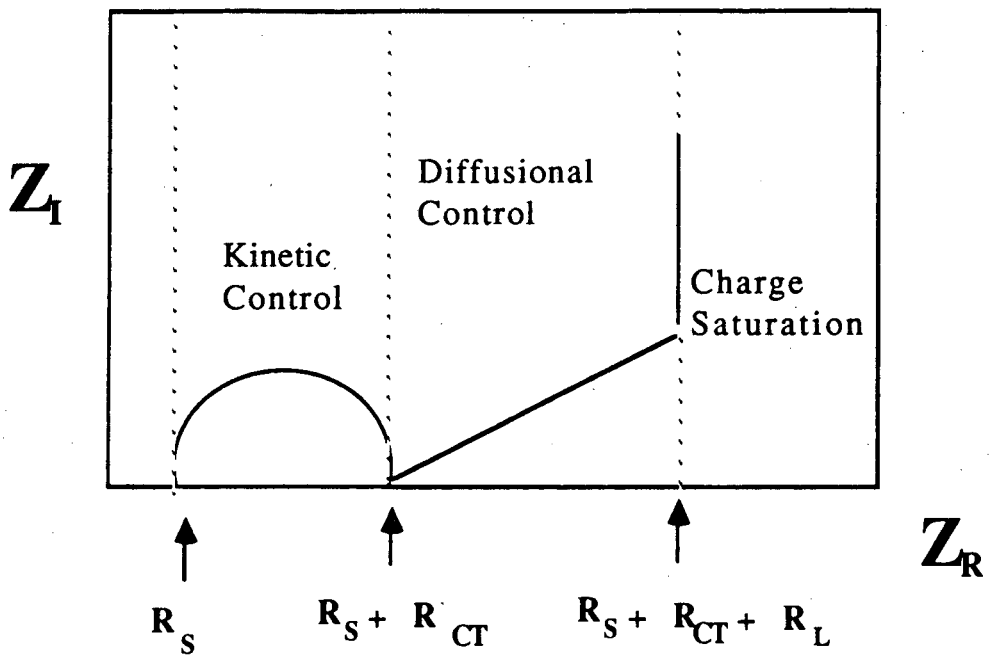

Figure 12. Simulated Impedance Display for PVF

PREVIOUS STUDIES OF IMPEDANCE ON V_6O_{13}

Impedance studies on lithium insertion in single crystal V_6O_{13} have been reported (4-6). The equivalent circuit was modeled similarly to the electroactive film circuit by Ho (1). The charge transfer resistance is in series with the Warburg impedance and these two components are in parallel with the double layer capacitance. The effective diffusion coefficient is given by:

$$D_{eff} = \left(\frac{dE}{dx}\right)^2 \left(\frac{1}{C_1 Z_W \sqrt{j\omega}}\right)^2 \qquad (4)$$

x = number of lithium ions inserted per V_6O_{13} ($Li_xV_6O_{13}$)

C_1 = volume concentration of lithium inserted for x=1

dE/dx is obtained either directly or from very slow scan cyclic voltammetry

Results for (010), (001) and (100) surfaces:

The (010) surface is perpendicular to the structural channels. When the oxide is grown as a single crystal, growth occurs along the monoclinic b axis (same direction as structural channels). Li^+ ion diffusion is one-dimensional and proceeds along these b-axis channels. Impedance at this surface should show the highest values for D_{eff}, as was found. The impedance plot (Z_R versus Z_I) showed a depressed semi-circle and a Warburg diffusion region at potentials above 2.5 V vs Li. The calculated diffusion coefficient for this surface was 6.0×10^{-8} to 4.0×10^{-9} cm/s^2 for Li^+.

For the (001) surface, parallel to the cavity channels , a diffusion coefficient of about 2 orders of magnitude lower than that for the (010) surface was obtained.

For the (100) surface, a high frequency semi-circle was obtained but the diffusion region was very small and the semi-circle was followed at lower frequencies by a capacitive region. Explanations are that any diffusion in (100) and (001) are due to kinks and defects which expose the transporting channels. Effective diffusion is in the b-direction only.

RESULTS AND DISCUSSION

PVF as a model system

The main focus of work to date has been to explore the impedance behavior of spin coated PVF as a model system for electroactive films to be investigated here. PVF is being used initially because it is possible to spin-coat thin, flat films for analysis. These films are electrochemically stable for long periods of time. Also, there is a large amount of data available in the literature on the electrochemical properties of PVF.

Electrode fabrication

Previous work (3) indicated some instability of films of PVF cast by solvent evaporation. The method of spin-coating results in a very stable film. In this process, a small amount of PVF, solubilized in methylene chloride, is spun onto a silica wafer coated with 500-1000 Å of gold.

Silica wafers are convenient to use as a substrate because they have a highly polished, uniformly flat surface and are available as circular wafers ideal for use with the 3" chuck used for the spin-coating apparatus. Gold was vapor deposited on the wafers to a total thickness of 1000 Å. Profilometry showed that the gold surface was very flat and of uniform thickness. Gold was chosen as a substrate because of its relatively inert nature. Any gold exposed through cracks or holes in the PVF film will not react chemically with the electrolyte solution at the voltages being applied. Several coatings of PVF were applied on top of the gold by spin-coating.

After polymer deposition, the wafers were baked at 90° C for about 5 minutes to remove residual solvent. The silica wafers were then cut with a diamond glass cutter into rectangular sections of about 1-2 cm^2 surface area and a wire lead was attached to one end using silver conductive epoxy. The edges of the silica and the wire lead were completely covered with an epoxy resin which is non-soluble in organic solvents. The edges had to be coated as the gold tended to delaminate from the silica when exposed to solvent, because

the solvent penetrated underneath the film. The electrical lead was covered so that the entire electrode could be immersed in electrolyte, with the only electroactive surface exposed being the PVF film. A schematic of the two methods of preparations of PVF electrodes is shown in Fig. 13.

Since the wire lead was attached to one edge of the gold film, rather than an entire circular current collector as used previously (3), the resistivity of the gold film may cause the current and potential distributions to be somewhat nonuniform at high currents. The first electrodes prepared were rather thin, about 500-700 Å. Increasing the concentration of the PVF solution (molecular weight 80,000 gm/mole) to about 3 grams/100 ml of methylene chloride has yielded films of 5000-8000 Å. (Higher PVF concentrations tend to form crystalline films during the spin-coating process.)

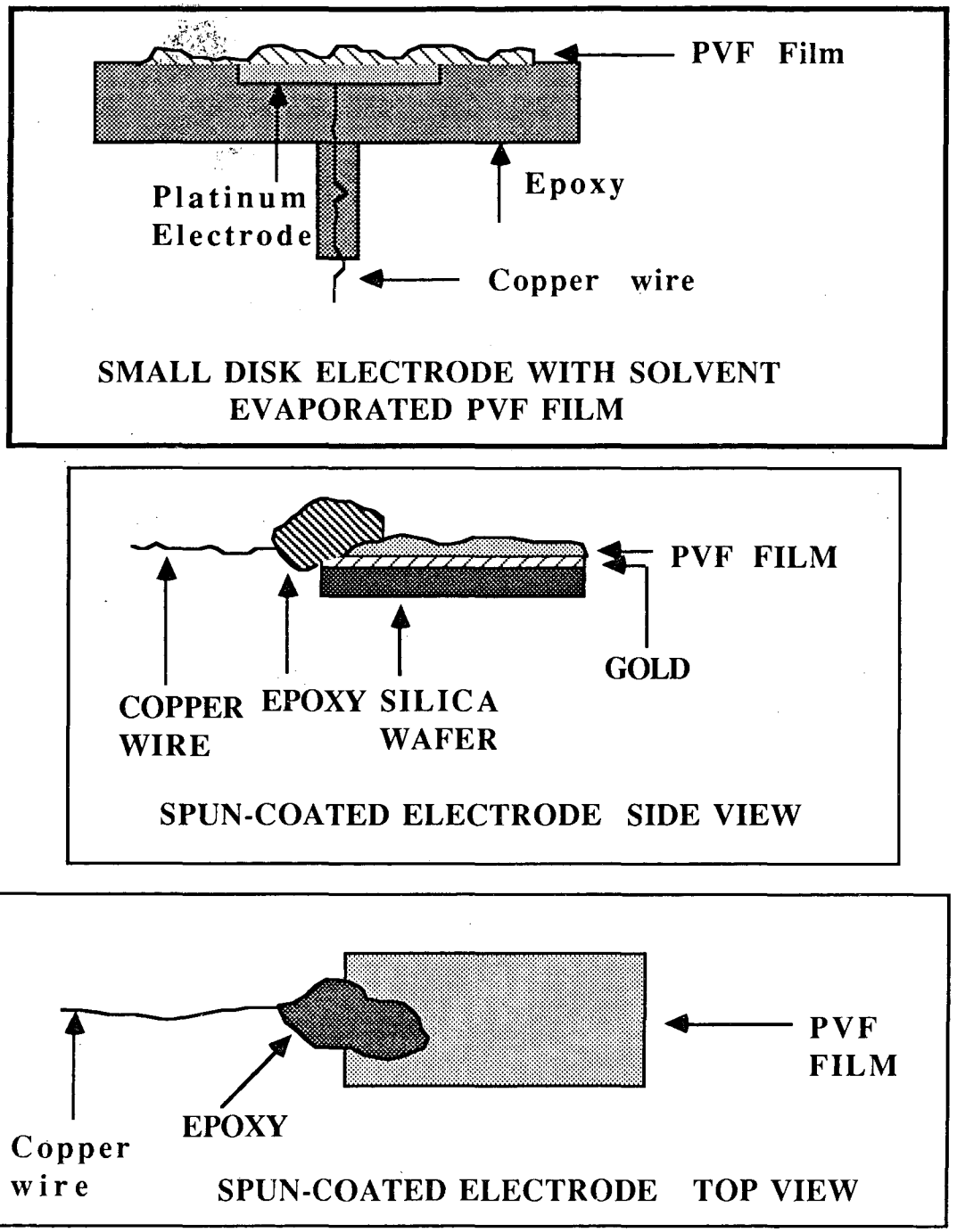

Figure 13. Schematic of small disk electrodes (solvent evaporation) versus spin coated silica wafer electrodes

Cyclic voltammetry of PVF films in liquid electrolytes

A typical cyclic voltammogram of a 500 Å PVF film in 0.1 M $LiClO_4$/acetonitrile is shown in figure 14. The figure shows that only about 9% deterioration in peak current occurred over 30 cycles. Films stored for several days after cycling have exhibited peak currents and characteristic wave shapes identical to the last previous cycle. This indicates that spin-coated PVF films are extremely stable, both chemically and electrochemically.

Figure 14 shows a peak separation of ΔE_{peak} = 65 mv. Other films have shown an increasing separation with scan rate. ΔE_{peak} values in excess of 60 mv are generally indicative of slow electron transfer between the electrode and the redox centers in the polymer, but can also be caused by film (or solution) resistance effects.

Integrating the area under the upper peak gives the total amount of anodic charge and conversely, the area of the lower peak gives the total cathodic charge. The ratio $\frac{\text{anodic charge}}{\text{cathodic charge}}$ gives a measure of reversibility and was equal to 1 for these films, indicating that the electrochemical process was reversible. The variation of peak current vs. sweep rate calculated for a typical 750 Å film is:

$\frac{\text{anodic peak current}}{\text{ma}}$	$\frac{\text{sweep rate}}{\text{mv/sec}}$	$\frac{\sqrt{\text{sweep rate}}}{(\text{mv/sec})^{.5}}$	$\frac{(\text{sweep rate})^{0.75}}{(\text{mv/sec})^{.75}}$
.5	10	3.16	5.62
.9	20	4.47	9.46
2.0	50	7.07	18.8
3.3	100	10.00	31.6

The peak current increased directly with sweep rate at the lower sweep rates (10, 20 mv/sec), and at the higher sweep rates varied as $\upsilon^{0.75}$ at 50 and 100 mv/sec. Thicker films

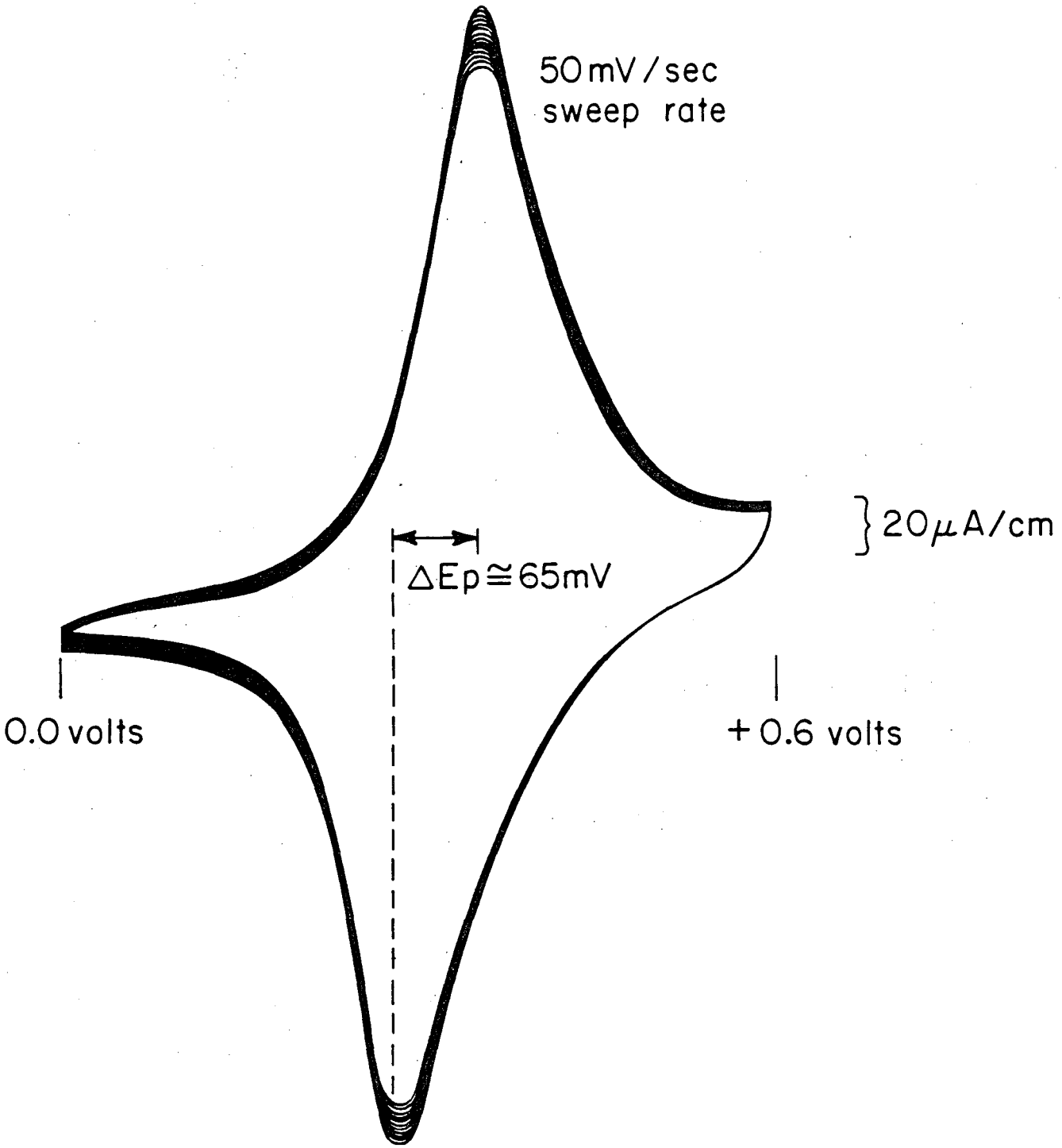

Fig. 14. Cyclic voltammetry of 500 Angstrom PVF film in 0.1 M $LiClO_4$/ acetonitrile

exhibited diffusion-controlled behavior; i_{peak} proportional to $\upsilon^{0.5}$ at low sweep rates (see figure 15).

The current increased with each successive cycle until a steady-state was reached, indicating an activation of the film by swelling (2). This was particularly noticeable with the thicker films (5000 Å).

Film thickness

The thicknesses of spun-coated PVF calculated by coulometry using a previously reported number of 2 x 10^{-3} mol/cm^3 for active polymer sites (3), have been compared with results obtained by profilometry and ellipsometry. Results on two films are as follows:

Coulometry	Profilometry	Ellipsometry
532 Å	300 Å	325 Å
4900	4500	

Profilometry values may be low because the mechanical stylus penetrated the surface layer and gave low readings. Ellipsometry values are based on measurement of the degree of refraction and should be very accurate. Very thin films were more difficult to measure accurately, due to the increased sensitivity of the profilometer to vibration and other noise at very low measurement levels.

If ellipsometry is chosen as a standard, with profilometry values in reasonable agreement, the coulometry values appear to be too high. If spin-coating results in a more porous structure, as indicated by impedance results to be discussed later, the value of 2 x 10^{-3} active sites/cm^3 used in coulometric calculation should be too high. An even higher value is needed to give results similar to ellipsometric measurements, however. Therefore, this limited data does not support the theory that spin-coating results in more porous films.

Other values for plasma-polymerized films have been reported. A value of 2.4 x 10^{-3} sites/cm^3 was obtained by assuming a ferrocene density of 0.5 gm/cm^3. Other

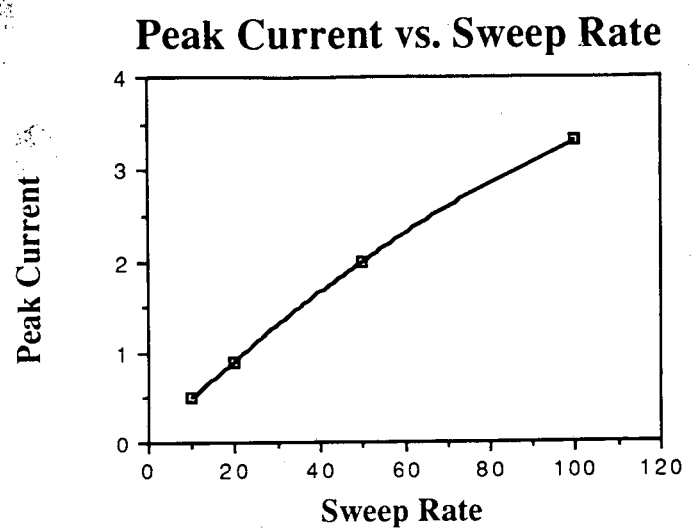

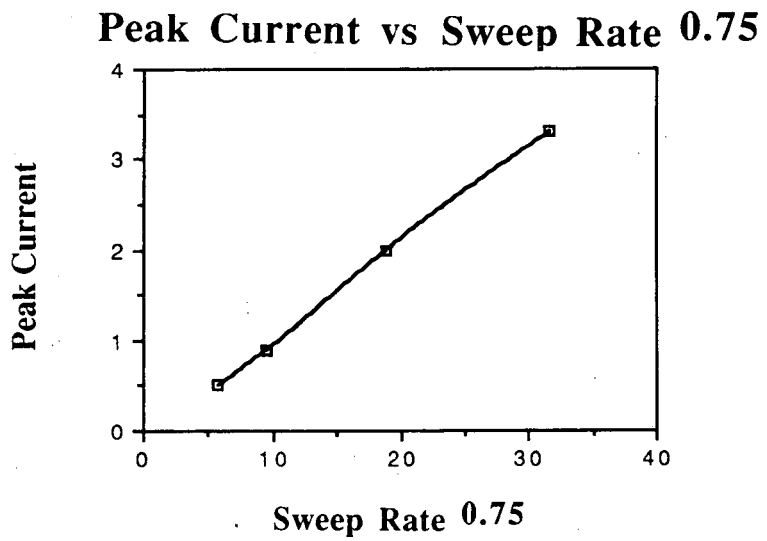

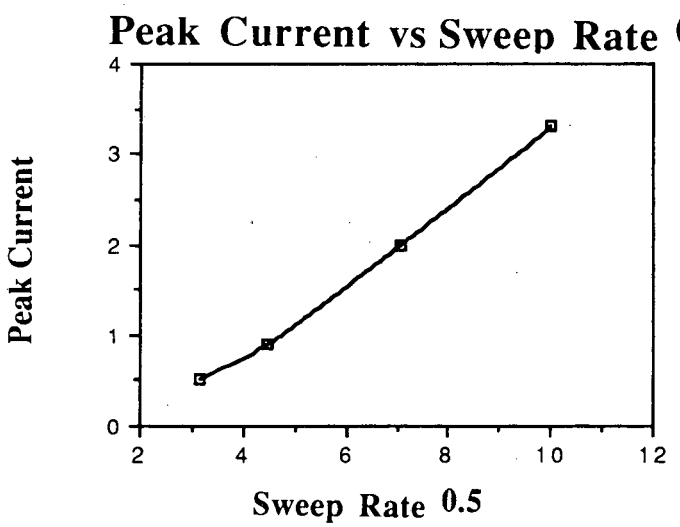

Figure 15. Peak current versus sweep rate

workers have assumed that PVF has a density similar to polystyrene (7,8). Further work must be done to obtain true values for the number of active sites/cm^3 for spin-coated PVF films. Films must be prepared over a wide range of thicknesses, which will be measured in the dry state immediately after spin-coating by profilometry and ellipsometry. Electrodes will then be prepared and the value of active sites/cm^3 will be calculated by coulometry, assuming that the ellipsometric thickness measurements are correct.

Impedance experiments

The strategy was to begin with simple systems which have been studied previously and proceed to more complex systems. Comparison of the effects of the different types of electrolyte will be made.

1) Liquid Electrolyte System (0.1 M $LiClO_4$ in acetonitrile)

   Impedance analysis similar to previous experiments by Tyler et al. (3) were run on spun-coated PVF. The spun-coated cells were much larger in the present study (about 1 cm^2) as compared to 0.1 cm^2 in the study by Tyler, et. al., and the resistivity of the gold film may cause nonuniform current and potential distribution at high currents.

2) Low Molecular Weight PEO System

   Using 1000 MW PEO (with $LiClO_4$) at 100 °C (a viscous liquid) - a small PVF electrode will be dipped into the bulk solution, along with a reference electrode and a Pt counter electrode. This system represents a transition between bulk liquid methods and the thin film cells which are sometimes mechanically difficult to construct.

3) Thin Film System

Previous work by Tyler et al. (3) indicated that films in the range 2500-7000 Å showed all 3 regions of behavior (charge-transfer, diffusion, and charge saturation control) in impedance analysis. We have generally been unable to get a spin-coated film thick enough to obtain a diffusion-controlled region of slope = 1 on Z_{REAL} versus $Z_{IMAGINARY}$ plots. It was shown by Tyler et al. (3) that in the diffusion controlled region, both the real and imaginary parts of the impedance are proportional to $\frac{1}{\sqrt{\text{frequency}}}$, and thus are proportional to one another. This is consistent with diffusion into a semi-infinite medium from a flat interface. Two films of thicknesses 4400 and 4900 Å did show a definite diffusion region at voltages corresponding to highly reduced and highly oxidized states. However, the slope (Z_{REAL} vs. $Z_{IMAGINARY}$) was about $\pi/4$, indicating a porous or rough structure of the electrode. Diffusion in porous electrode structures have been shown to demonstrate a characteristic slope of 0.41 (Z_{REAL} vs. $Z_{IMAGINARY}$). In addition, from our plots of Z_i versus ω, diffusion coefficients of about 10^{-7} cm^2/sec were calculated, which are about 100 times larger than previously observed for solvent-cast films (3). Both TBAP (tetrabutylammonium perchlorate) and $LiClO_4$ showed the same results.

Possible explanations for the large values of D_{CT} in the spin-coated films are:

1) Films prepared in this manner are more porous which enhances electrolyte incorporation into the film and aids in counterion transport. This explanation is supported by impedance results which indicate a porous or rough electrode. The preliminary coulometry results of film thickness appear to be in disagreement with this conclusion.
2) Films are amorphous rather than crystalline due to rapid solvent evaporation by this method.

Film porosity causing large values of D_{CT} is the more likely explanation. Impedance data indicates the presence of a porous electrode and the large diffusion coefficient observed would be expected in a highly porous electrode.

Cyclic voltammetry in low molecular weight PEO was attempted. It was not successful because the silver wire used as a reference electrode did not give a stable potential. Shifts in the peak voltage for the oxidation and reduction waves varied by as much as 1 volt over a 4-hour period. Before impedance analysis can be performed, a stable reference must be found.

CONCLUSION

Spin-coating has resulted in extremely stable, relatively porous and uniformly flat films. Diffusion coefficients for counterion transport in liquid electrolytes are much larger than previously observed (3). Impedance plots of Z_{REAL} versus $Z_{IMAGINARY}$ have been obtained exhibiting 3 regions of behavior (charge-transfer, diffusion, and charge saturation).

Profilometry and ellipsometry measurements of film thicknesses have been made and are in close agreement with each other and rough agreement with coulometric measurements. Profilometry of the films indicate a uniform, flat surface.

The use of PVF as a starting point for developing techniques and methodology has proved useful. Comparison of results with those of previous workers has revealed significant differences in structure of spin-coated films. Comparison of thickness measurements by 3 different methods has indicated a need to determine new values for the number of active sites/cm^3 in spin-coated PVF. The techniques developed during this investigation will be extended to other thin-film materials.

References

1. C. Ho,I.D. Raistrick, R.A. Huggins, J. Electrochem. Soc., Feb 1980, vol. 127 (2), p. 343-350.
2. A.H. Schroeder and F.B. Kaufman, J. Electroanal. Chem., 113, (1980) p. 209-224.

3. P.S. Tyler, T.B. Hunter, W.H. Smyrl, and H.S. White, J. Electrochem. Soc., 134, p. 2198-2204. (September 1987) 9, (1985) p. 1205-1208.

4. T.Jacobsen, K. West, B. Zachau-Christiansen, S. Atlung, Electrochimica Acta, 30, 9, (1985) p. 1205-1208, J. Power Sources, 14, (1985) p. 235-245.

5. T.Jacobsen, K. West, B. Zachau-Christiansen, S. Atlung, State Ionics, 5, (1981) p. 335-338.

6. P.C. Spurdens, J. Drennan, J.R. Owen, B.C.H. Steele, Solid

7. P.J. Peerce and A.J. Bard, J. Electroanal. Chem., 112 (1980) p. 97-115.

8. P.J. Peerce and A.J. Bard, J. Electroanal. Chem., 114 (1980) p. 89-115.

2B. IMPEDANCE CHARACTERIZATION OF ELECTRONICALLY CONDUCTING POLYMERS

-W.H. Smyrl, Chi-Hum Paik

INTRODUCTION

Recent interest in poly(acetylene) and other conducting polymers such as poly(thiophene), and poly(pyrrole) have stimulated a number of studies of their properties, including their electrochemistry. The latter properties suggest several applications in light-weight batteries, corrosion protection, sensors, and microelectronic and photovoltaic devices. Conducting polymers have a large range of conductivity and redox characteristics, and the redox characteristics are of interest in this investigation. The electronically conductive polymers listed above may be oxidized by simultaneously injecting a hole and an anion into the polymer. The positively charged hole becomes delocalized on the polymer backbone, and the anion is injected to maintain charge neutrality. The charging and discharging may be accomplished either by chemical or electrochemical means. The electrochemical charging and discharging of conducting polymers is of interest in batteries, and is the subject of this report.

The technique of Digital Impedance for Faradaic Analysis (DIFA) was used in the present study, specifically that developed in our laboratory. In a DIFA experiment, the polymer is charged to a specific state and maintained in equilibrium. A modulating input voltage perturbation is applied at multiple frequencies to observe the response of the polymer, and to characterize the relaxation processes as a function of frequency. In this study, the rate of charge injection, the diffusion in the polymer, and the redox capacity were measured as a function of applied voltage, anion injected, and electrolyte resistivity. If the polymer is porous and the electrolyte penetrates the polymer film on the substrate metal, charging and discharging would be distributed into the interior of the porous structure of the polymer. The details of the distribution of the charging reaction will depend on the relative resistivities of the electrolyte, polymer fibers, and the interfacial

resistance to charge transfer from the solution to the polymer. There are several similarities of the charge-discharge process to classical porous electrode behavior, and this study is intended to elucidate such similarities.

Comparison to earlier work (2) on the redox polymer poly(vinylferrocene) showed similarities, and as will be shown below, there were 3 fundamental relaxation processes. At high frequencies, the relaxation process was charge injection into the polymer film. The heterogeneous rate constant of the charge-injection process is reported as a function of the concentration of charge in the polymer, the latter being a function of the equilibrium voltage. In addition, the diffusion coefficient was a function of charge, and was found to be a stronger function of concentration than in the earlier study (2) of poly(vinylferrocene).

Results are reported on three polymers, poly(thiophene), poly(3-methylthiophene), and poly(pyrrole), prepared from monomers of heterocyclic aromatic compounds. The electropolymerized materials have been used for sensors (3), for microelectronic applications, including devices (4,5), and as electrodes in batteries and fuel cells (5). The materials exhibit a non-Nernstian relationship between charge concentration and electrochemical potential, and in that regard, they are similar to intercalation materials such as TiS_2, V_6O_{13}, WO_3, and graphite.

Impedance Theory Applied to Electronically Conductive Polymer Films

We propose that for an electroactive polymer phase, the rate of charge injection (charge transfer) reflects interfacial properties and is combined with the interfacial (double layer) capacitance to produce an RC relaxation process similar to intercalation at a V_6O_{13}/electrolyte interface, for example. The rate of the charge transfer process can be characterized by a heterogeneous rate constant, K_s, or equivalently by an exchange current density, i_o, and the two are related by

$$i_o = nFK_sAC_o^{(1-\alpha)}C_R^{\alpha} \qquad [1]$$

Here, α is the transfer coefficient, A is the electrode area, F is the Faraday constant, n is the number of equivalents/mole reacted, and C_O and C_R are the concentrations (mol/cm^3) of the oxidized and reduced species, respectively. The charge transfer resistance of the faradaic process, R_f, is defined by

$$R_f = RT/ni_oF \qquad [2]$$

The characteristic time constant for the charge-transfer process is related to the product of R_f and the double layer capacitance of the oxide/electrolyte interface, C_{dl}. The inverse of this quantity is defined as the characteristic relaxation frequency for the process, i.e.,

$$\omega_c = 1/(R_fC_{dl}) \qquad [3]$$

Following our work on poly(vinylferrocene), it is expected that the impedance of the electroactive polymer films will follow the general behavior shown in Fig. 12. At high frequency, one observes a charge-transfer-dominated regime, and the characteristic parameters which define the behavior are obtained from the above analysis. At lower frequencies, diffusion of charge in the polymer film dominates the impedance results. The frequency range of the diffusion behavior is controlled by the diffusion coefficient and film thickness (see below). Finally, the finite thickness of the polymer film will limit the extent of the diffusion behavior at low frequencies, and a "redox capacitance" is observed. From the several regions of impedance behavior, one may determine the kinetic and mass transfer parameters of the polymer film. In addition, it is possible to characterize how the parameters depend on the voltage and oxidation state for a particular system.

Properties such as the conductivity of the phase, be it polymer or oxide, are also important and in this case, ohmic drop across the film is expected to control the extent and distribution of charge transfer in films of low conductivity. The resistance of the film would be expected to be in series with the charge transfer process. If so, it would be

observed as part of the high frequency intercept, R_s, along the real axis. Changes in the film resistance would displace the intercept along the real axis. These effects were not seen in the present investigation so we assume they were negligible. A different resistance effect could come from transient changes in the composition of the solution phase that swells the films as the film is oxidized or reduced. Since the film to was at equilibrium at each electrode potential, and was perturbed only slightly with the impedance excitation, no resistance effects of this type should be expected and none were observed.

Determination of charge-transfer kinetic parameters. - Rf was determined from the diameter of the charge-transfer semicircle at high frequencies. The characteristic frequency at which the imaginary component of the impedance, Z_i, is at a maximum on the semi-circle defines the product R_f and R_{dl} from Eq. [4]. Therefore C_{dl} may be calculated for the polymer/electrolyte interface.

Determination of the diffusion coefficient and redox capacitance of thin films (7). In the diffusion controlled regime, the magnitude of the impedance is given by Eq. [5]

$$|Z| = (dE/dQ)*L/(D_{CT}^{1/2}\omega^{1/2}) \qquad [5]$$

where $(dE/dQ)^{-1}$ is the low frequency redox capacitance, C_l (farads, F). D_{CT} is the diffusion coefficient for charge transport in the polymer film, and L is the polymer film thickness. The impedance phase angle in the diffusion regime is $\pi/4$ and independent of frequency.

Values of C_L were obtained from the low-frequency impedance data. In this frequency range, $\omega << L^2/D_{CT}$, the phase angle approaches $\pi/2$ and C_L is given by

$$C_L^{-1} = d(-Z_i)(d\omega^{-1}) \qquad [6]$$

The low-frequency polymer resistance, R_L, was obtained by extrapolating the low frequency data to the x-axis (Fig. 1). R_L is related to the redox capacitance and diffusional relaxation time, L^2/D_{CT}, by Eq. [7]

$$R_L = (1/C_L)*L^2/3D_{CT} \quad [7]$$

Impedance of Porous Electroactive Polymers

Porous electrodes will have impedance behavior with an equivalent circuit described in general by the transmission line model shown in Figure 16. The current to a porous electrode with such an equivalent circuit has been shown (8) to be nonuniformly distributed in general. Simple arguments, in part following Armstrong et al. (9), will help to introduce the ideas. For a porous, metallic electrode with uniform, cylindrical pores, the resistance of an electrolyte filled pore is

$$R_{PORE} = l\rho/\pi r^2 \quad [8]$$

where l is the length of the pore, r is the radius, and ρ is the resistivity of the electrolyte. The impedance of the pore interface is

$$Z/2\pi rl \quad [9]$$

For

$$R_{PORE} << Z/2\pi rl \quad [10]$$

the current distribution is uniform (planar electrode, kinetic control), but for the reverse, i.e.,

$$R_{PORE} > Z/2\pi rl \quad [11]$$

the current distribution is nonuniform (porous behavior, ohmic control) and current flows preferentially to the outer part of the pore. If the resistivity of the electrode material is large, the impedance of the conductor plus its interface is approximately

$$R_c + Z/2\pi rl \quad [12]$$

instead of [9]. If the resistivity of the pore is much larger than [12], the current distribution is nonuniform (porous behavior), and more current would flow to the outer pore walls. For

$$R_c + Z/2\pi rl > R_{PORE} \quad [13]$$

and the current distribution will be uniform only for the special case

$$Z/2\pi rl >> R_c > R_{PORE} \quad [14]$$

If condition [13] is obeyed, but not [14], the position of the current collector becomes important and its location at the bottom of the pore will, in general, cause the current flow to the electrode to be higher at the bottom of the pore (no direct current passes from the solution to the current collector, however). Thus, for a material like poly(3-methylthiophene) whose resistivity changes as the charging/discharging reaction proceeds, the current distribution would change as well. Porous electrode behavior would be expected in general, but the competing influences would cause a range of current and potential distribution determined by particular conditions.

Poly(3-methylthiophene) electrodes, being both resistive and porous in the lightly doped or undoped state, would be expected to behave as in the latter case above. The electrochemical charging reaction would be nonuniform in the early stages, and spread through the polymer matrix as the reaction continued. This macroscopic nonuniformity of current would create gradients of dopant concentration. Relaxation of the gradients upon interruption of the current may occur by diffusion within the polymer, or by bipolar redistribution through the electrolyte phase driven by the voltage difference between lightly doped and heavily doped regions. Discharge of the relaxed, uniformly doped polymer would be expected to be nonuniform as well. Unless the polymer had a resistivity much lower than the electrolyte, the current would be higher at points closest to the current collector. The net effect would be to undope the high current areas first and to increase the resistivity there. A resistive layer in the polymer adjacent to the current collector would be

built up and would dominate the discharge behavior. Any discharge current to more highly doped regions would have to flow through the polymer resistive layer to the current collector. The discharge of the doped polymer would be difficult. Incomplete discharge would cause low coulombic efficiency on cycling. The efficiency could be improved by special cycling techniques, such as that of Kaneto et al. [10]. There, 50% of the charge was recovered at constant current and the remainder at constant voltage.

In addition to interest in the charge-discharge behavior of conducting polymer films, the impedance behavior of uniformly doped material in electrolytes is of interest as well. As the frequency is changed for porous electrodes, the current distribution will change according to the transmission line model (Figure 16). This arises because the predominance of the resistivity of either the pores or the interface (or interface + electrode resistivity) will depend on the frequency of the applied signal. At low frequencies where for example

$$Z/2\pi rl > R_{PORE}$$

the pore is uniformly accessible. But at higher frequencies where the interfacial impedance decreases, the current distribution will become nonuniform and the signal will only penetrate the outer portion of the pore. A more detailed analysis by de Levie (8), has found that for several simple limiting cases, the impedance of a porous electrode will have a "squared" relationship to the equivalent planar electrode. That is, the phase angle of the impedance of a porous electrode is half that of a planar electrode with the same process, and the magnitude of the impedance is proportional to the square root of the impedance of the equivalent planar electrode. Further, simple charge-transfer processes are found to be characterized in the following way on porous electrode:

(1) The imaginary part of the measured impedance depends on frequency as $\omega^{+1/2}$ and $\omega^{-1/2}$ respectively at frequencies less than or greater than the characteristic

frequency of the process. This is to be compared to ω^{+1} and ω^{-1} dependences for the equivalent process on a planar electrode.

(2) A 45° high frequency phase angle. This is 90° on a planar electrode.

(3) A general lemniscate shape for Z(IMAG) vs Z(REAL). The curve is a semicircle on a planar electrode.

These characteristics, especially (1), will be used below to identify porous electrode behavior.

EXPERIMENTAL

Materials - The electronically conducting polymers investigated were poly(thiophene), poly(3-methylthiophene), and poly(pyrrole). The polymers were prepared electrochemically by oxidation of the appropriate monomers. The monomers, thiophene, 3-methylthiophene, and pyrrole (Alfa Products) were distilled at atmospheric pressure and kept under refrigeration. The electrolyte used for all the experiments was tetraethylammonium tetrafluoroborate (TEAFB) (Southwestern Analytical Chemicals), and was recrystallized twice with methanol/ether and stored in a drying oven. The solvent, acetonitrile (Aldrich, HPLC grade) was dried over molecular sieves until use. The electrode on which the polymer was deposited was a platinum wire whose cross-sectional area (0.78×10^{-2} cm^2) was exposed to the solution and the remainder sealed in epoxy. The exposed Pt disk surface was polished before use on a metallography wheel successively down to 0.05 micron alumina suspended in water. The reference electrode was sodium chloride saturated calomel electrode (SSCE), and the auxiliary electrode was another Pt wire.

Preparation - The monomer solution of 0.2 M TEAFB and 0.05M thiophene (or other monomers) dissolved in acetonitrile was deaerated with nitrogen for about 15 minutes. The Pt electrode was immersed into the solution, and the potential was increased to about +2.0V (vs SSCE) for electropolymerization (4). A red-colored film appeared on the Pt indicating polymer deposition, but at high film thicknesses the film became black.

Film thicknesses between 0.6 and 2 microns were used in the studies. The film was rinsed with acetonitrile to remove excess monomer, and the electrode was immersed into the solution of deaerated 0.1M TEAFB in acetonitrile.

Electrochemical procedure and apparatus - Cyclic voltammograms were run with a potentiostat (Pine RDE4) and X-Y recorder (Hewlett-Packard 7044B). Impedance measurements were made using the system previously described (1). A voltage signal of 51 superposed sinusoids (Maximum amplitude = 5 mV peak-to-peak) was applied to the cell as a perturbation to the constant voltage, and the response was filtered and digitized along with the voltage input. The complex impedance of the system was calculated as a function of frequency using a Fast Fourier Transform (FFT) at all 51 frequencies simultaneously. The range of frequencies applied was 0.01 to 50,000 Hz. The computer-controller was PDP 11/44, enhanced with an Analogic array processor for FFT calculations. The digitizer was a Biomation Model 1015 transient recorder. The signal generator gave a signal of known frequency content (Hewlett-Packard 3722A). Krohn-Hite low pass filters were used to prevent "aliasing". Preston differential amplifiers were used to adjust signal gain to the digitizer. The 51 frequencies covered a frequency range of 1 1/2 orders of magnitude. The range from 0.01 Hz to 50 kHz was covered by 6 frequency settings. Multiple runs were made at each setting to reduce stray noise effects.

All electrochemical experiments were run in acetonitrile with 0.1 M TEAFB as the electrolyte. Solutions were thoroughly purged with nitrogen before each run, and nitrogen was blown over the solution during all experiments to minimize oxygen contamination.

ELECTROCHEMICAL RESULTS AND DISCUSSION

In the results to be described below, each polymer will be discussed separately. In each case, cyclic voltammetry will be presented first, followed by charge vs voltage data, and finally the impedance data. For the latter, the charge transfer rate and double layer capacitance were calculated from the data, along with the diffusion coefficient for transport

of the charged species in the polymer phase. The results are more complete for poly(3-methlylthiophene), but the other polymer films behaved in a similar way. Qualitatively, the behavior agrees with the general description given above for PVF films.

I. Poly(3-methylthiophene) (P3MT). The cyclic voltammetry of a PMT film is shown in Fig 17. The behavior is similar to that reported in the literature for other electrolytes. The anodic peak occurs at approximately 0.6V (vs SSCE) and the cathodic peak is almost at the same voltage. Furthermore, both the anodic and cathodic peaks are linear functions of sweep rate, as expected for reversible polymer films. The second cathodic peak at about +0.3V is characteristic of P3MT films reported in the literature (4).

Charge concentration in the film (expressed as coulombs/cm^2) increased with voltage as shown in Fig. 18. Both the magnitude and slope of the curves agree with literature data (4), and other work in our laboratory (11) for films on Pt and glassy carbon substrates in other solvents. The non-Nernstian behavior is characteristic of many electroactive polymers, and has some similarities to intercalation in oxides.

Impedance data were taken at several different voltages. The films were allowed to equilibrate at the control voltage, as evidenced by the drop of the charging current to zero. The voltage was perturbed about the control voltage and the current response was measured from 0.01 to 50 kHz at each control voltage. The impedance at three different voltages is shown in Fig. 19 for P3MT. At each voltage, three relaxation regions are evident. At low charge concentrations (V in Fig. 19), the rate of charge injection is slow and this leads to a large value of R_{ct} and a large semicircle at high frequencies. At intermediate frequencies the impedance was controlled by diffusional transport in the polymer. At the lowest frequencies, diffusion was fast enough in the finite thickness of the polymer to maintain uniform concentration throughout the voltage cycle, and the film behaved as a "redox capacitor". Overlap of the controlling processes is evident at certain film thicknesses and charge concentrations. In the diffusional transport region, the slope of Z(real) vs Z(imag)

was approximately $(\pi)/8$, characteristic of porous electrode behavior. Porous electrode behavior is also evident at lower frequencies where the slope is finite (porous electrode) rather than infinite (planar electrode).

Analysis of the impedance gave the results summarized in Table 3. The double layer capacitance is characteristic of other electrochemical charge-transfer interfaces. The most interesting results are the diffusion coefficients, D_{CT}, which show a large increase with increased charge concentration. The earlier results on PVF (2), by contrast, revealed that the diffusion coefficient only changed by a factor of two. In the PVF system, the maximum of D_{CT} occurred at the reversible potential of the redox polymer where the concentrations of oxidized and reduced sites were equal. The large increase in D_{CT} occurred at the reversible potential of the redox polymer where the concentrations of oxidized and reduced sites were equal. The large increase in D_{CT} for P3MT films occurred between 0.45 and 0.5V, where the charge concentration began to increase in the polymer. The electronic conductivity of the polymer increased in this region as well (but we did not measure it). The magnitude of the diffusion coefficient, i.e., 10^{-7} cm^2/sec, is large, but of the same order as that found recently for spin-coated PVF films (12). The spin-coated PVF films also behaved as "porous electrodes."

The impedance behavior of P3MT is compared at several different voltages in Fig. 20, all for the same film of thickness (1.84 μm). The impedance overlapped in the diffusion-control region, but the transition to the redox capacitance region occurred at different frequencies as the voltage changed. The transition to redox capacitance occurs at a frequency which is controlled by the film thickness and D_{CT}. For the films in Fig. 20, the film thickness was constant and the change of R_L was due to the change of D_{CT} in the films. The redox capacitance also increased with voltage, as shown in Table 1. C_L was calculated from impedance data according to [6], and is consistant with results for similar systems. Only estimates of the double layer capacitance, C_{de}, could be obtained for this

system, but the values appear to be reasonable. (Note that the values of C_{de} reported in Table 4 must be divided by area to obtain the double layer capacitance.)

II. Polythiophene (PT). Cyclic voltammograms for PT are shown in Fig. 21 at several different sweep rates. The anodic peaks occurred at approximately 0.95V and the peak currents were a linear function of sweep rate. The cathodic peaks were also a linear function of sweep rate. The small peak separation between anodic and cathodic processes indicated a high degree of reversibility at these sweep rates. The total charge for the anodic charging reaction was dependent on the sweep rates. At high sweep rates the film were not operating in the redox capacitance region for voltages larger than about 0.65V, so that the data in Fig. 22 may not be used to calculate C_L for the films. Values of C_L from impedance data are reported below.

Impedance behavior as a function of voltage for PT films are given in Fig. 23. The three regions of behavior are not resolved as well as for the P3MT films, but all three relaxation processes are apparent. Values of the characteristic parameters are given in Table 4. It should be noted that the charge transfer resistance R_{CT} for the PT films goes through the minimum at approximately 1V. This striking result is not the result of film degradation, although films may be degraded by cycling to larger voltages, i.e., larger than 1.2V. It is possible that a change in the charge-injection mechanism may be indicated by this result, but we were unable to verify that such a change occurs. The values of D_{CT} and C_L for PT films are smaller than for the P3MT films described above.

III. Polypyrrole (PPY). Cyclic voltammograms of PPY films are shown in Fig. 24 at several different sweep rates. The anodic and cathodic peaks are linear functions of sweep rate. The charge concentration in the films was measured as a function of voltage and is shown in Fig. 25. Impedance results for PPY films were similar to that reported above for P3MT and PT films, but were less extensive. Three relaxation processes were apparent,

but not enough data were obtained to report the characteristic parameters due to degradation of the electrodeposited films.

REFERENCES

1. Smyrl, W.H. (a) J. Electrochem. Soc. 132, 1552 (1985).
   (b) ibid, 1555 (1985).
   (c) ibid, 1559 (1985).

2. Hunter, T.B., Tyler, P.S., Smyrl, W.H., and White, H.S., ibid, 2198 (1987).

3. Hanawa, T., Kuwabata, S., and Yoneyama, H., J. Chem. Soc. Faraday Trans. 84, 1587 (1988).

4. Thackeray, J.W., White, H.S., and Wrighton, M.S., J. Phys. Chem. 89, 5133 (1985).

5. Chao, S., Wrighton, M.S., J. Am. Chem. Soc. 109, 2197 (1987).

6. (a) Nigrey, P.J., McInnes, D., Nairns, D.P., MacDiarmid, A.G., and Heeger, A.J., J. Electrochem. Soc. 128, 1651 (1981).

7. Ho, C., Raistrick, I.D., and Huggins, R.A., J. Electrochem Soc. 127, 343 (1980).

8. deLevie, R., in Advances in Electrochemistry and Electrochemical Engineering, eds. P. Delahay and C.W. Tobias, Interscience, New York, 1967.

9. Armstrong, R.D., Edmondson, K., and Lee, J.A., J. Electroanal. Chem. 63, 287 (1975).

10. Kaneto, K., Maxfield, M., Niarns, D.P., and MacDiarmid, A.G., J. Chem. Soc. Faraday Trans. 78, 3417 (1982).

11. Deng, Z., Smyrl, W.H., and White, H.S. (submitted to J. Electrochem. Soc.).

12. Lien, M., unpublished data.

Fig. 16. **EQUIVALENT CIRCUIT OF A POROUS ELECTRODE**

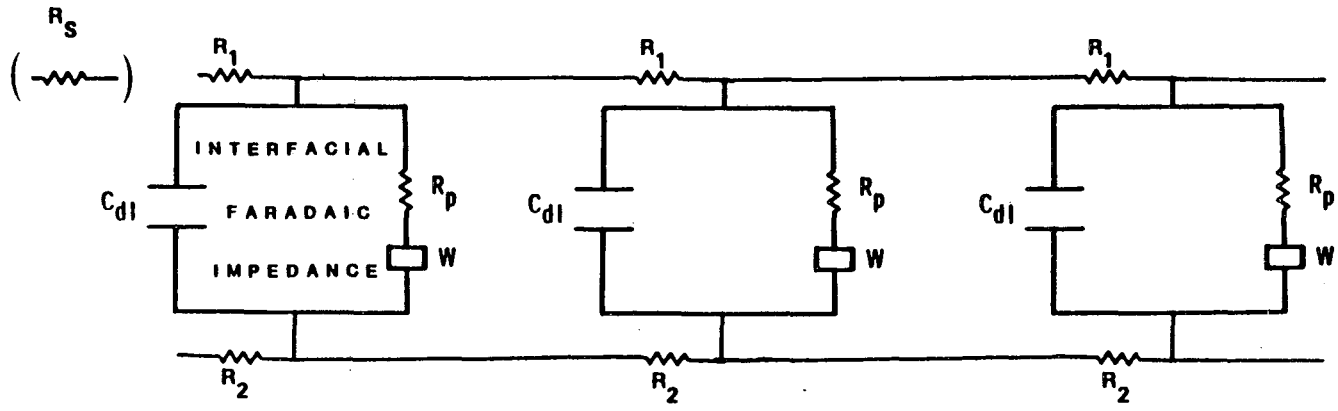

Fig. 17. Cyclic Voltammogram of Pt/Poly(3-methylthiophene) in MeCN Containing 0.1M TBAFB.

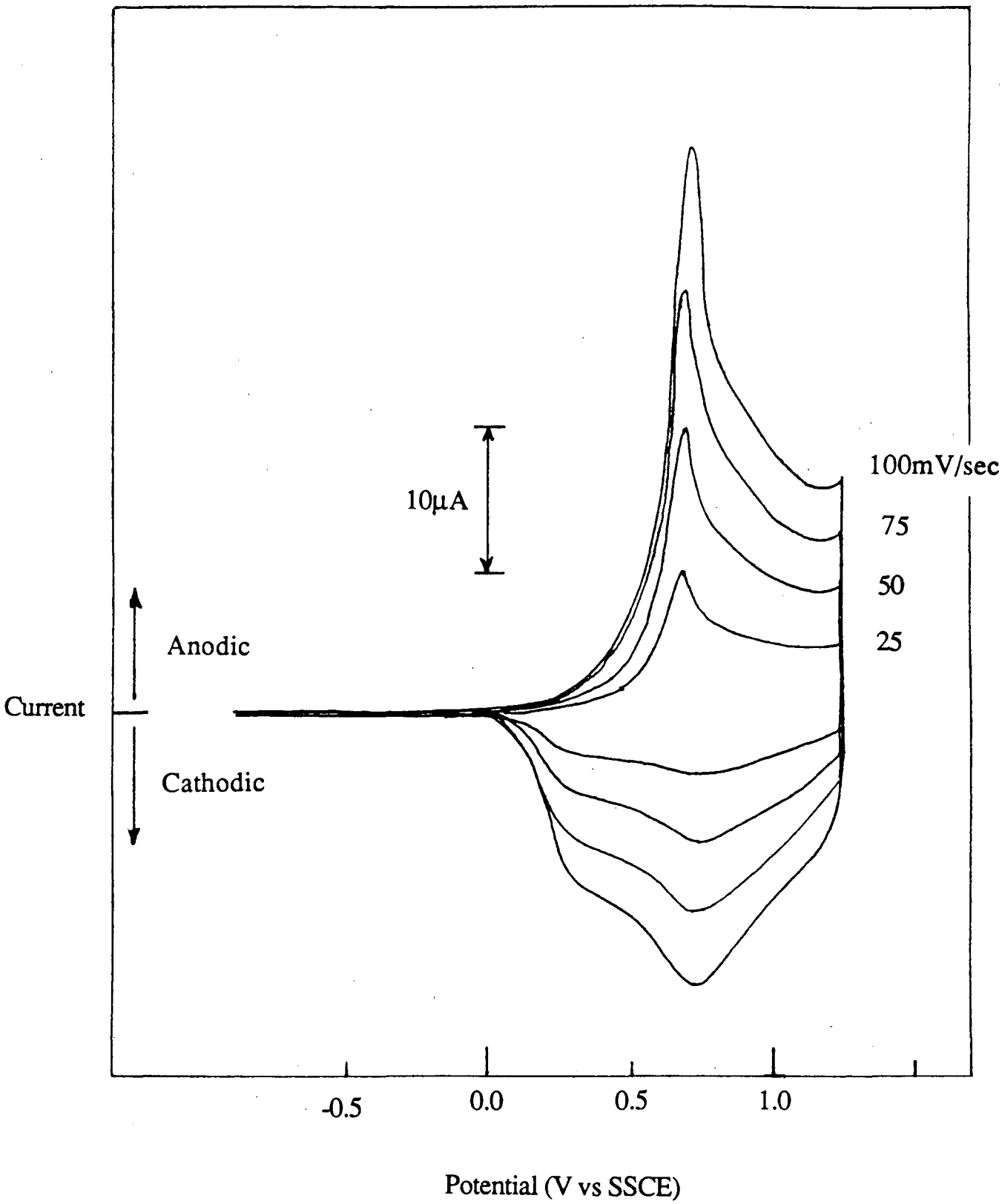

Fig. 18. Charge vs Potential for Pt/Poly(3-methylthiophene)

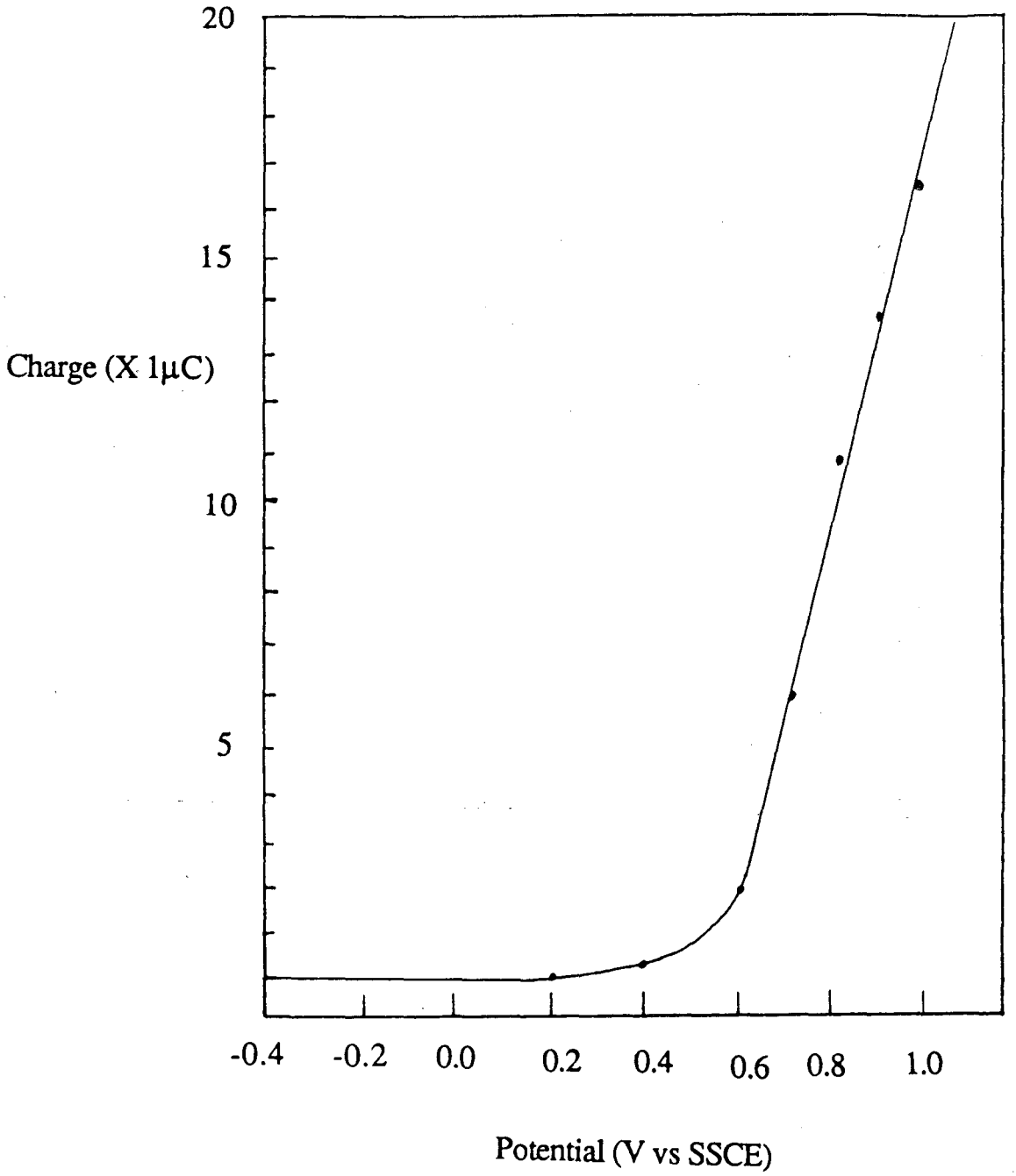

Fig. 19. Complex impedance data for Pt/P(3MT) in MeCN containing 0.1M TBAFB. Applied DC potential of +0.4, +0.45, and +0.5V vs SSCE. Film Thickness = 1.79 μm.

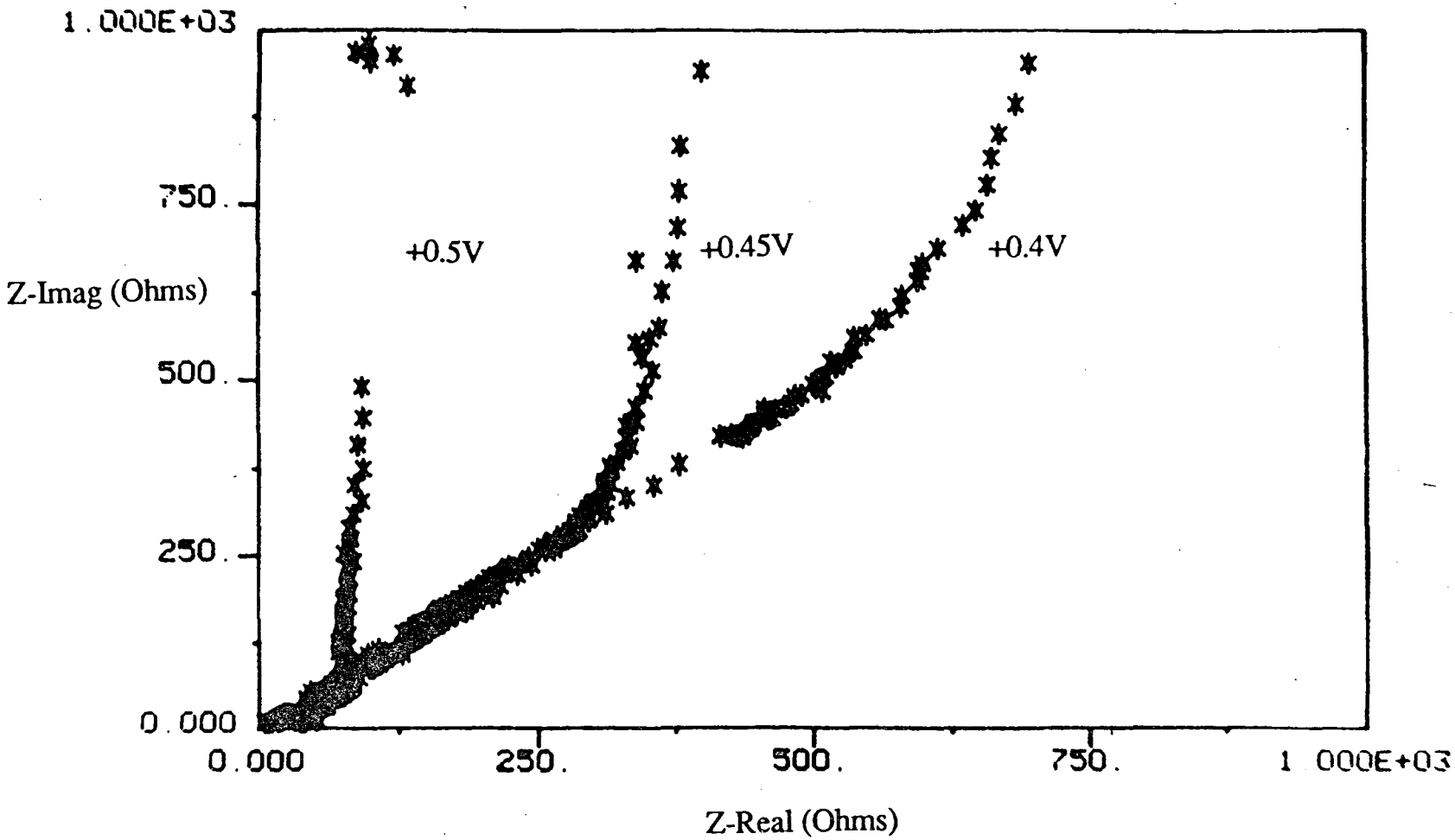

Fig. 20. Complex impedance data for Pt/P(3MT) in MeCN containing 0.1M TBAFB. Applied DC potential of +0.2, 0.3, 0.4, and 0.5V vs SSCE. Film Thickness = 1.84μm.

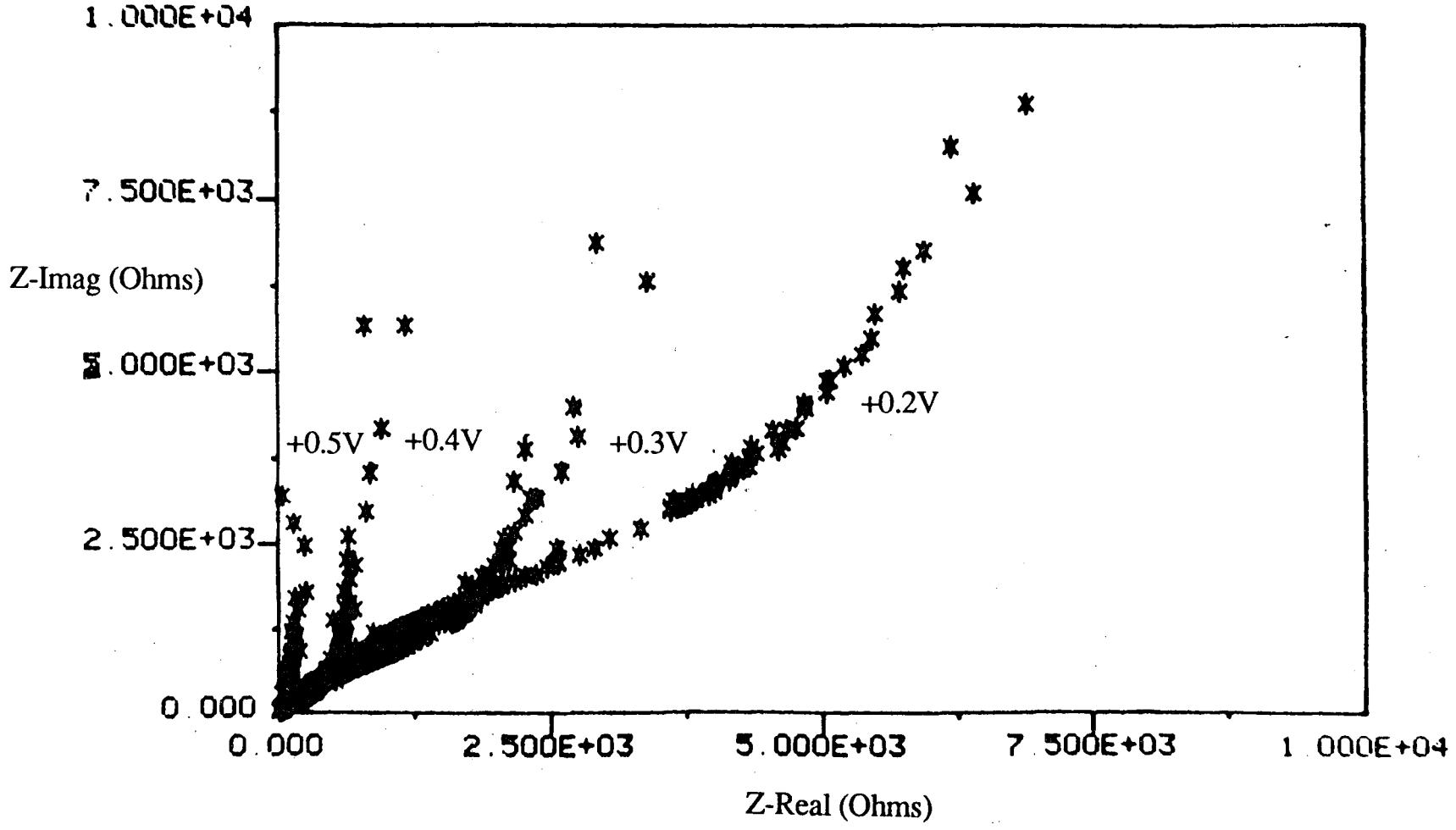

Fig. 21. Cyclic Voltammogram of Pt/Polythiophene in MeCN Containing 0.1M TBAFB.

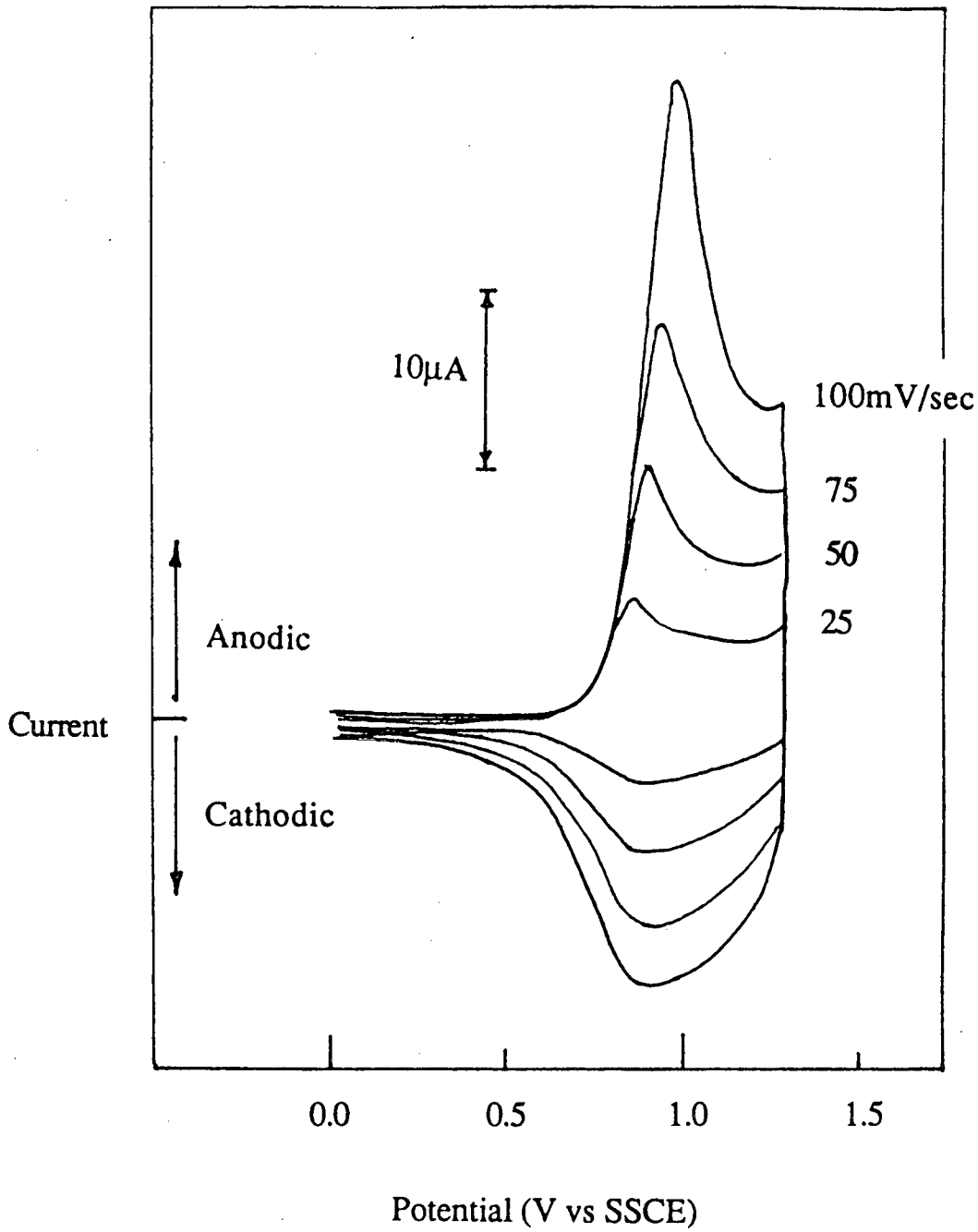

Fig. 22. Charge vs Potential for Pt/Polythiophene

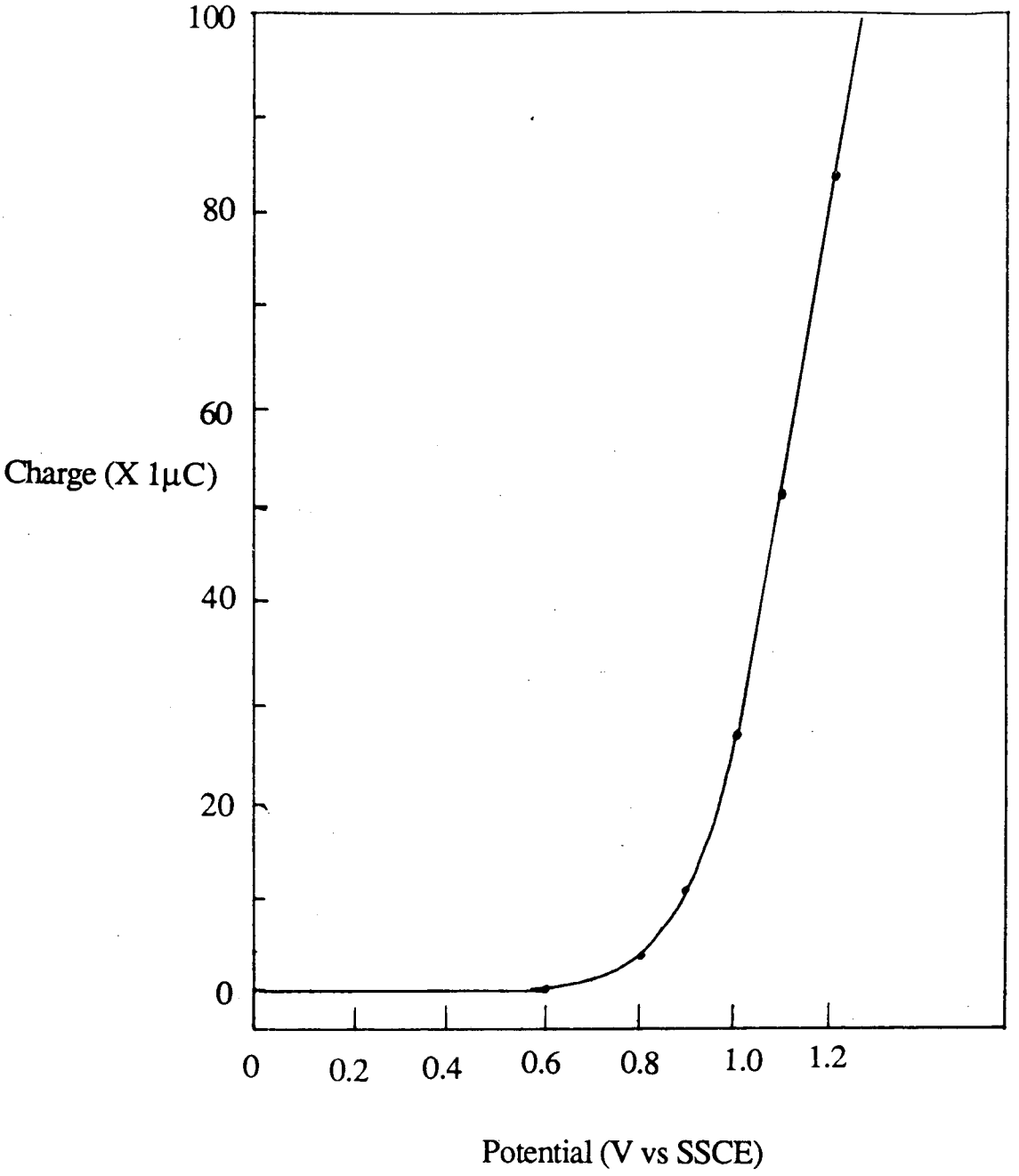

Fig. 23. Complex impedance data for Pt/Polythiophene in MeCN containing 0.1M TBAFB. Applied DC potential of +0.8 V and +1.0V vs SSCE.

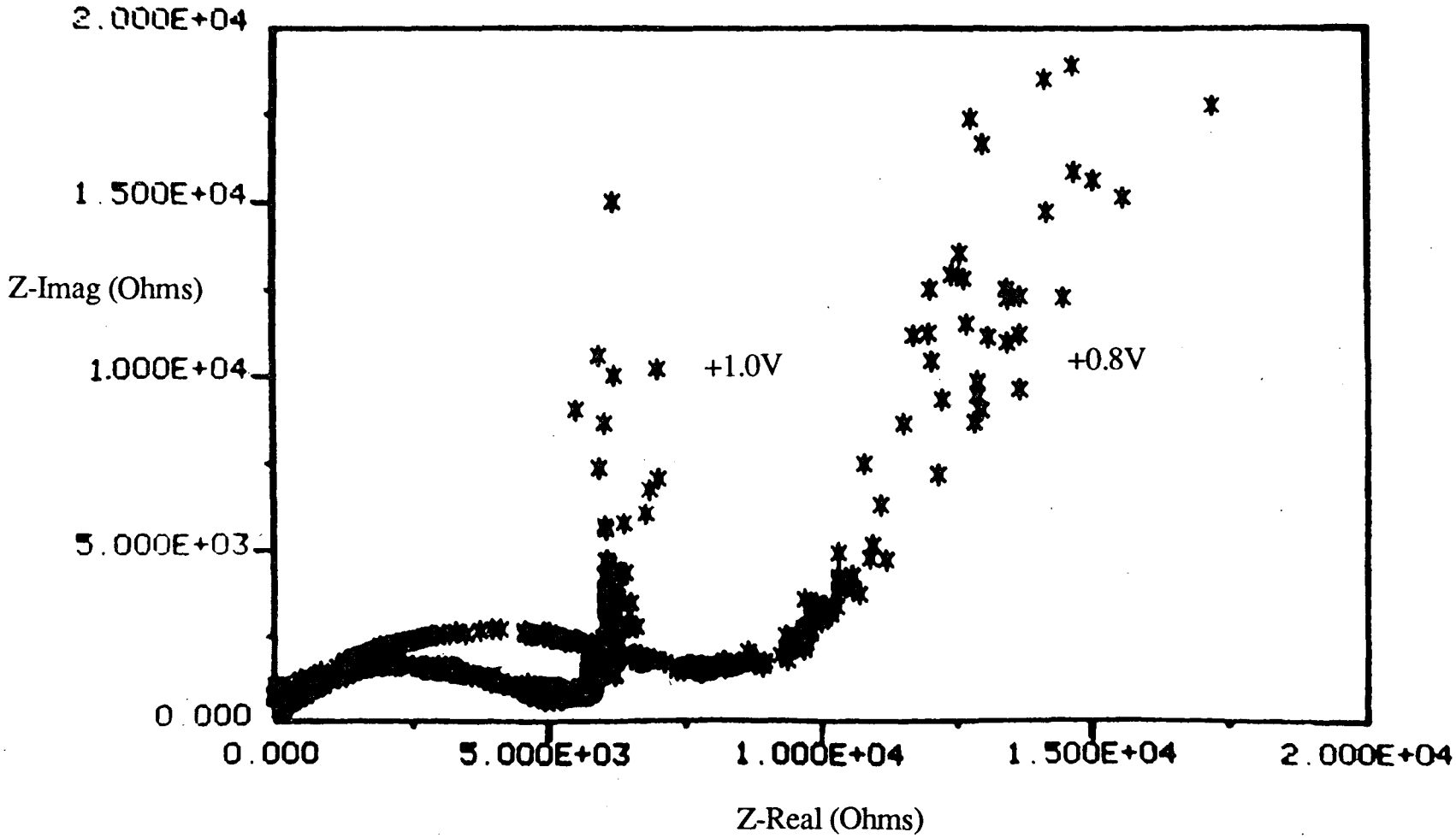

Fig. 24. Cyclic Voltammogram of Pt/Polypyrrole in MeCN Containing 0.1M TBAFB.

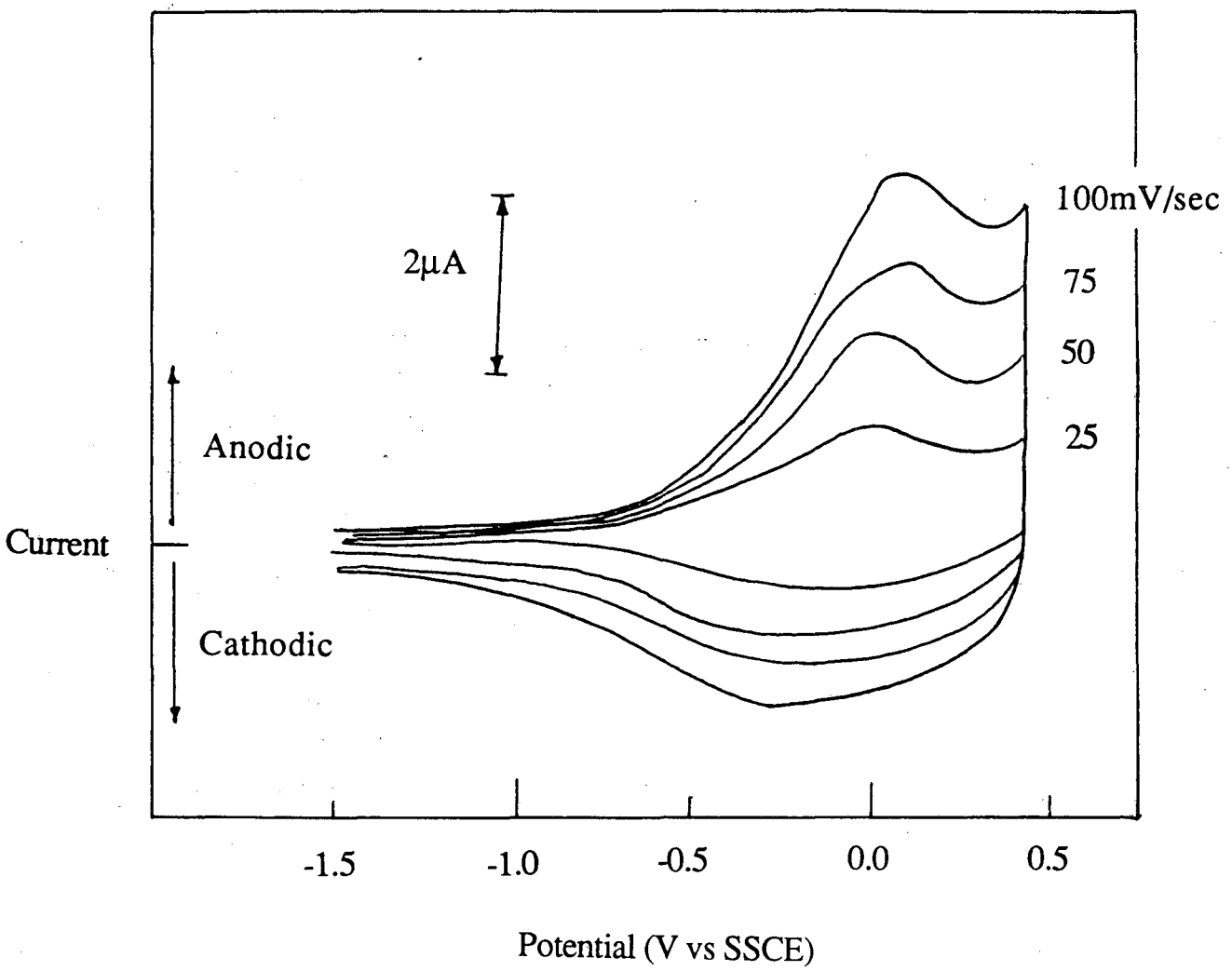

Fig. 25. Charge vs Potential for Pt/Polypyrrole

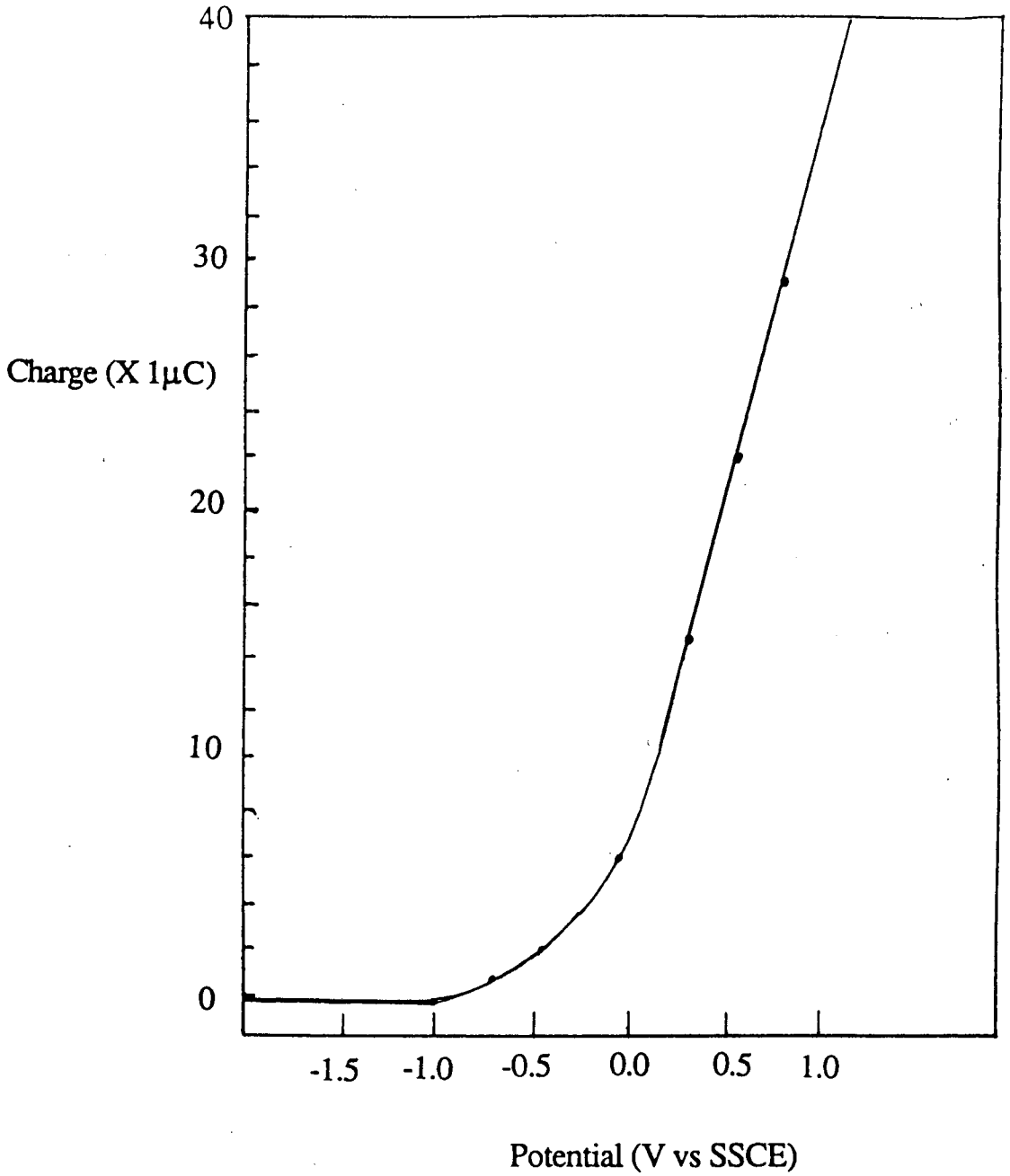

Table 3. Summary of Impedance Data for Pt/Poly(3-methylthiophene)
a) Film Thickness = 1.79 μm; b) Film Thickness = 1.87 μm.

	$E_{applied}$ (V vs SCE)	R_{ct} (Ohms)	Cdl (F X 10^6)	C_l (F X 10^4)	D_{ct} (cm^2/sec X 10^7)
a)	+0.4	50	0.5	4.2	0.5
	+0.45	40	0.4	6.3	0.7
	+0.5	40	0.3	7.9	4
b)	+0.2	110	0.1	0.3	3
	+0.3	40	0.5	1.5	0.6
	+0.4	25	0.8	2.4	2
	+0.5	20	1	21	2

R_{ct} = Charge Transfer Resistance (Ohms)

C_{dl} = Double Layer Capacitance (Farads)

C_L = Redox Capacitance (Farads)

D_{ct} = Diffusion Coefficient based on PVF model (cm^2/sec)

Table 4. Summary of Impedance Data for Pt/Polythiophene

$E_{applied}$ (V vs SCE)	R_{ct} (Ohms)	C_{cl} (F X 10^6)
+0.6	--	--
+0.8	7500	0.03
+1.0	5000	0.03
+1.2	7500	0.03

2C. CATION INTERCALATION IN V_6O_{13} SINGLE CRYSTALS

- M.Z.A. Munshi

INTRODUCTION

The intercalation of Li^+ in V_6O_{13} has received popular attention due to the potential application in high-energy-density secondary solid-state batteries [1,2]. The motivation for using lithium as the anode material lies in the fact that it is the lightest metal and also has a high negative electrode potential in the electromotive series.

From a battery point of view, V_6O_{13} is a promising lithium cathode material because of its large reversible insertion capacity (the maximum lithium stoichiometry attainable in V_6O_{13} is $Li_8V_6O_{13}$) and high theoretical specific energy of 890 Wh/kg [3]. This is considerably greater than some of the other intercalation cathodes such as TiS_2 (480 Wh/kg calculated for $LiTiS_2$). The exceptional insertion properties have been attributed to a crystal structure which contains channels of linked perovskite - like cavities extending in the [010] direction [4]. Lithium ions reside on sites within these cavities and are mobile both along the channels and between adjacent channel pairs. The equilibrium open-circuit voltage - composition data and the chemical diffusion coefficient of lithium within this structure are important parameters in determining whether an active V_6O_{13} cathode will be able to sustain a satisfactory voltage and current density, respectively. In this respect, high equilibrium voltages (>2V) and high diffusion coefficients (10^{-9} - 10^{-8} cm^2s^{-1}) in the cathode have been demonstrated with the Li/V_6O_{13} couple, making it a very promising cathode in rechargeable lithium batteries. Nonetheless the high reactivity of elemental lithium anodes may cause some concern as to the safety and cycle life of ambient-temperature secondary lithium batteries. In addition, because of the limited world supply, the material may become expensive in the long run. These problems may be overcome, however, by finding alternative anodes such as Na,Mg, Zn, Cu, etc., which may be more stable, have reasonable energy densities and which are also highly desirable both from a cost-effective point of view and materials availability.

The major thrust on the V_6O_{13} positive active material has been made using lithium as the negative electrode. In addition, previous emphasis has been placed on studying polycrystalline V_6O_{13}. The use of polycrystalline samples in pressed pellet poses a serious problem in any kinetic-properties determination because of severe ion-transport impedance across the dry interparticle boundaries. Furthermore, since the diffusion is anisotropic [8], the results will depend on the crystal orientation. To overcome these and other obstacles, single-crystal cathodes of V_6O_{13} will be contacted on particular crystallographic faces by a solid polymer electrolyte (poly(ethylene oxide) doped with the appropriate salt) so as to allow electrochemical insertion of cations into the crystal in specific crystallographic orientation. However, in to carry out this task, the initial intercalation study will be made using non-aqueous organic solvents as the electrolyte so as to screen potential anode materials. This study will then be extended to cover polymer electrolytes. The work will cover:

(1) growth of single crystals

(2) intercalation studies using Li anode

(3) intercalation studies using Zn, Cu, Na, Mg, Al anodes.

EXPERIMENTAL

Preparation of Polycrystalline V_6O_{13}

Non-stoichiometric V_6O_{13} was prepared by the thermal decomposition of NH_4VO_3. Analytical grade, ball-milled, vacuum dried NH_4VO_3 (Alfa) was thermally decomposed under a dry Ar stream. In a typical preparation, 35-40 g of NH_4VO_3 was placed in a alumina crucible and heated in an Ar stream (100-150 cm^3/min) from room temperature to 500°C at a rate of 4-5°C/min. After one hour at 500°C when ammonia was no longer detected, the temperature was increased to 550°C for an additional hour. The product was slowly cooled to room temperature while maintaining the Ar flow. The

powder obtained varied in color from blue-grey to navy blue. The stoichiometry of the product was determined by monitoring the mass charge upon oxidizing the samples to V_2O_5, and it ranged between $V_6O_{13.45}$ and $V_6O_{13.11}$. The x-ray powder diffraction patterns were similar to that of V_6O_{13}. Non-stoichiometric V_6O_{13+x}, prepared by the above method has a higher reported capacity for lithium than the stoichiometric material. This excess capacity has been attributed to its small particle size (1-5μm), although the influence of lattice defects is unknown. It has been suggested that the defect responsible for the excess oxygen in V_6O_{13+x} might be an additional single chain of VO_6 octahedra inserted between the double chains of the V_6O_{13} structure.

Preparation of V_6O_{13} Single Crystals

Polycrystalline V_6O_{13} was used to grow V_6O_{13} single crystals using the method of Saeki et al. [5]. About 5 g of V_6O_{13} and 300 mg of $TeCl_4$ were sealed in an evacuated silica glass tube of length 16 cm and diameter 2 cm. This tube was held in a horizontal two-zone tube furnace with the charge zone at 600°C and the growth zone at 550°C for 6-10 days. This method yielded well-shaped but small blue-black crystals with needle or extended plate-like morphologies (8-mm long x 0.5-mm wide x 0.1-mm thick). After 10 days the crystals were regrown by inverting the tube so that the needle-like crystals were now at the charge zone. In this way, crystals of dimensions (12-mm long x 2-mm wide x 1-mm thick) were obtained. The crystals were removed from the tube and washed with dichloromethane to remove residual $TeCl_4$ from the surface. X-ray powder diffraction revealed no traces of phases other than V_6O_{13}. Single-crystal diffraction was used to show that the direction of preferred growth was always the monoclinic b axis and that the cleavage plane was (001) [5,6]. Figure 26 shows an optical micrograph of the V_6O_{13} single crystals.

Intercalation with Lithium

Preliminary intercalation studies in V_6O_{13} single crystals were performed using lithium anodes in order to reproduce earlier reported work. Single-crystal slices were prepared as electrodes oriented for Li^+ diffusion perpendicular to the (001) plane, with the diffusion direction being made as thin as possible. (010) sections were obtained from crystals with needle-like morphologies by sawing into 1-mm long sections perpendicular to the b axis. One of the (010) faces, typically 2-3 mm^2 in area, was mounted to a Pt wire with silver epoxy. The whole crystal was then set in an electrically insulating epoxy and once hardened, the opposite crystal (010) face exposed by polishing with 0.3-μm diamond paste.

Thicknesses were measured to 0.001 mm with a micrometer screw gauge and the samples were measured to 0.02 mg on a microbalance.

Simple two-electrode cells were constructed with a lithium anode, a single-crystal V_6O_{13} cathode and an electrolyte consisting of 1M $LiClO_4$ in propylene carbonate (Burdick and Jackson) that was pre-distilled. Subsequent measurements were carried out in a He atmosphere glove box at room temperature. Cell voltages were measured to 1 mV using a high input impedance digital electrometer (Keithley 617). Currents were measured using a Keithley 175 multimeter.

RESULTS AND DISCUSSION

Open-circuit voltage (OCV) - composition curves were obtained by coulometric titration. Constant currents of 0.2-10 $mAcm^{-2}$ were applied for known times, so as to pass known amounts of lithium into the crystal. After each titration, the cells were allowed to stand at open-circuit to return to equilibrium, this being assumed to have been reached when the cell voltage changed by less than 1 mV in 24 hours. The results of such an experiment performed on different crystals at room temperature is shown in Figures 27 and

28. The highest lithium concentration that could be reached before cell failure varied considerably, but was probably limited by crystal cracking caused by lattice expansion which accompanies lithium insertion. Separating the components of the failed cells to confirm this proved difficult because they were invariably firmly stuck together.

From the continuously falling region of the coulometric titration curves (Figure 28), a single phase region was identified in the range $0 \leq x \leq 0.1$ in $Li_xV_6O_{13}$, while beyond x = 0.10 a constant-voltage revealed the presence of a two phase region, extending to at least x = 0.6. These findings are in good agreement with previous reports indicating the technique to be sound [3,7]. The lithium result was the control with which other anodes could be correlated and assessed.

Preliminary Results on Zn and Cu Intercalation

Several Zn|V_6O_{13} and Cu|V_6O_{13} cells in 50:50 DMSO:PC as the electrolytes have been built and open-circuit voltage measurements made. However, almost all the cells tested behaved indifferently from the lithium cells. The OCV's of the zinc cells with no electrochemical intercalation varied between 0.9 and 1.35V, whereas the copper cells varied between 0.50 - 0.60V. However, in the case of the copper cells, the voltages appear to stabilize over a period of several days to about 0.3 V. EDAX measurements on the V_6O_{13} single crystals obtained from the Cu|V_6O_{13} cells with no electrochemical intercalation failed to show Cu in the crystals, indicating perhaps that the falling OCV is not due to chemical intercalation. In some cases, the epoxy mount holding the single crystal was also found to dissolve in the electrolyte. Further work is continuing to clarify some of the above results.

With the zinc cell, the OCV also decreased with time. However, in some cases electrochemical intercalation was possible. Although very little data has been obtained at this time, qualitatively it has been shown by EDAX (Figure 29) that Zn intercalation is taking place.

Future Plan

The work is aimed at investigating the reversible nature of V_6O_{13} towards monovalent, divalent and trivalent cations. After the initial screening study using non-aqueous solvents as the electrolyte, the emphasis will be to construct solid-state cells consisting of the appropriate anode, a solid polymer electrolyte (poly(ethylene oxide) complexed with the appropriate salt) and a V_6O_{13} single crystal as the cathode. In addition to coulometric studies on the above system, the a.c. ionic conductivity of the crystal will be measured as a function of composition and temperature. In this way the transport properties of the various cations in V_6O_{13} single crystals can be evaluated. The work should prove useful in screening potential anode materials for use in solid polymer electrolyte batteries.

References

1. D.W. Murphy, P.A. Christian, F.J. DiSalvo and J.N. Carides, J. Electrochem. Soc. 126, 497 (1979).

2. D.W. Murphy and P.A. Christian, Science, 205, 651 (1979).

3. K. West, B. Zachau-Christiansen and T. Jacobsen, Electrochim. Acta, 28, 1829 (1983).

4. D.W. Murphy, P.A. Christian, J.N. Carides and F.J. DiSalvo, in "Fast Ion Transport in Solids," (Eds) P. Vashista, J.N. Mundy and G.K. Shenoy, p. 137, (North-Holland), (1979).

5. M. Saeki, N. Kimizuka, M. Ishii, I. Kawada, M. Nakano, A. Ichinose and M. Nakahira, J. Cryst. Growth, 18, 101 (1973).

6. P.D. Dernier, Mat. Res. Bull. 9, 955 (1974).

7. P.C. Spurdens, J. Drennan, J.R. Owen, B.C.H. Steele, J.M. Gonzales-Calbet, and D.A. Jefferson, Solid State Ionics, 5, 335 (1981).

8. P.C. Spurdens and B.C.H. Steele, Solid State Ionics, 21, 151 (1986).

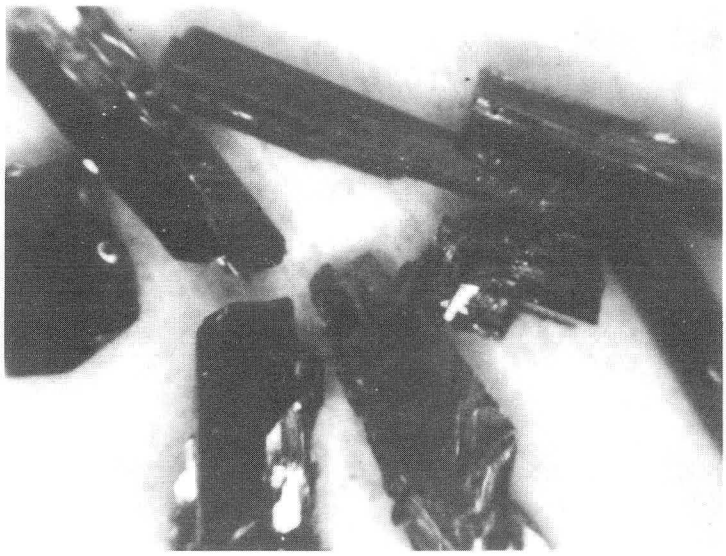

Figure 26. Optical micrograph of V_6O_{13} single crystals (mag. = 15X).

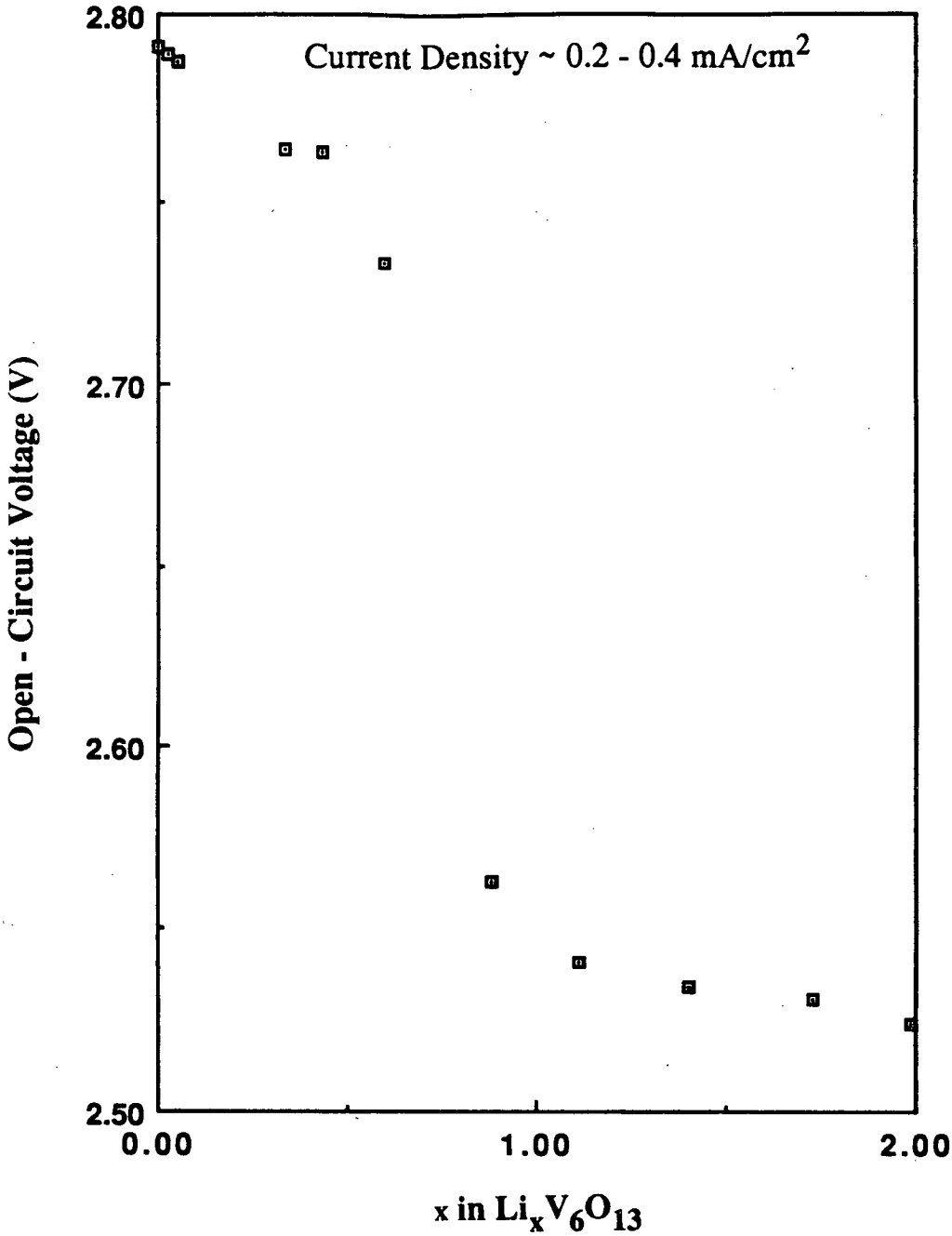

Figure 27. Lithium insertion in V_6O_{13} single crystal.

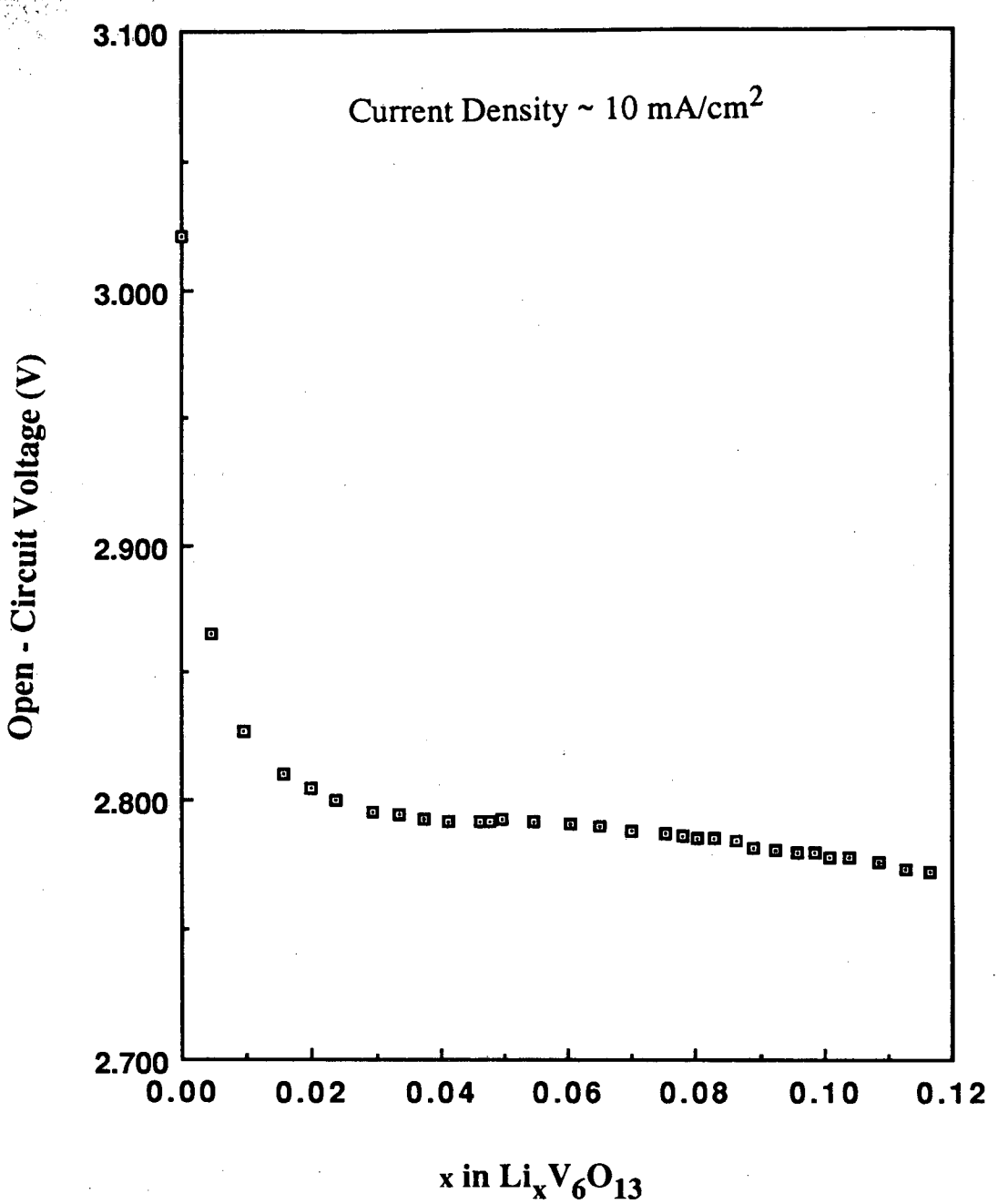

Figure 28. Lithium insertion in V_6O_{13} single crystal.

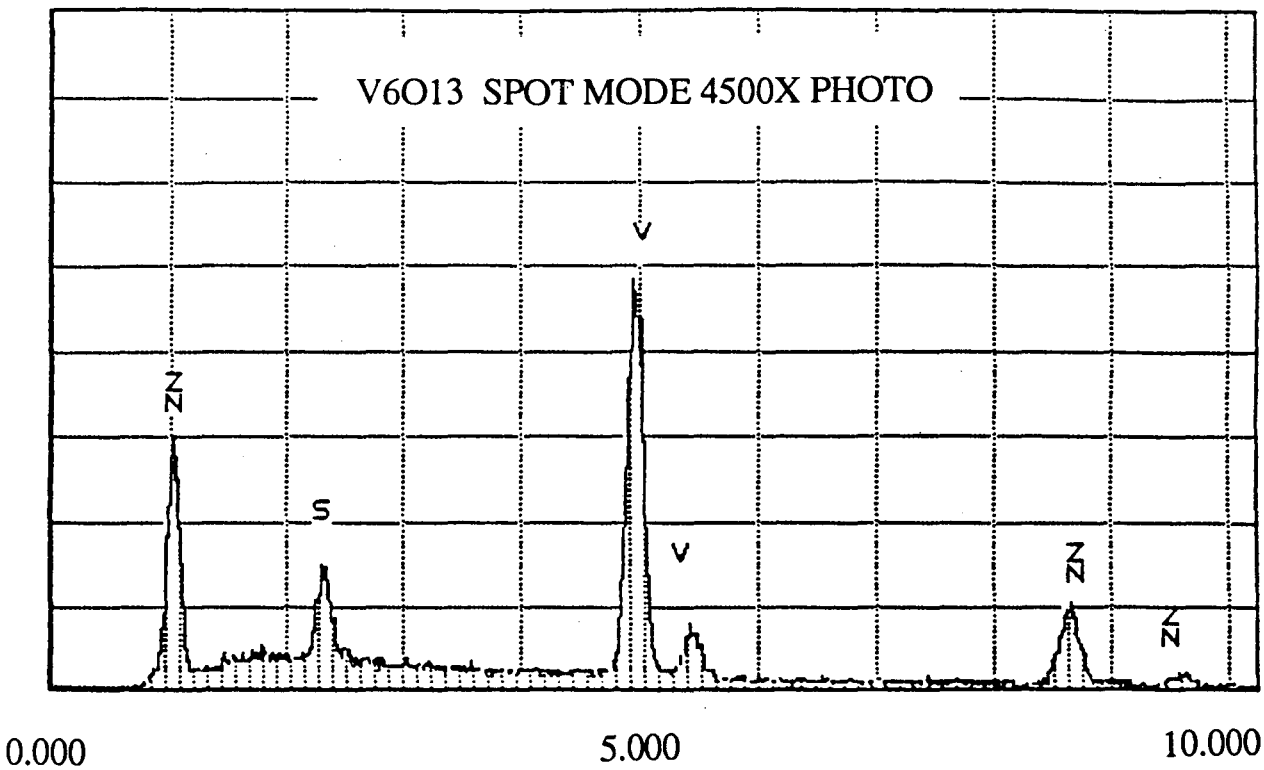

Figure 29. EDAX scan of V_6O_{13} single crystal from zinc cell.

2D. TRANSPORT IN POLYMERIC ELECTROLYTES

- W.H. Smyrl, J.Y. Cherng, Mary Lien

In this work, effort was focussed on the fundamentals of transport in polymeric electrolytes and the techniques of measuring transference numbers at steady state. The mathematics of both dilute solution and concentrated solution transport in electrolytes have been used to develop the fundamental framework. Only the dilute solution development will be reported here. The conclusions are at variance with the literature on the subject and may be the basis for new techniques for transference number determination in polymer electrolytes. The steady-state treatment for measurement of diffusion coefficients, transference numbers, and conductivity may be summarized in the following steps:

1. Measurement of the steady voltage difference between identical electrodes reversible to the cation, the initial concentration of electrolyte, and cell thickness will yield a value for D_+, from steady-state measurements.
2. Supplemented by a measurement of the initial conductivity, one may also calculate D_-.
3. Taken together, these may be used to calculate t_+, and hence $(1-t_+)$.
4. The concentration profile in steady state is independent of t_+.
5. The transient change from the initial uniform concentration to the final steady-state distribution depends on t_+. The nearer t_+ is to 1, the longer the transition time.
6. At $t_+ = 1$, there is no change from the initial distribution, and the concentration remains uniform.

In addition, a preliminary discussion of a completely new technique for measuring transference numbers is presented. It is based on the use of microstructured electrodes and offers the advantage of being rapid, and broadly applicable to all solid electrolytes.

Transport in a solid polymeric electrolyte

For a binary electrolyte in general, since

$$z_+C_+ = -z_-C_-$$

$$\underline{v} = 0$$

$$\frac{\partial C}{\partial t} = \frac{z_+D_+F}{RT}\nabla\cdot(C\nabla\phi) + D_+\nabla^2C \tag{1}$$

$$\frac{\partial C}{\partial t} = \frac{z_-D_-F}{RT}\nabla\cdot(C\nabla\phi) + D_-\nabla^2C \tag{2}$$

$$C = \frac{C_+}{\nu_+} = \frac{C_-}{\nu_-}$$

Subtraction of (2) from (1) gives a general equation, for all times including steady state

$$\left(\frac{z_+D_+}{RT} - \frac{z_-D_-}{RT}\right)\nabla\cdot(C\nabla\phi) + (D_+ - D_-)\nabla^2C = 0 \tag{3}$$

Equation (3) can be used to eliminate the potential from (1) or (2), i.e.,

$$\frac{\partial C}{\partial t} = D\nabla^2C \qquad \text{or} \qquad \frac{\partial C}{\partial t} = \nabla\cdot(D\nabla C) - \frac{i\nabla t_+}{z_+\nu_+F} \qquad \text{(variable D and } t_+\text{)} \tag{4}$$

$$D = \left(\frac{z_+D_+D_- - z_-D_-D_+}{z_+D_+ - z_-D_-}\right) \tag{5}$$

The Boltzmann similarity transformation is used to solve transient concentration problems, if the boundary conditions may also be transformed. We note that the concentration distribution in a solution of a single salt is governed by the same equation as the concentration distribution of neutral species, even when current is passed.

From Equation (3), integrating once yields

$$-\frac{i}{z_+\nu_+F} = \left(\frac{z_+D_+}{RT} - \frac{z_-D_-}{RT}\right)FC\nabla\phi + (D_+ - D_-)\nabla C) \tag{6}$$

If only cations react,

$$N_+ = \frac{i}{z_+F} = -\frac{z_+D_+}{RT}F\nu_+C\frac{d\phi}{dy} - D_+\nu_+\left(\frac{dC}{dy}\right) \tag{7}$$

$$N_- = 0 = \frac{-z_-D_-F}{RT}\nu_-C\frac{d\phi}{dy} - D_-\nu_-\left(\frac{dC}{dy}\right) \tag{8}$$

Eliminating the potential gives an expression that can be used in integrating transients in (4), i.e.,

$$\frac{i}{z_+\nu_+F} = -\left(\frac{z_-D_-D_+ - z_+D_+D_-}{z_-D_-}\right)\left(\frac{dC}{dy}\right) \tag{9}$$

$$= -D_+\left(1 - \frac{z_+}{z_-}\right)\left(\frac{dC}{dy}\right) \tag{9'}$$

In the steady-state case, this equation can be integrated immediately to

$$(C_L - C_o) = -\frac{i\,(L)}{z_+\nu_+F\,D_+\left(1 - \frac{z_+}{z_-}\right)} \tag{10}$$

where L is the cell electrolyte thickness. This concentration profile does not depend on transference number, only on the diffusion coefficient of the cation, or

$$(C_L - C_o) = \frac{i\,(L)}{-\nu_-F\,D_+\,(z_- - z_+)} \tag{10'}$$

From (9') and (6), (eliminating current)

$$D_+\left(1 - \frac{z_+}{z_-}\right)\frac{dC}{dy} = (z_+D_+ - z_-D_-)\,C\,\frac{F}{RT}\left(\frac{d\phi}{dy}\right) + (D_+ - D_-)\left(\frac{dC}{dy}\right) \tag{11}$$

Collecting the $\frac{dC}{dy}$ terms,

$$\frac{dC}{dy}\left[-D_+\,\frac{z_+}{z_-} + D_-\right]\frac{1}{C} = (z_+D_+ - z_-D_-)\,\frac{F}{RT}\left(\frac{d\phi}{dy}\right)$$

or

$$-\frac{1}{z_-C}\left(\frac{dC}{dy}\right)\left[D_+z_+ - D_-z_-\right] = (z_+D_+ - D_-z_-)\,\frac{F}{RT}\left(\frac{d\phi}{dy}\right)$$

$$-\frac{1}{z_-}\,\frac{d\,\ln C}{dy} = \frac{F}{RT}\left(\frac{d\phi}{dy}\right)$$

$$\ln\left(\frac{C_L}{C_o}\right) = -\frac{z_- F}{RT}(\phi_L - \phi_o) \tag{12}$$

Measurement of $(\phi_L - \phi_o)$ immediately yields

$$\left(\frac{C_L}{C_o}\right) = \exp\left[-\frac{z_- F}{RT}(\phi_L - \phi_o)\right]$$

Knowledge of C_L/C_o yields

$$\frac{C_L}{C_o} = 1 + \frac{i\,(L)}{\nu_- F\, D_+\, (z_- - z_+)\, C_o}$$

or

$$\left[\frac{L}{D_+ C_o}\right] = \frac{\nu_- F\,(z_- - z_+)}{i}\left[\frac{C_L}{C_o} - 1\right] \tag{13}$$

The terms on the right hand side of (13) is measurable directly, i.e., by measuring the constant voltage drop or the current density. Thus, we obtain the ratio $\left(\frac{L}{D_+ C_o}\right)$, and D_+ is determined by measuring L and C_o.

If the current is raised to the level that

$$C_L = 0, \qquad i = i_{limit}, \qquad (\phi_L - \phi_o) \rightarrow -\infty$$

$$\frac{L}{D_+ C_o} = \frac{-\nu_- F\,(z_- - z_+)}{i_{limit}}$$

$$D_+ \bar{C}_o = -\frac{i_{limit}\,(L)}{\nu_- F\,(z_- - z_+)} \tag{14}$$

$$C_L - C_o = -\frac{i}{i_{limit}}$$

$$\frac{C_L}{C_o} - 1 = -\frac{i}{i_{limit}}\frac{\bar{C}_o}{C_o} = \frac{i\,(L)}{\nu_- F\, D_+\,(z_- - z_+) C_o}$$

The concentration at the midpoint $\left(\frac{L}{2}\right)$ should be unchanged from the initial concentration. If this is so,

$$C_{L/2} - C_L = C_o - C_{L/2}$$

At currents where $C_L \rightarrow 0$,

$$\bar{C}_o = 2(C_{L/2}) = 2(C_{init})$$

From Equation 15

$$D_+ = \frac{- i_{limit}(L)}{\nu_- F (z_- - z_+) 2C_{init}} \tag{16}$$

If we can measure the conductivity for the initial concentration,

$$\kappa = \frac{F^2}{RT} [z_+^2 D_+ C_+ + z_-^2 D_- C_-]$$

$$= \frac{F^2 C}{RT} [\nu_+ z_+^2 D_+ + \nu_- z_-^2 D_-]$$

$$= \frac{F^2 C_{init}}{RT} [z_+ \nu_+ (z_+ D_+ - z_- D_-)]$$

$$D_- = - \left(\frac{\kappa RT}{z_- F^2 C_{init}}\right) \left(\frac{1}{z_+ \nu_+}\right) + D_+ \left(\frac{z_+}{z_-}\right) \tag{17}$$

$$= - \left(\frac{\kappa RT}{F^2 C_{init} z_-}\right) \left(\frac{1}{z_+ \nu_+}\right) - \frac{i_{limit}(L) \left(\frac{z_+}{z_-}\right)}{\nu_- F (z_- - z_+)(2C_{init})}$$

The transference number with respect to the polymer matrix is measured, i.e.,

$$t_+ = \frac{z_+ D_+}{z_+ D_+ - z_- D_-}$$

$$= z_+ \left\{ - \frac{i_{limit}(L)}{\nu_- F (z_- - z_+)(2C_{init})} \right\} \tag{18}$$

$$z_+ \left\{ - \frac{i_{limit}(L)}{\nu_- F (z_- - z_+)(2C_{init})} \right\} + z_- \left\{ \left(\frac{\kappa RT}{F^2 C_{init} z_-}\right) \left(\frac{1}{z_+ \nu_+}\right) - \frac{\left(\frac{z_+}{z_-}\right) i_{limit}(L)}{\nu_- F (z_- - z_+)(2C_{init})} \right\}$$

C_{init} is eliminated from both the numerator and denominator so that the limiting current (i_{limit}), κ, and L are used to calculate t_+.

i.e., $$t_+ = -\frac{Fz_+^2\nu_+ i_{limit} L}{2\kappa RT(z_- - z_+)\nu_-} = \frac{z_+\nu_+ i_{limit}(LF)}{2\kappa RT(\nu_+ + \nu_-)} \quad (19)$$

Since

$$C_L + C_o = 2C_{L/2} = 2C_{init}$$

from (19) and (10),

$$C_L = \frac{i(L)}{2\nu_- FD_+(z_- - z^+)} + C_{init}$$

$$C_o = C_{init} - \frac{i\,(L)}{2\nu_- FD_+(z_- - z_+)}$$

$$\frac{1}{D_+} = \frac{\nu_- F(z_- - z_+)}{i\,(L)}\left[\frac{C_L}{C_o} - 1\right]\left\{C_{init} - \frac{i\,(L)}{2\nu_- D_+ F(z_- - z_+)}\right\} \quad (20)$$

$$\frac{C_L}{C_o} = \exp\left[-\frac{z\text{-}F}{RT}(\phi_L - \phi_o)\right] \quad (21)$$

The relationship between D_+ and the potential difference, current density, thickness, and initial concentration is given by

$$\frac{1}{D_+} = \frac{\nu_- F(z_- - z_+)}{i\,(L)}\left\{\exp\left[-\frac{z\text{-}F}{RT}(\phi_L - \phi_o)\right] - 1\right\}\left\{C_{init} - \frac{i\,(L)}{2\nu_- D_+ F(z_- - z_+)}\right\} \quad (22)$$

A series of measurements of current and voltage drop would lead to

$$(\phi_L - \phi_o) = -\frac{RT}{z\text{-}F}\ln\left[1 + \frac{1}{\left(\frac{\nu_- F(z_- - z_+)C_{init}D_+}{i\,(L)} - \frac{1}{2}\right)}\right]$$

One would get a semilog plot of

$$(\phi_L - \phi_o) \qquad \text{vs} \qquad \ln\left[\frac{1}{\left(\frac{C_{init}\nu_- F(z_- - z_+)D_+}{i\,(L)} - \frac{1}{2}\right)} + 1\right]$$

with 59 mv/decade slope (when $z_- = -1$).

The transient problem is solved with the boundary conditions

$C = C_{init}$ at $y = L/2$

and

$$\frac{i}{z_+\nu_+F} = -\left[\frac{(z_-D_-D_+ - z_+D_+D_-)D_+}{z_-D_-}\right]\left(\frac{dC}{dy}\right) \text{ at } y = 0$$

The other half of the domain from $\frac{L}{2}$ to L is antisymmetric with this behavior.

Let $\eta = \frac{y}{\sqrt{4Dt}}$

$$\frac{\partial C}{\partial t} = \frac{dC}{d\eta}\frac{\partial \eta}{\partial t} = \frac{dC}{d\eta}\left[-\eta\frac{1}{2t}\right]$$

$$\frac{\partial C}{\partial t} = \frac{dC}{d\eta}\frac{\partial \eta}{\partial y} = \frac{dC}{d\eta}\left(\frac{1}{\sqrt{4DT}}\right)$$

$$\frac{\partial^2 C}{\partial t^2} = \frac{d^2C}{d\eta^2}\left(\frac{\partial \eta}{\partial y}\right)^2 = \frac{d^2C}{d\eta^2}\left(\frac{1}{(4DT)}\right)$$

so that (4) becomes

$$\frac{dC}{d\eta}\left[-\frac{1}{2}\frac{\eta}{t}\right] = \frac{d^2C}{d\eta^2}\left(\frac{1}{4t}\right)$$

and

$$\frac{d^2C}{d\eta^2} + 2\eta\frac{dC}{d\eta} = 0 \qquad (23)$$

Subject to the boundary conditions

(a) $C = C_{init}$ at $\eta = \left[\frac{L/2}{\sqrt{4Dt}}\right]$

this corresponds to (∞) at short times. This suggests another solution must be sought at long times.

(b) $$\frac{i}{z_+\nu_+F} = -\frac{(z_- - z_+)D_+}{z_-}\left(\frac{dC}{d\eta}\right)\left(\frac{1}{\sqrt{4Dt}}\right) \text{ at } \eta = 0$$

This boundary condition requires $i = i(\frac{i}{\sqrt{t}})$ in order for the similarity transformation to work, i.e., "clamp" voltage to $\phi = \phi_0$ at $\eta = 0$ and $\phi = \phi_L$ at $\eta = 1$. That is, if

$$\frac{i\ (\sqrt{4Dt})(z_-)D_+}{z_+\nu_+F(z_- - z_+)} = -\frac{dC}{d\eta} \text{ at } \eta = 0$$

becomes independent of t, the problem is solved with the technique used here.

If $t_+ = 1$, from (18)

$$\frac{\kappa RT}{F^2 z_-}\left(\frac{1}{z_+\nu_+}\right)' = -\frac{i_{lim}(L)\left(\frac{z_+}{z_-}\right)}{\nu_- F(z_- - z_+)}$$

$$C_{init}(z_+D_+ - z_-D_-) = C_{init}z_+D_+$$

or

$$D_- = 0,$$

as expected. The concentration distributions and potential distributions were derived above without any assumption about the transference number, and (9), (10), and (12) are all written with no explicit appearance of D_- or t_-. Therefore they should be general.

In (6), with $D_- = 0$

$$\frac{i}{z_+\nu_+F} = \frac{z_+D_+FC\nabla\phi}{RT} + D_+\nabla C \tag{24}$$

and passage of current will still lead to the same concentration profile in the steady state.

As a final note, the literature suggests that the transference number may be measured as a ratio of the steady-state current to the initial current for constant (potentiostatted) voltage. We find from the above equations that

$$\frac{i(\text{steady state})}{i(\text{init})} = \frac{t_+(z_- - z_+)\left[\exp\{-\frac{z_-F}{RT}(\phi_L - \phi_0)\} - 1\right]}{\left(\frac{z_+z_-}{RT}\right)(\phi_L - \phi_0)\left\{1 + \frac{1}{2}\left[\exp\{-\frac{z_-F}{RT}(\phi_L - \phi_0)\} - 1\right]\right\}} \tag{25}$$

This never yields the transference number. At small voltages, the exponentials may be expanded and

$$\frac{i(\text{steady state})}{i(\text{init})} = - t_+ \left(\frac{z_-}{z_+} - 1\right)$$

One may confirm that this approximation yields a constant times the transference number. It is clear that the i(steady state)/i(initial) ratio is affected by the applied voltage. Since the current at steady state is limited by the concentration of salt and the diffusivity of cations and the initial current is determined by the conductivity of a polymeric electrolyte and the applied voltage, the ratio will approach zero at a large applied voltage. At 100°C, the applied voltage needs to be in the region of 0.116-0.131 V so that i(steady state)/i(initial) = t_+ within 5 percent. If the equation is used to check literature results, a lower value of transference number was obtained at 0.01 V applied voltage. Values larger than 1 were obtained at 1 V applied voltage. This suggests new and careful measurements based on solid principles need to be made.

Transient transport in polymer electrolytes

Since the transport of ions greatly affects the design of electrodes, a mathematical model at constant current has been derived to describe the concentration distribution of salt in the polymer electrolyte.

$$C = C_0 - \left(i/(z_+ \nu_+ F D_+)/(1 - z_+/z_-)\right)(x - L/2 + (4L/\pi^2)$$

$$\sum_{n=0}^{\infty} (1/(2/n + 1)^2)\exp(-(2n + 1)^2\pi^2 tD/L^2) \cos((2n + 1)\pi x/L)) \qquad [1]$$

C_0: initial concentration of electrolyte (mole/cm^3),

z_+: charge of cation D_+: diffusivity of cation (cm^2/s),

L: thickness of electrolyte (cm), x: location in electrolyte (cm)

t: time (s), D: diffusivity of electrolyte (cm^2/s)

v_+: number of cations into which a mole of electrolyte dissociates

The concentration distribution of $LiClO_4$ at 90°C and 3 mA/cm^2 is shown in Figure 30. It can be clearly seen that after 15 minutes, the steady state is well established. The mathematical model also shows that the limiting current through the polymeric electrolyte is proportional to the concentration of salt and the diffusivity of the cation. A limiting current of 6 mA/cm^2 (C=0 at x=0 or x=L=100 μm) can be obtained in the $LiClO_4$•PEO_8 electrolyte at 90°C. The diffusivities of salt and cation affects the length of time to reach steady state. However, only the diffusivity of cation affects the concentration distribution of salt at steady state as described above.

Fig. 30. Concentration Distribution of Lithium Perchlorate

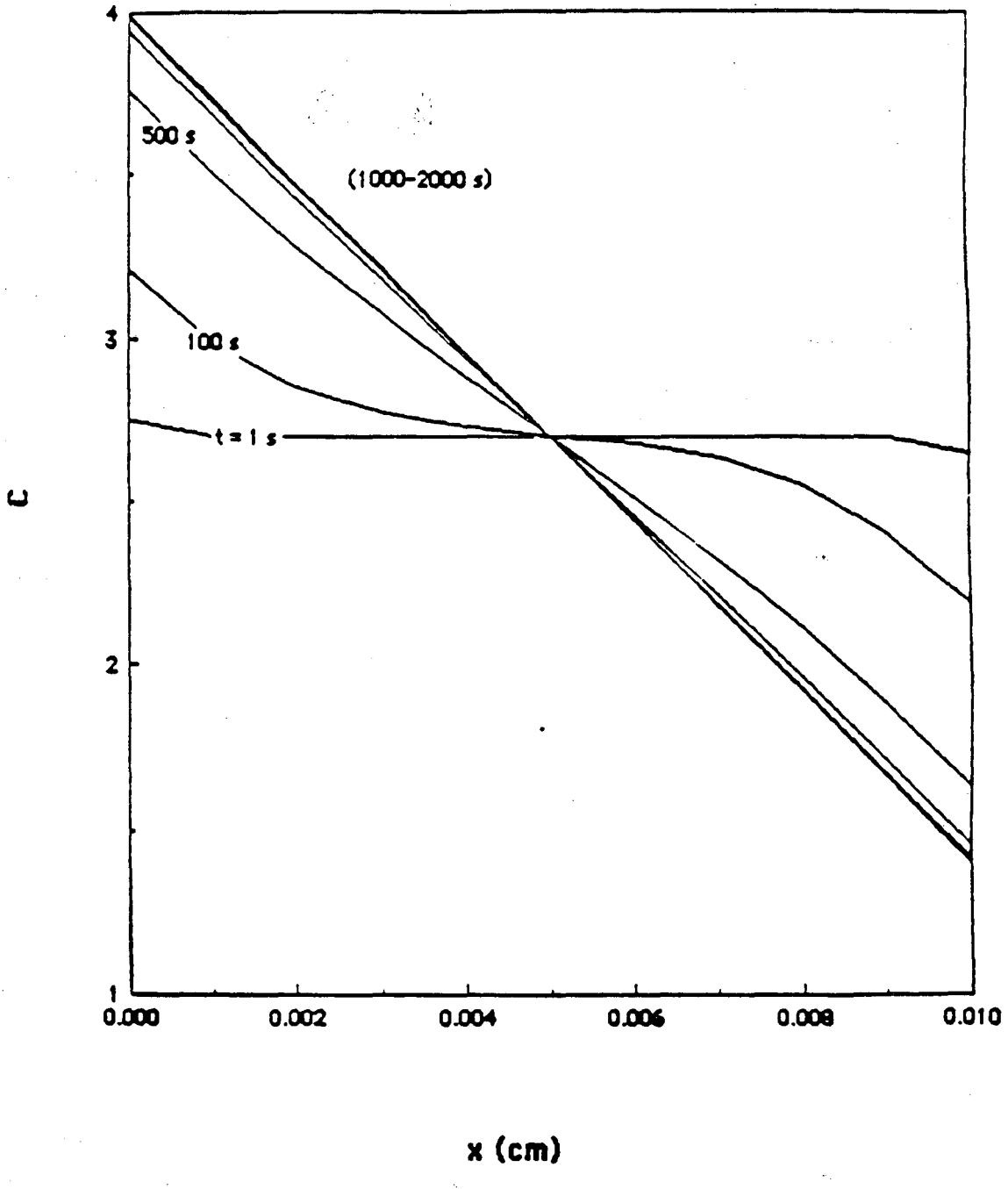

2E. ELECTROCHEMICAL PROPERTIES OF POLY(1-TRIMETHYLSILYL-2-BROMO ACETYLENE) IN THE SOLUBLE AND INSOLUBLE STATE

- Laura Douglas, Kathryn Podolski, W.H. Smyrl

Conducting polymers have been researched extensively in recent years for many possible uses. However, the study of these materials has been limited to polymer films which are usually insoluble in a given solution either in the oxidized or reduced state. This exploratory research was conducted to determine if poly(1-trimethylsilyl-2-bromo acetylene) is soluble in an electrolytic solution in both neutral and oxidized states and to determine if its thermodynamic properties during the charging/discharging processes were Nernstian. The material for the studies was contributed by Dr. John Ziegler of Sandia National Laboratory. The results described here are the first of their kind to be reported for a high molecular weight polymer (50,000 MW).

Studies on the polymer in the soluble state

The solvent used was a mixture of toluene (C_7H_8) and acetonitrile (C_2H_3N) in the ratio of 4:1 (both the toluene and acetonitrile were spectroscopic grade). This mixture was necessary in order to dissolve both the nonpolar polymer and the polar electrolyte. The electrolyte salt employed in these experiments was tetrabutylammonium tetrafluoroborate (TBATFB). The TBATFB was recrystallized twice in ethanol (C_2H_6O) and was stored, along with the polymer, in a vacuum to keep them as dry as possible. A salt concentration of 0.1M used. The quantity of the polymer (50,000 MW) used was 1.0 mg/ml of solution. The blank electrolyte was a clear, colorless solution, but the addition of the polymer resulted in a clear, golden-brown solution.

Voltammetry was first run on the electrolyte solution to determine the potential window over which the current response of the background was minimal and to determine if the polymer remained in solution. Nitrogen was bubbled through the solution for 10 minutes to eliminate oxygen. The window obtained for this solution was 3.6 V wide, i.e., from -1.8 V to +1.8 V.

The polymer solution was tested within the potential limits of the background. Two oxidation peaks and one reduction peak were found. The oxidation peaks were located at +0.72 V, and a reduction peak for the reverse reaction was observed at slow scan rates. The disappearance of this peak at fast scan rates indicated that the reduction reaction was slow, even though the forward (oxidation) reaction was fast. In the range of scan rates where both peaks were seen, the peak current for both anodic and cathodic reactions was proportional to the square root of scan rate, indicating that both oxidized and reduced species were soluble and remained in solution. No precipitates was observed on the working electrode during the cyclic voltammetry experiments.

Coulometric experiments were carried out to determine the concentration-voltage relationship for the system. A digital coulometer measured the amount of charge passed, and periodically the current was interrupted to measure the potential of a Pt indicator electrode dipping into the solution. In all the experiments, a stirring bar and nitrogen bubbling were used to stir the solution and to eliminate oxygen. The measurements were taken on solutions containing 3 different concentrations of polymer, and on the background solution as well. The three polymer concentrations were 0.1, 0.5, and 1.0 mg per ml of solution respectively. From plots of the logarithm of concentration (Ox/Red) vs voltage, straight lines of slope 53 mV/decade, 62 mV/decade, and 49 mV/decade were obtained for the three solutions, respectively. This clearly demonstrated that the polymer in the soluble form obeyed Nernstian thermodynamics.

When the polymer was reduced at -1.4 V, buildup of a film was observed. That is, the current continued to increase with cycling in this region, and a film could be observed on the electrode after long cycling. Also, the peak reduction current was proportional to sweep rate as would be expected for a surface-attached film. The film was removed by sweeping to the oxidation peaks at 0.72 V and 1.08 V.

Studies on the polymer in the insoluble state

The above experiments were repeated with the same polymer, but under conditions where the polymer was solution cast from toluene as a film on the Pt working electrode, and it was insoluble in all conditions. The solvent in this case was acetonitrile only, and the electrolyte was 0.1 M TBATFB. Cyclic voltammetry showed that there was an oxidation peak at approximately 0.7 V that was rather irreversible at slow scan rates as seen in the studies above. The anodic peak was proportional to the scan rate at slow scan rates.

Coulometry on the polymer film gave concentration-voltage behavior that was completely different from that obtained from studies in the soluble state. There was no region of Nernstian behavior, and the tangent to the curve was greater than 150 mV/decade throughout. This is characteristic of all films of both electronically conducting and redox polymers, and appears to be consistent with intercalation thermodynamics developed for other materials.

3. VOLTAMMETRY STUDIES WITH MICROSTRUCTURED ELECTRODES

Prototype dual-band microelectrodes and single microelectrodes for measuring transport rates have been constructed and tested in polymer electrolytes containing Li^{+}, Fe^{+2}, Fe^{+3}, and Cu^{+2} ions. Cyclic voltammetry under semi-infinite solution conditions were used to measure the apparent diffusion coefficients of the metal ions. The electrochemical reversibility of these metal ions was also qualitatively determined.

The use of microelectrodes provided a quick and reliable means of electrochemical measurements in PEO electrolytes. The single most important advantage of using microelectrodes is that faradaic currents, corresponding to the cell reactions, are reduced to values that yield small and often insignificant iR potential losses in the electrolyte. This allows for a more quantitative evaluation of voltammetric behavior. We have used this advantage to explore the reaction behavior of Cu^{2+} reduction in PEO, which appears mechanistically different than in aqueous solution. A second advantage of using microelectrodes is that a standard reference electrode can be conveniently employed in the cell. This is obviously important in obtaining accurate thermodynamic data on cell reactions. Third, the placement of the counter electrode is not consequential in microelectrode voltammetric measurements and, in fact, is generally placed 1-2 cm away from the electrode under study. Interference from products generated at the counter electrode does not occur as it often does in thin-layer cells. Finally, the measurement of steady-state voltammetric limiting currents is the most direct method of measuring ion-fluxes in PEO presently available.

3A. MICROSTRUCTURED ELECTRODES FOR TRANSPORT STUDIES
- H.S. White, T. Hunter

I) An electrochemical microcell has been constructed for directly measuring d.c. conductivities and diffusion coefficients in thin polymeric electrolytes, Fig. 31A. The prototype cell consists of two Pt or Au electrodes, ca. 0.5-cm long and 100-Å wide, separated by 1 -100 μm layer of muscovite mica. Polymer electrolyte layers are solvent cast onto the surface of the structure, Fig. 31B, to form a Pt/solid electrolyte/Pt cell. There are

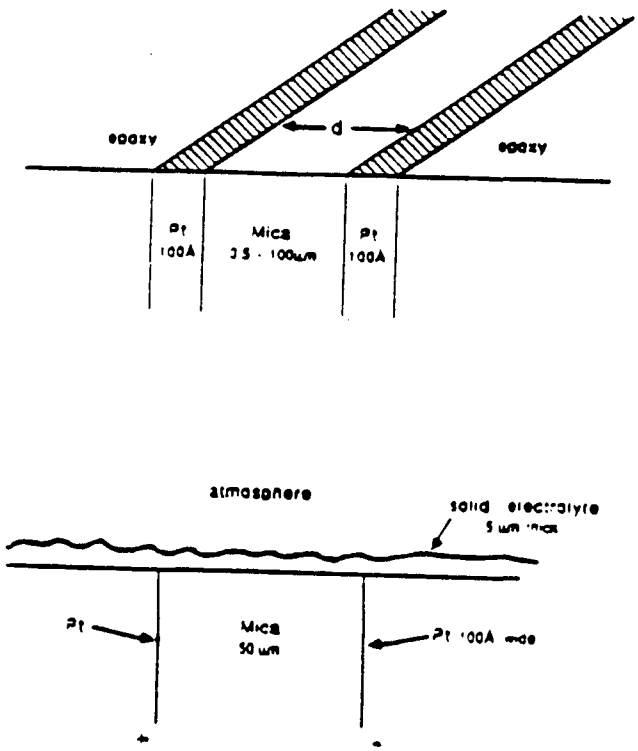

Fig. 31. (A) Cut-away of microcell showing Pt electrodes and mica spacer. (Not drawn to scale).

(B) Side-view of 50-μm thick Pt/Mica/Pt microcell coated with 5-μm solid electrolyte.

several advantages of this cell design in measuring transport properties relative to the standard multilayer cell. First, the electrolyte thickness, d, can be reduced to micron or submicron dimensions without electrical shorting of the cathode and anode. This allows investigations of transport behavior over a wider range of electrolyte thicknesses including ultra-thin separations (<1 μm). Second, the thickness d is precisely determined by the mica thickness which is readily measured to within 10Å by interferometry. Thus, changes in the electrolyte morphology during operation or uncertainties in the roughness of the film due to solvent casting do not enter into the analysis.

Approximately 25 of these prototype cells were constructed. The voltammetric response of these microcells in liquid electrolytes containing a redox active species were studied to unambiguously define the effective electrodes and cell geometry for future transport studies in solid electrolytes. For example, Fig. 32 shows the results of an

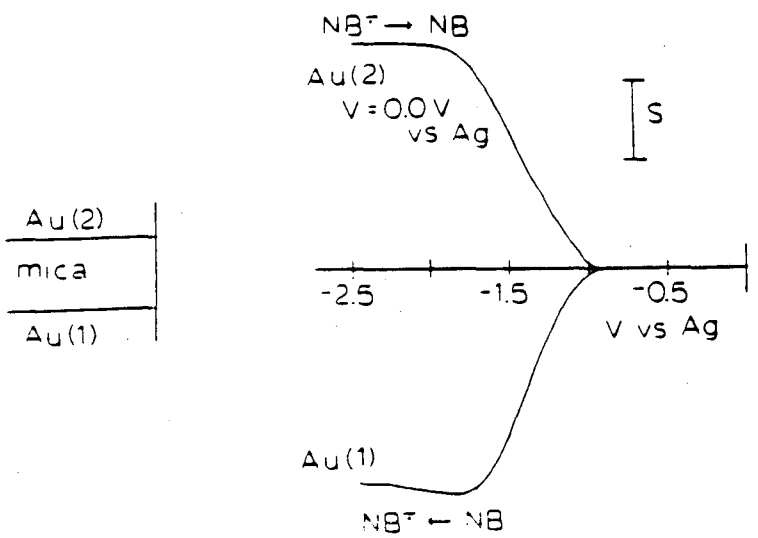

Fig. 32.Generator-collector experiment with microcell shown in Fig. 31. The potential of electrode #1 was scanned (20 mV/s) over the indicated potential range. The potential of electrode #2 was poised at 0.0V vs. Ag.

experiment where one electrode is used to reduce nitrobenzene radical anion generated at the first electrode. The second electrode is poised at a sufficiently positive potential to re-oxidize any nitrobenzene radical anion generated at the first electrode. This diffusion experiment is referred to as a collector-generator experiment and is analogous to rotating-ring disk measurements.

We have verified that the diffusion-limited response at a single electrode is in quantitative agreement to that expected for cylindrical diffusion to a thin-line electrode. For instance, in Fig. 32 the limiting quasi-steady-state current at electrode 1 due to reduction is 5.8 μA, in good agreement with theory. We have also measured the collection efficiencies in the generator-collector experiment over the range of separation thicknesses 1-10 μm. In Fig. 32, for example, approximately 40% of the nitrobenzene reduced at electrode 1 diffuses to electrode 2 where it is re-oxidized. This value is within 10% of the theoretical value based on a 5-μm mica separation.

Direct measurements of Li^+ diffusion coefficients were carried out with a Pt disk microelectrode, as a first step toward using the dual microband electrodes. We report direct measurements of the diffusion coefficient of Li^+ in an 8:1 PEO:$LiClO_4$ (M.W. = 1000) electrolyte using this microvoltammetric technique. A key finding in these studies is that voltammetric analysis of cation reduction in bulk PEO samples is possible using conventional electrochemical hardware including the use of a 3-electrode cell configuration that allows stable potential control of the working electrode. This latter result is especially significant in that general examination of electrode processes in PEO electrolytes may now be accomplished at a similar level of quantitative analysis associated with voltammetry in conventional fluid electrolytes, and without construction of thin-film devices.

The key to our measurements is the use of very small Pt electrodes (i.e., microelectrodes). The small size (nominal 12.5-μm radius) reduces the magnitude of the cell current, and thus, the resistive ohmic losses associated with the bulk electrolyte to values acceptable in quantitative voltammetric analysis.

The electrochemical cell was a standard three-neck roundbottom flask equipped with a Ag/Ag^+ quasi-reference electrode, a Pt wire counter electrode, and a 12.5-μm radius Pt disk (area = 5×10^{-6} cm^2). The spacing between the working and counter electrodes was 1 cm and the spacing between reference and working electrodes was 1 mm. The cell was heated in an oil bath and equipped with a N_2 inlet. In a typical experiment, ca. 2 grams of premixed PEO:$LiClO_4$ powder was placed in the cell and heated to 110°C overnight under a constant flux of N_2. The electrodes were immersed in the viscous mixture for several hours prior to experimentation.

Fig. 33 shows the voltammetric response of the Pt microdisk in PEO:$LiClO_4$ at a 20 mV/s scan rate. When the electrolyte is carefully dried, the voltammogram appears relatively featureless between +1V and -3V (vs Ag/Ag^+). At a potential of ca. -3.2V the cathodic current rapidly increases and reaches a constant value of 1.85 μA. This plateau current is constant over a 1 V range and corresponds to the steady-state diffusion limited reduction. The return sweep shows a peak at -3.0 V that corresponds to the oxidation of Li metal. The smaller anodic peak at -1.5 V is due to the reduction of a small quantity of Fe^{2+}, which was added intentionally to the electrolyte to establish a quantitative potential reference scale. The difference in potential between the Li^+ and Fe^{2+} wave is ca. 2.3 V, in quantitative agreement with the tabulated free energies of these two couples.

The diffusion coefficient of Li^+ in 8:1 PEO:$LiClO_4$ is obtained from the limiting current, i_{lim}, using the relationship

$$D_{Li^+} = \frac{i_{lim}}{nFC_{Li^+}\,4r_o} \qquad (1)$$

where r_o is the electrode radius. The concentration of Li^+ in the electrolyte is 2.9×10^{-3} mol/cm^3. The equation is valid when the thickness of the deposited metal layer, d, does not exceed the electrode radius. From coulometric analysis of the Li metal oxidation wave

in Fig. 33, we determine that d = 11 μm. Analysis using the current plateau in Fig. 32 yields a value of $D_{Li^+} = 2 \times 10^{-6}$ cm^2/s in the 1000 M.W. PEO electrolyte.

The voltammetric response in PEO:$LiClO_4$ that has not been carefully dried is qualitatively different from that shown in Fig. 33. First, the Li/Li^+ wave is distorted and the anodic "stripping peak" is no longer observed. This finding suggests that the metallic Li deposit is unstable in "wet" PEO. Second, several cathodic waves are observed between 0 and -2.5 V that probably correspond to the reduction of water or the formation of surface hydrides. These waves are noticeably absent after rigorous drying of the electrolyte.

Although quantitative analysis of Li^+ transport and electroreduction in PEO is now feasible using microelectrodes, the ohmic drop in the bulk PEO:$LiClO_4$ remains significant. For example, we estimate from Fig. 33 that iR_s is ca. 0.5 V, which corresponds to an electrolyte conductivity of about 6.5×10^{-4} $(ohm.cm)^{-1}$, in reasonable agreement with literature values. However, the ohmic drop has a minimal effect on i_{lim} and the determination of diffusivities.

Measurements of limiting-current on the 25-μm Pt disks were used to determine the diffusivity of lithium in PEO as a function of Li^+ concentration. The results show (Table 5) that the maximum value of the product of diffusivity and concentration, DC_{Li}, is 5.6×10^{-10} mole/cm sec for molar ratio of 8:1. The Li^+ concentration was calculated by assuming a solid density of 1.21 g/cm^3. After correction for Li^+ concentration, a maximum diffusivity of 2.71×10^{-7} cm^2/sec was calculated for a molar ratio of 8:0.7. Preliminary measurements of Fe^{+2} and Fe^{+3} diffusivity were also made in 3×10^5 MW PEO. The diffusivity of Fe^{+2} is at least 3 times smaller than Fe^{+3} in PEO.

Table 5

WE	Graph#	Scan#	Molar Ratio	ilim(A)	$D_{Li+}C_{Li+}$ (mole/cm sec)	C_{Li+} (mole/cm3)	D_{Li+} (cm2/sec)	mass total(g)	mass $LiClO_4$(g)	moles Li+	*volume (cm3)
2	5-I	1	8/1	$2.7x10^{-7}$	$5.60x10^{-10}$	$2.64x10^{-3}$	$2.12x10^{-7}$	3.256	0.756	$7.11x10^{-3}$	2.69
2	6-II	1	8/1	$2.7x10^{-7}$	$5.60x10^{-10}$	$2.64x10^{-3}$	$2.12x10^{-7}$	3.256	0.756	$7.11x10^{-3}$	2.69
2	9-I	1	8/0.7	$2.6x10^{-7}$	$5.39x10^{-10}$	$1.99x10^{-3}$	$2.71x10^{-7}$	3.029	0.529	$4.97x10^{-3}$	2.50
2	9-III	1	8/0.5	$1.25x10^{-7}$	$2.59x10^{-10}$	$1.49x10^{-3}$	$1.73x10^{-7}$	2.877	0.377	$3.54x10^{-3}$	2.37
2	9-IV	1	8/0.2	$4.50x10^{-8}$	$9.33X10^{-11}$	$6.48x10^{-4}$	$1.44x10^{-7}$	2.651	0.151	$1.42x10^{-3}$	2.19
2	9-V	1	8/2	$5.00x10^{-8}$	$1.04x10^{-10}$	$4.29x10^{-3}$	$2.42x10^{-8}$	4.011	1.511	$1.42x10^{-2}$	3.31

*Calculations based on a density of 1.21 g/cm^3

The measurements were performed on solutions in low molecular weight PEO (MW = 1000 g/mol). The studies were extended to 3 x 10^5 and 5 x 10^6 MW PEO using slow scan rates (20-50 mV/sec) on the microdisk electrodes. A well-defined limiting current corresponding to diffusion-limited transport of Li^+ was obtained. Analysis of limiting currents as described above yielded values of the diffusivities reported in Table 6.

Table 6. Diffusivities of Li^+ in PEO Solution

MW PEO	D_{Li^+} (Dm^2/sec)
1000	2 x 10^{-6}
3 x 10^5	2 x 10^{-6}
5 x 10^6	0.5-1 x 10^{-7}

The results demonstrate the utility of microelectrode voltammetry in solid-state battery research, specifically in relation to transport phenomena in the more viscous high-molecular-weight polymer used in batteries.

II. VOLTAMMETRIC MEASUREMENT OF METAL ION DIFFUSIVITIES IN PEO-SALT SOLUTIONS

- A. Thakur, H.S. White

The electrolyte was prepared using PEO of 0.5 x 10^6 molecular weight. Metal (Cu^{+2},Fe^{+2}, Fe^{+3}) salts were dried under a vacuum of 25 mm Hg and 60°C for at least a week. After drying, PEO was dissolved in a minimum volume of either ethanol or acetonitrile, e.g., 1 ml. of acetonitrile per gram of PEO. Similarly, the metal salts were also dissolved in a minimum volume of either ethanol or acetonitrile. The solutions were well stirred and stored for 48 hours to ensure homogeneity. After complete dissolution, the PEO and salt solutions were mixed in the electrochemical cell so as to form the electrolyte solution. This solution was stirred for 4 days under N_2. The organic solvents were allowed to evaporate, initially at room temperature under vacuum and then at a higher temperature of 80°C for 24 hours. After complete evaporation of the solvents, the

viscous solution was used for cyclic voltammetry. The cell was placed in an oil bath so as to control temperature. Platinum disk microelectrodes of diamter 25 microns were polished with 1 μm alumina.

The voltammetric behavior of Cu^{2+} in PEO (PEO/$CuCl_2$:8/1) is shown in Fig. 34 for temperatures between 110 and 160°C (voltammetric scan rate = 10 mv/sec). One irreversible wave is observed for the reduction of Cu^{2+} to Cu^{+}. On the reverse scan, no anodic peak is observed corresponding to the reoxidation of Cu^{+}. This behavior is consistent with the voltammetric response at a microdisk of dimensions <100 μm.

For a disk microelectrode, the limiting plateau current is given by

$$i_l = rnFDCr_o \qquad (1)$$

Here n is the number of electrons, F is the Faraday, D is an apparent diffusion coefficient of metal ion, C is the concentration of the metal ions, and r_o is the radius of the microelectrode. The product of the diffusion coefficient and concentration of Cu^{2+}, D•C, can be calculated from eq. 1 from measurement of the limiting currents (Table 7). These values range from 2 to 70 mol/cm•s and are of the same magnitude as reported for Li^{+}. The limiting current for Cu^{2+} reduction increases with increasing temperature, Fig. 35, although the shape of the voltammogram essentially remains the same. In Fig. 36, the log of the product of the metal ion diffusivity and concentration, log(D•C), is plotted vs 1/T(K) for PEO/$CuCl_2$ ratios between 80:1 and 8:1. The slopes of these plots yield activation energies of 2.5-4.0 kcal/mol, independent of Cu^{2+} concentration.

The dependence of log(D•C) on the PEO/$CuCl_2$ mole ratio is plotted in Figure 37 for experiments performed at 110, 130 and 150°C. All three plots show linear behavior up to an 8:1 PEO/$CuCl_2$ ratio, in agreement with eq. 1, which predicts a linear increase of current with Cu^{2+} concentration. The results suggest that the diffusivity of Cu_2^{+} in PEO, to a first approximation, remains constant over a wide range. At the highest Cu^{2+} concentrations, values of (D•C) decrease slightly, similar to previously results reported for Li^{+}.

From estimates of the solution Cu^{2+} concentration, the diffusivity of the Cu^{2+} in 8:1 PEO/$CuCl_2$ mixture is calculated to be ~4 x 10^{-7} cm^2/s. This estimate, which is based upon eq. (1), assumes that migration and convection are negligible. Although these assumptions are incorrect, we have shown that eq. (1) yields estimates of the diffusivity that is within a factor of 2 of the correct bulk value (1). Furthermore, a gradual increase or decrease of the diffusivity within the reaction layer thickness does not significantly affect the measured limiting current.

Preliminary experiments have also been performed with the PEO•$FeCl_3$ system. The reduction of Fe^{3+} ion in PEO is a 2-step process as shown in Fig. 38. The first cathodic wave at -0.2 V corresponds to the reduction of Fe^{3+} to Fe^{2+}. Both halves of this redox couple are soluble in PEO resulting in a nearly sigmoidal shaped voltammogram. The second wave at -0.9 V corresponds to the 2-electron reduction of Fe^{2+} to metallic Fe. As predicted by the above eq. 1, the height of this wave is approximately twice that of the 1-e^- reduction of Fe^{2+}. The second reduction wave is more reversible in comparison to the reduction of Cu^{2+}. For instance, the voltammetric oxidation peak at -0.5 V corresponds to reoxidation of the metal deposit.

Table 7

$CuCl_2$/PEO molar ratio = 0.0125/1

S.No	Temperature (°K)	Limiting Current (nA)	$D_{Cu^{2+}}*C_{Cu^{2+}}*10^{11}$ (mol/cm*sec)
1.	383	24	2.49
2.	395	48	4.97
3.	403	53	5.49
4.	413	59	6.11
5.	425	65	6.74
6.	433	62	6.42

$CuCl_2$/PEO molar ratio = 0.0375/1

S.No	Temperature (°K)	Limiting Current (nA)	$D_{Cu^{2+}}*C_{Cu^{2+}}*10^{11}$ (mol/cm*sec)
1.	383	56	5.8
2.	389	64	6.63
3.	401	92	9.53
4.	411	116	12.02
5.	421	200	20.73
6.	433	190	19.69

$CuCl_2$/PEO molar ratio = 0.125/1

S.No	Temperature (°K)	Limiting Current (nA)	$D_{Cu^{2+}}*C_{Cu^{2+}}*10^{11}$ (mol/cm*sec)
1.	383	200	20.73
2.	398	240	24.87
3.	413	495	51.30
4.	443	740	76.68
5.	453	680	70.47
6.	463	675	68.38

$CuCl_2$/PEO molar ratio = 0.1375/1

S.No	Temperature (°K)	Limiting Current (nA)	$D_{Cu^{2+}}*C_{Cu^{2+}}*10^{11}$ (mol/cm*sec)
1.	383	200	20.73
2.	398	225	23.32
3.	413	350	36.27
4.	428	560	58.03
5.	443	640	66.32
6.	453	620	64.27

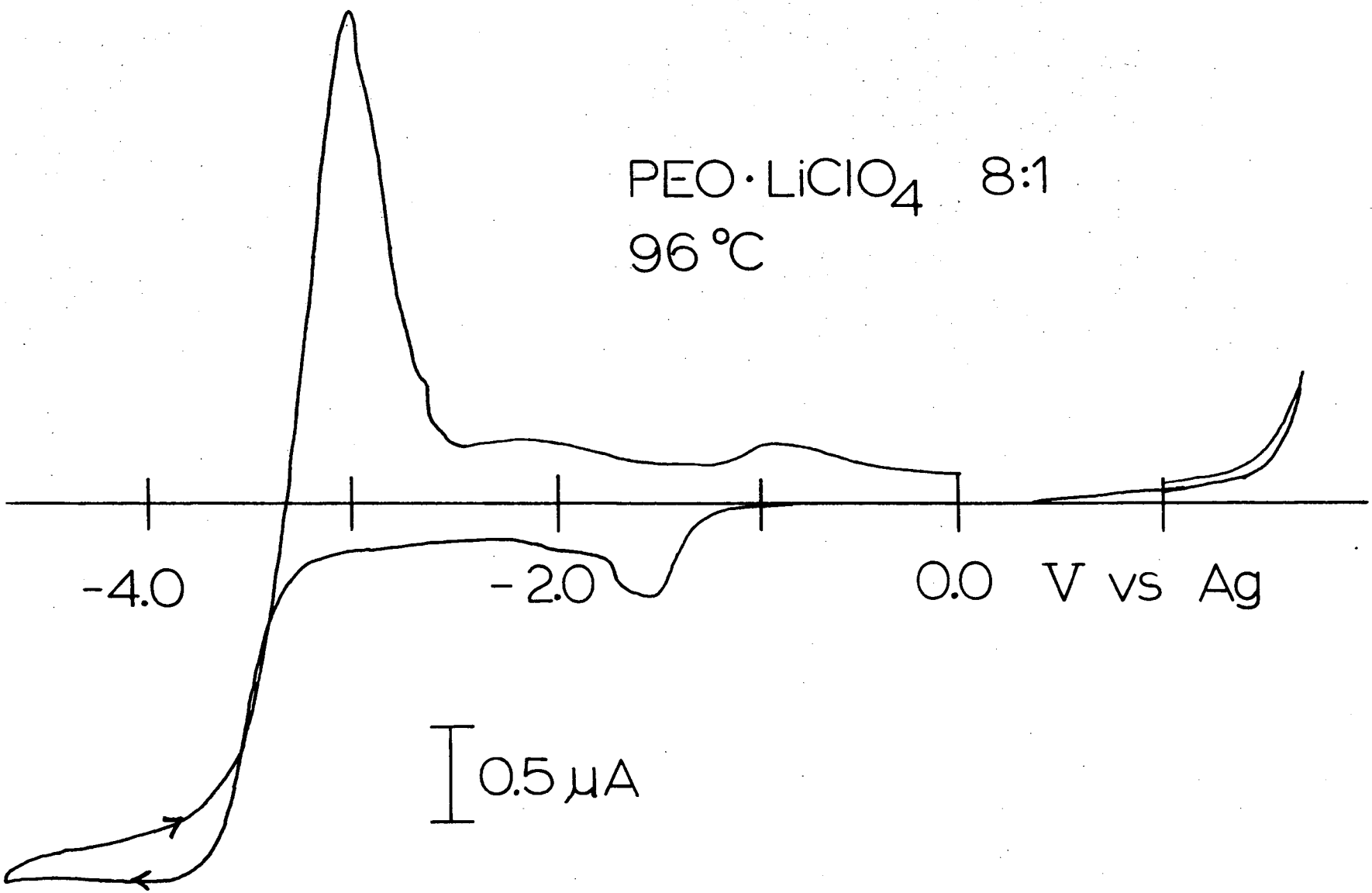

Fig. 33. Cyclic Voltammetric response of a 25 μm diameter Pt disk in a PEO·$LiClO_4$ solution

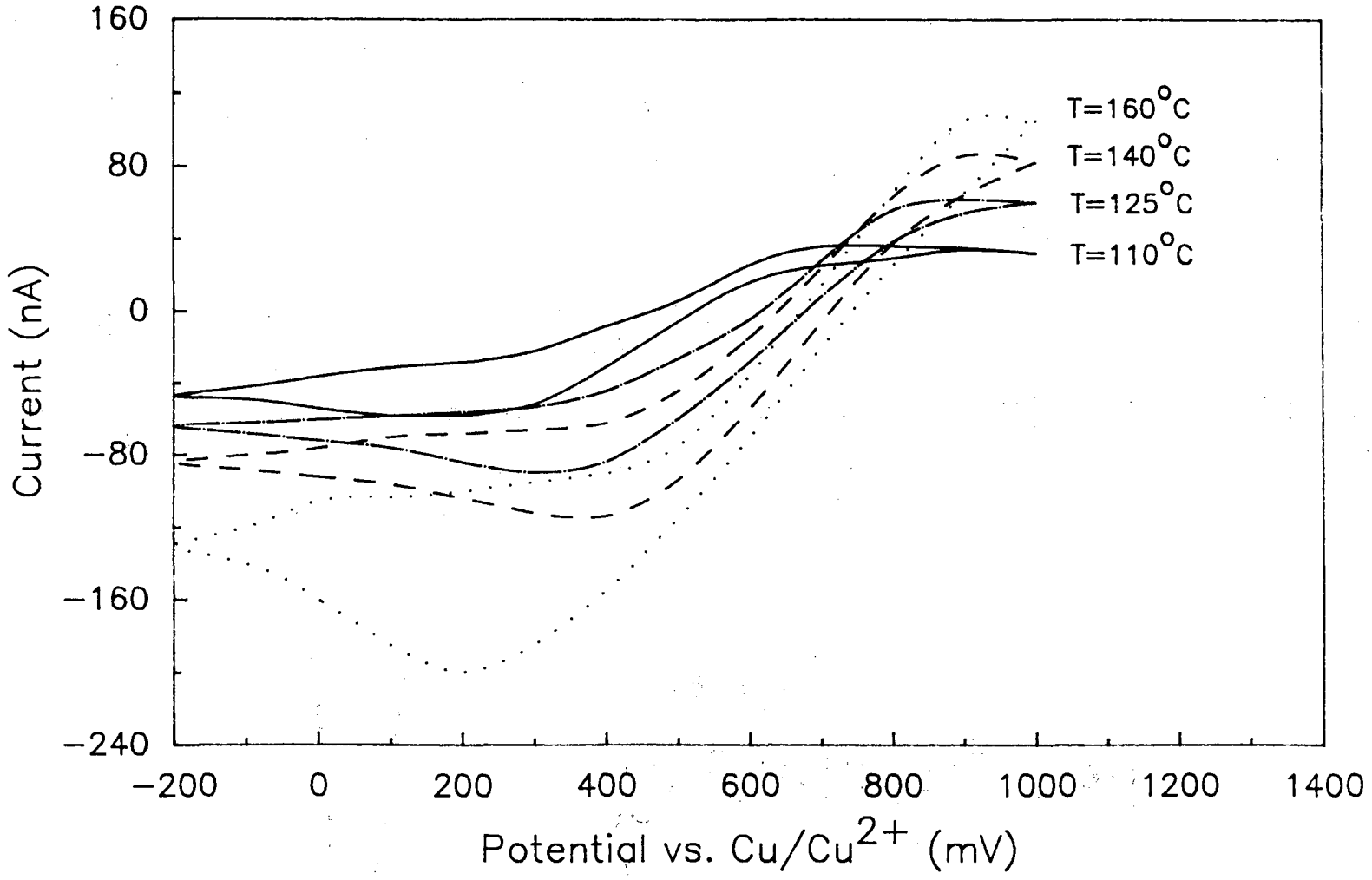

Fig. 34. Cyclic voltammograms of the $CuCl_2$: PEO system

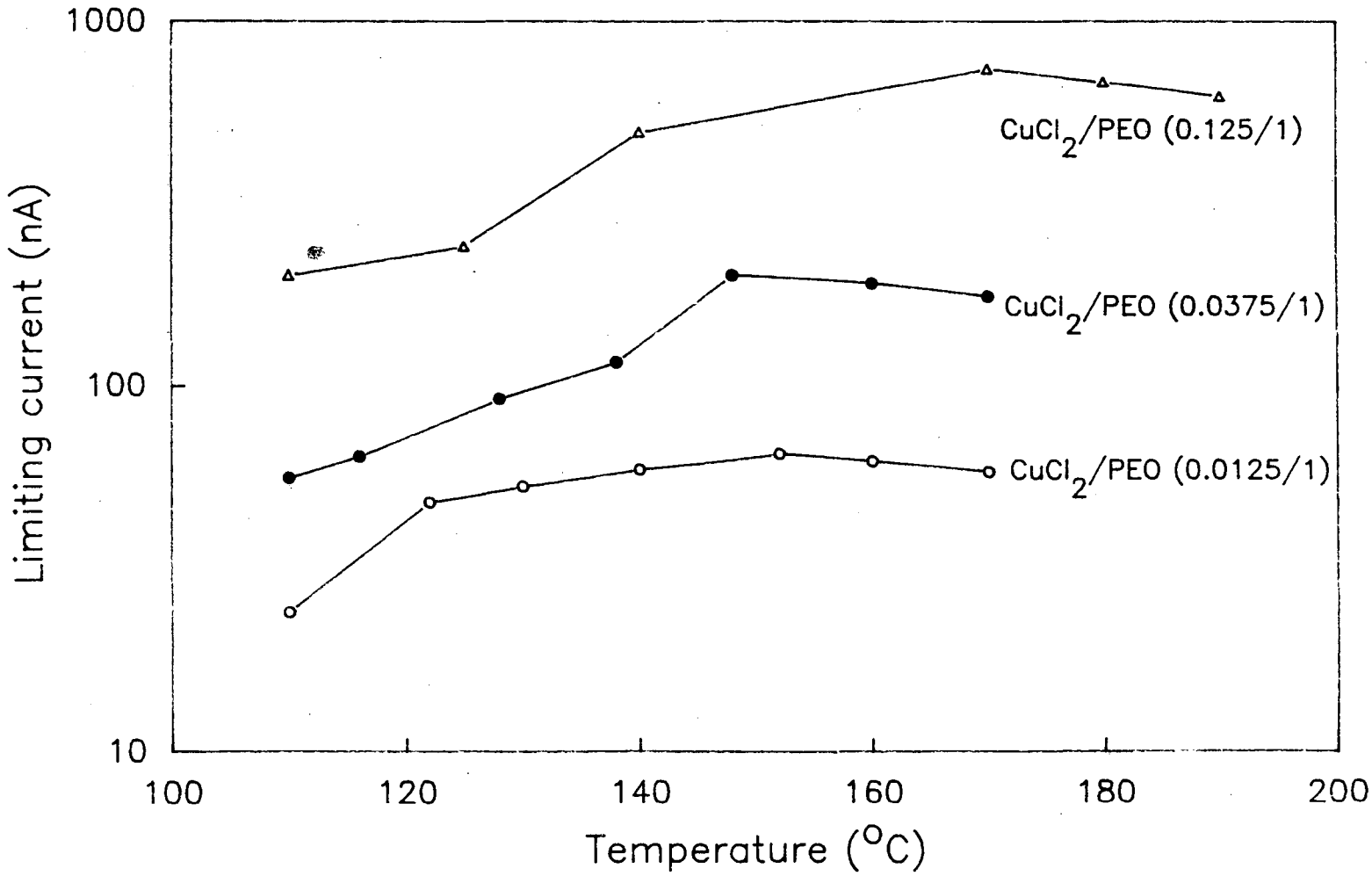

Fig. 35. Limiting current as a function of temperature.

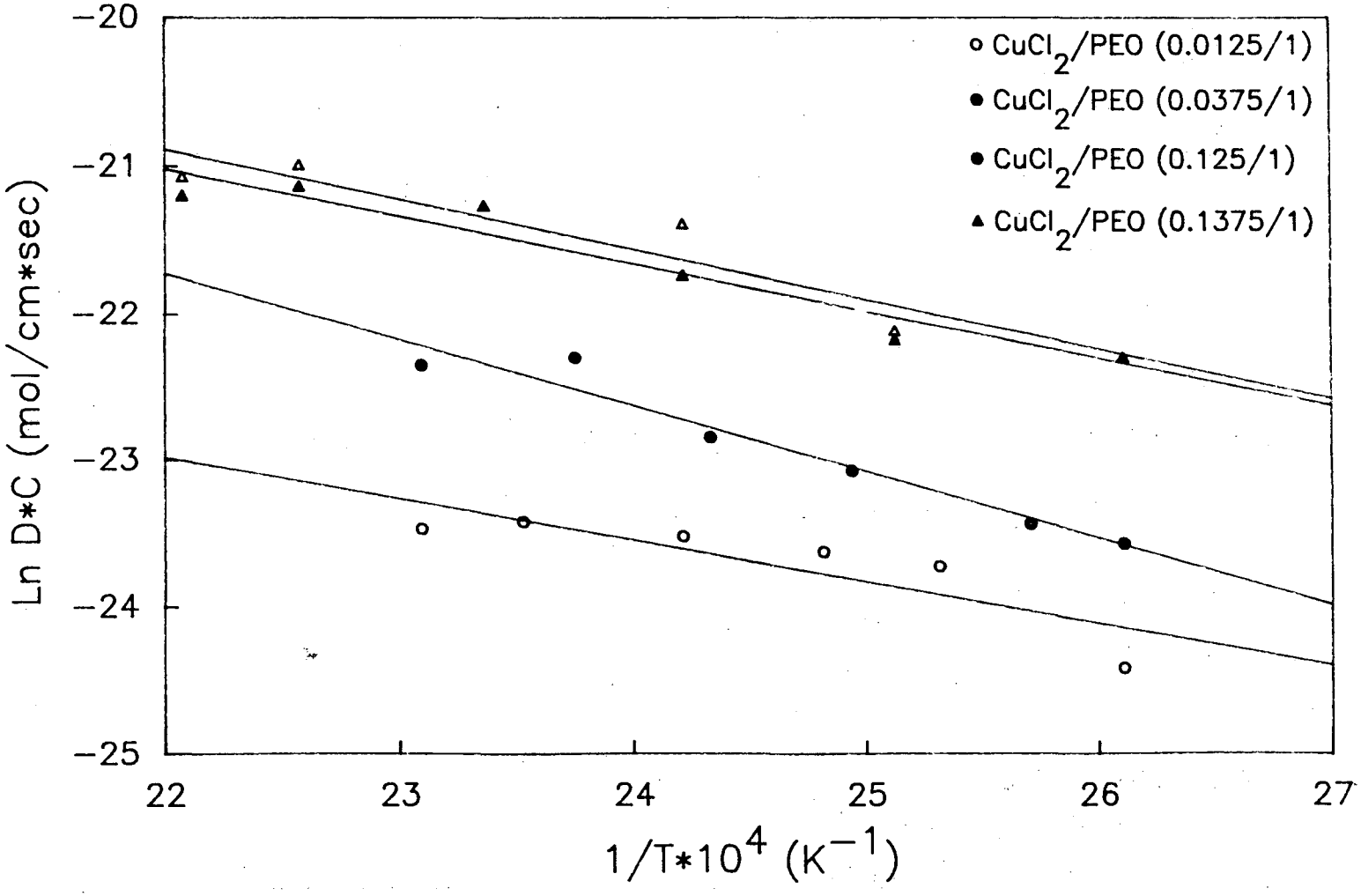

Fig. 36. Ln of Diffusion Coefficient Concentration Products as a Function of Inverse of Absolute Temperature

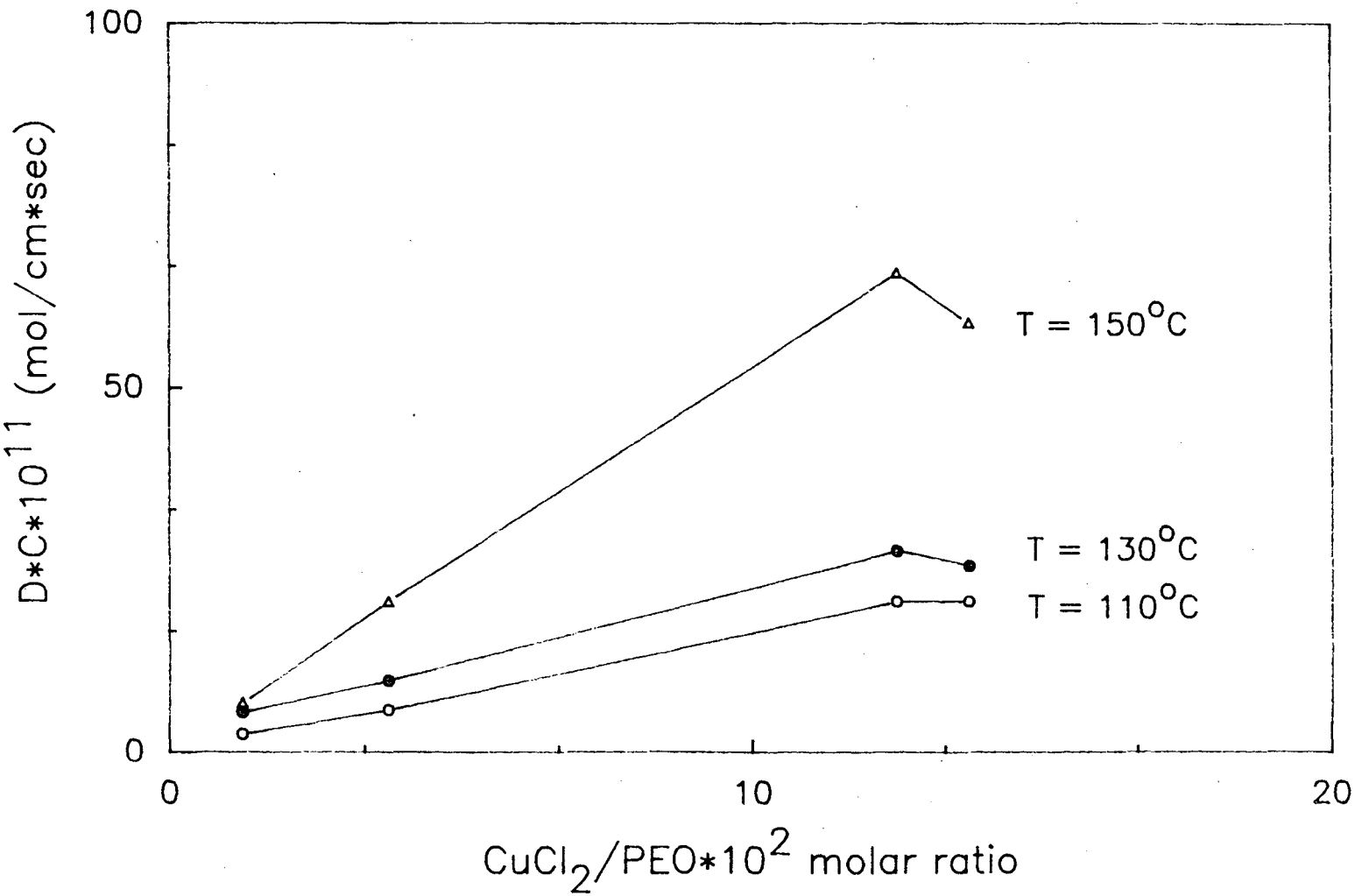

Fig. 37. Diffusion Coefficient Concentration Product as a Function of $CuCl_2$/PEO Molar Ratio

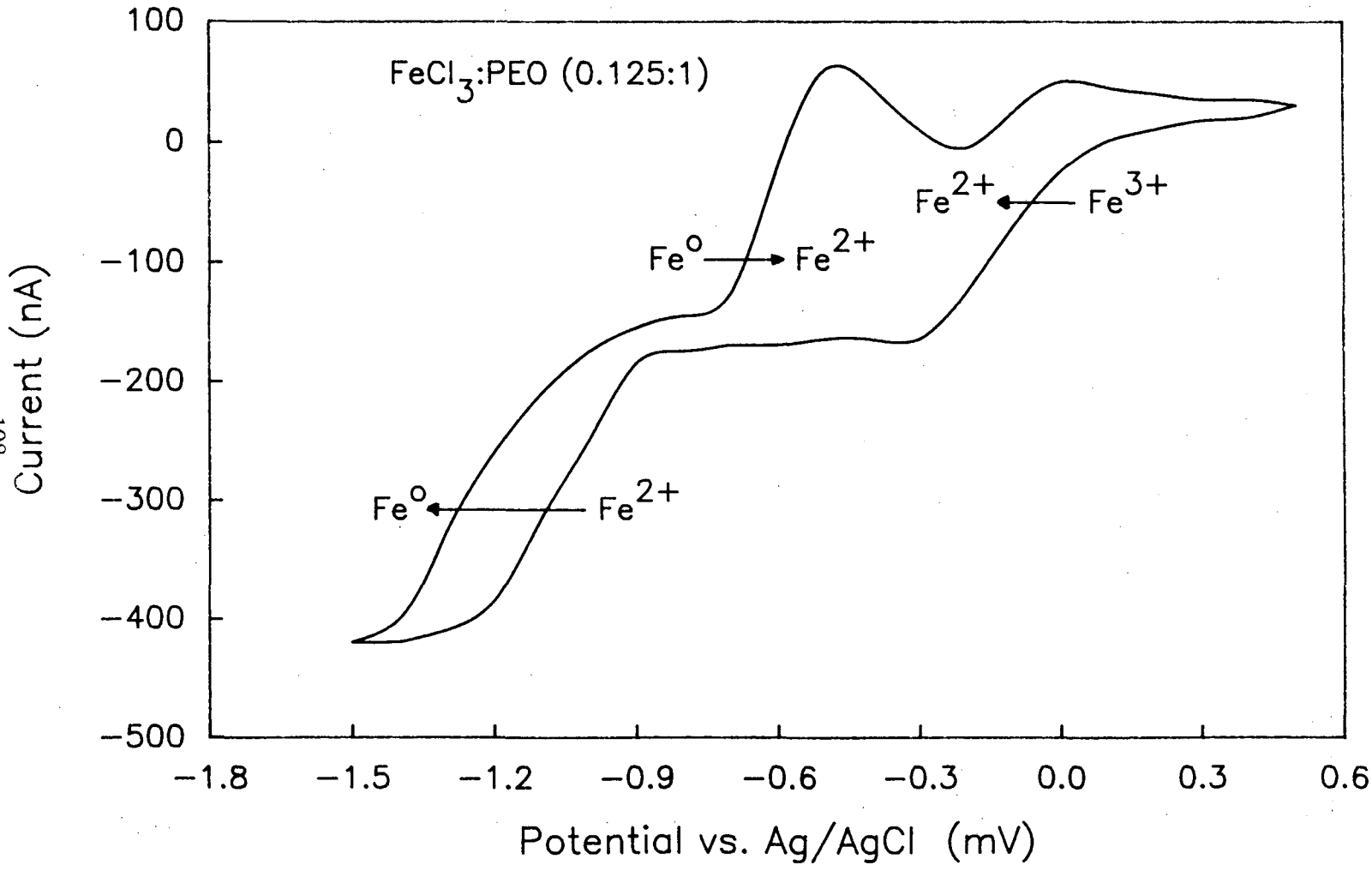

Fig. 38. Cyclic voltammogram of the $FeCl_3$: PEO system

LAWRENCE BERKELEY LABORATORY
TECHNICAL INFORMATION DEPARTMENT
1 CYCLOTRON ROAD
BERKELEY, CALIFORNIA 94720